Dissertation

submitted to the

Combined Faculties for the Natural Sciences and for Mathematics

of the Ruperto–Carola University of Heidelberg, Germany

for the degree of

Doctor of Natural Sciences

presented by

M.Sc. Alexander Matthias Goebel

born in Buenos Aires (Argentina)

Oral examination: July 16^{th} 2008

Manipulation of Multi-Photon-Entanglement

* * *

Applications in Quantum Information Processing

Referees: Prof. Dr. Jian-Wei Pan
Prof. Dr. Jörg Schmiedmayer

Zusammenfassung

Manipulation von Multi-Photonen-Verschränkung

Die Quanteninformationsverarbeitung (QIV) hat in den letzten zwanzig Jahren das Interesse zahlreicher Wissenschaftler geweckt, da sie beeindruckende Verbesserungen unter anderem auf den Gebieten der Rechengeschwindigkeit, Kommunikationssicherheit und die Fähigkeit zur Simulation von quantenmechanischen Prozessen verspricht. Diese Dissertation beschreibt eine experimentelle Arbeit zur Physik der Verschränkung mehrerer Photonen und ihre Anwendung auf dem Gebiet der QIV. Es wurden neuartige Techniken entwickelt, die zur Erzeugung der Verschränkung von bis zu sechs Photonen benötigt werden. In dieser Dissertation werden grundlegenden Experimente beschrieben, die mit Hilfe des entwickelten Sechs-Photonen Interferometers durchgeführt wurden. Im einzelnen sind dies die erste experimentelle Quanten Teleportation eines zusammengesetzten Zwei-Teilchen Zustandes, die Realisierung von Verschränkungsübertragung über mehrere Abschnitte, die Implementierung eines teleportationsbasierten "bedingten-NICHT-Gatters" für eine fehlertolerante Quantenrechnung, die erste Erzeugung eines Graph-Zustandes mit sechs Photonen und die Realisierung eines Einwegquantencomputers mit Hilfe eines Zwei-Photonen-Vier-Qubit Cluster Zustandes. Die entwickelten Methoden sollen einen Beitrag leisten sowohl für die weitere Erforschung von QIV als auch für zukünftige grundlegende Experimente der Quantenmechanik.

Abstract

Manipulation of Multi-Photon-Entanglement

Over the last twenty years the field of quantum information processing (QIP) has attracted the attention of many scientists, due to the promise of impressive improvements in the areas of computational speed, communication security and the ability to simulate nature on the micro scale. This thesis describes an experimental work on the physics of multi-photon entanglement and its application in the field of QIP. We have thoroughly developed the necessary techniques to generate multipartite entanglement between up to six photons. By exploiting the developed six-photon interferometer, in this thesis we report for the first time the experimental quantum teleportation of a two-qubit composite system, the realization of multi-stage entanglement swapping, the implementation of a teleportation-based controlled-NOT gate for fault-tolerant quantum computation, the first generation of entanglement in six-partite photonic graph states and the realization of 'one-way' quantum computation with two-photon four-qubit cluster states. The methods developed in these experiments are of great significance both for exploring the field of QIP and for future experiments on the fundamental tests of quantum mechanics.

Contents

List of Figures

Chapter 1

Introduction

The fundamental concept of quantum mechanics (QM) is superposition. Following classical physics and general human conception, a system can only be in one state at a time. However, in QM a system can be in a superposition of arbitrary many states at the same time. This has been shown in various analogs of Young's famous double-slit interference experiment, such as in an electron interferometer [1], neutron interferometer [2] and atom interferometer [3, 4].

This already puzzling feature leads to even more counterintuitive consequences for the combined system of two or more subsystems, as pointed out by Einstein, Podolsky and Rosen in their famous paper in 1935 [5]. They consider two distant particles that have interacted in the past and are in a superposition of states of the combined system. Depending on the choice of measurement (e.g. momentum or position) on particle A, particle B will collapse into a different state. This "spooky action at a distance" (Einstein) acts instantaneous and is completely independent of the distance between the two particles. Einstein, Podolsky and Rosen regarded this action as non-physical and therefore concluded, that QM must be considered incomplete.

For many years this effect, known as the EPR paradox, left the physics world puzzled. In 1964, Bell proposed an experimental test of a local hidden variable model (LHV), that was considered to complement QM and to thus circumvent its counterintuitive characteristics [6]. He noticed, that the expectation values for any LHV and QM differ for specific sets of measurements. More precisely, he formulated an inequality, which holds for any LHV, but is allowed to be violated by QM. This "Bell inequality" was first violated experimentally by Aspect et al. in 1982 [7, 8, 9] and has been tested further under various conditions [10, 11]. Today, QM is widely excepted by physicists. There still exist some loopholes of the Bell tests that up to now have not been closed simultaneously, however it is believed that this is only a question of a few years.

Quantum entanglement, the name for superposition in a multi-particle system was first noticed by Schrödinger [12]. In the beginning of the twentieth century, QM and in particular entanglement was viewed not without sceptism. However,

after the violation of Bell's inequality and at the latest after Feynman suggested the possibility of a *quantum computer*, entanglement has attracted the attention of many scientists.

Quantum entanglement lays at the heart of quantum information processing (QIP), which over the past twenty years has become an emerging field of modern physics. QIP can mainly be divided into the two areas of quantum communication and quantum computation [13, 14]. Quantum communication describes the transfer of quantum states over large distances, which can lead to drastic improvements in security – quantum cryptography [15, 16] – and channel capacity – quantum dense coding [17]. It further covers the distribution of bi- or multi-partite entanglement between different parties, separated by large distances [18, 19].

Quantum computation is dedicated to the implementation of algorithms that exploit the superposition character of quantum entanglement to dramatically speed up computational tasks such as a reduction of time needed to search an unsorted database of N elements. Any classical algorithm necessitates $\sim N$ operations to accomplish this task, whereas a quantum algorithm only needs $\sim \sqrt{N}$ operations [20]. Probably the most famous quantum algorithm is Shor's algorithm to factorize large numbers [21]. Its introduction in 1994 has jump started and fueled tremendous effort in the new field of QIP, both on the theoretical and experimental side. The algorithm is based on the quantum Fourier transform and yields an exponential improvement of required resources – i.e. as a function of the number of digits of the used number to factorize – compared to the best known classical algorithms. Several other quantum algorithms exist [22], many of which are also based on the quantum Fourier transform. Furthermore, a quantum computer can efficiently and accurately simulate the evolution of quantum many body systems and quantum field theories that cannot be simulated on classical computers without making unjustified approximations.

Remarkable experimental and theoretical effort has been employed to the implementation of different areas of QIP. Quantum cryptography, in particular quantum key distribution [15, 16] is an example for quantum communication, which is already at the verge to commercial use, whereas research on quantum repeaters [23, 24], essential building blocks for the realization of entanglement distribution over large distances, is still rather fundamental. Also, realizations of quantum computers to implement quantum algorithms are still at the very first stages and a great deal of fundamental research still lays ahead.

One of the exciting aspects of quantum information science is that there are several candidates of quite different physical systems that can in principle be used to implement QIP and it doesn't look like the race between them will be decided anytime soon. Promising candidates are, but not limited to, ion traps [25], nuclear magnetic resonance [26], quantum dots [27], super-conducting devices (Josephson junction) [28] and photons [29].

We try to implement QIP with photons and linear optics for various reasons such as very strong robustness against de-coherence, extremely fast and accurate implementations of universal single qubit operations and the vast availability of already existing electro-optic devices. We exploit spontaneous parametric down-conversion [30], which is still the best source for entangled photon pairs, together with basic linear optics elements to generate multi-photon entanglement. With these building blocks at hand, we on the one hand conduct experimental tests of the fundamental nature of quantum mechanics and on the other hand try to design and develop new techniques and methods necessary for future applications in QIP.

The work described within this thesis has been a step along this line, it is the aim to report the first quantum teleportation of a two-qubit composite system, to report the first realization of multi-stage entanglement swapping, to report the first implementation of a teleportation-based quantum gate for fault-tolerant quantum computation, to report the first generation of six-photon Schrödinger cat and cluster states and to report an implementation of the one-way quantum computer model with two-photon four-qubit cluster states. The main contents of the dissertation are organized as follow:

Chapter (1) is a brief introduction to the field of quantum entanglement and QIP and gives a short overview over the contents of this thesis.

In chapter (2) we present the theoretical background of some fundamental concepts of QIP that lay at the heart of all the work for this dissertation. We discuss in detail some features of bipartite entanglement and how it can be used to teleport an arbitrary quantum state from one place to another. We then proceed to multipartite entanglement by introducing ways to classify and verify it. We discuss the model of one-way quantum computation, which uses special multipartite entangled states. In the third section, we introduce the process of spontaneous parametric down-conversion as a source for polarization entangled photon pairs. We conclude the chapter with a detailed description of the implementation of a Bell state analyzer with linear optics.

Quantum teleportation of a single particle has first been demonstrated in 1997 with photons and with several other physical systems thereafter. However, teleportation of a composite system is a crucial task needed for many QIP protocols. In chapter (3) we demonstrate the first quantum teleportation of a two-qubit composite system. We depict the design and development of a six-photon interferometer that has been used in most of the experiments described within this dissertation.

Entanglement swapping is of fundamental interest since it can be used to entangle particles that have never physically interacted in the past. Its realization over multiple stages, however, is an essential exigency for the implementation of quantum repeaters. In chapter (4) we report the first experimental realization of multistage entanglement swapping. The experimental results clearly show the entanglement of the final outgoing photon pair.

The coupling of quantum states to their environment imposes a major challenge to the implementation of realistic quantum computers. Quantum error correcting codes and fault-tolerant quantum gates are thus of significant importance to QIP. In chapter (5) we present the first experimental realization of a teleportation-based controlled-NOT gate that can in principle be used for fault-tolerant quantum computation.

Multipartite entangled states are on the one hand of high interest for test of quantum mechanics, since certain classes of states show much stronger violations of locality and realism than any bipartite system. On the other hand they are a fundamental resource to several quantum computation models. However, the generation of highly entangled multipartite states remains a great experimental challenge. In chapter (6) we discuss the first generation of six-photon graph states such as a GHZ and a cluster state.

A recently developed scheme for 'one-way' quantum computation with highly entangled multipartite cluster states is a promising candidate for future implementations of quantum algorithms. In chapter (7) we demonstrate the realization of this model with a two-photon four-qubit cluster state. With our setup, we are able to increase the generation rate of a four-qubit cluster state by more than four orders of magnitude compared to recent experiments. This improvement constitutes an essential step towards the feasibility of realistic quantum computers.

We conclude this thesis by summarizing its main results and provide an outlook to future work and some further remarks in chapter (8).

Chapter 2

Multi-Photon-Entanglement

Quantum entanglement is, according to Schrödinger, the essential feature of quantum mechanics [12]. It describes correlations between quantum systems that are much stronger than any classical correlation could be and is a fundamental element of quantum information processing (QIP). From an early stage on, entanglement proved to be an essential tool of quantum physics, both in theory and experiment: early experimental realizations of entangled photon pairs were used to demonstrate the quantum nature of polarization correlations that can occur in decay processes [31, 32], to confirm quantum predictions of radiation theory and falsify semi-classical models [33, 34], or to test Bell's theorem and exclude local realistic descriptions of the observed quantum phenomena [6, 7, 8, 9]. It followed the discovery of QIP, partly triggered by the introduction of quantum cryptography[15, 16]. Quantum entanglement is a fundamental resource for QIP as a quantum channel in quantum communication (e.g. for quantum state teleportation [35, 36] or quantum dense coding [17, 37]) or as computational source. Quantum computing with photons has recently experienced a new boom by discovering the possibility of universal computing with linear optics and measurements alone [29].

In this chapter some basic concepts and procedures of quantum entanglement and QIP are introduced, which are essential to the work within the framework of this thesis. We start with the theoretical discussion of entanglement in bipartite systems, covering the Bell-state basis and quantum teleportation. We then proceed to multipartite entanglement and outline different classes of states, such as Greenberger-Horne-Zeilinger (GHZ) states and graph states. We show how they can be detected by quantum witnesses and why they can be used to perform scalable quantum computing. In the third section we briefly discuss the experimental realization of key elements that were used in all setups for this thesis. We describe the creation of entangled photons and the operation of a Bell-state analyzer.

2.1 Bipartite Entanglement

We start with the most simple case, the entanglement of two single particles. Many of the fascinating features of quantum entanglement can already be observed in such a bipartite system. Furthermore, many procedures in QIP can essentially be decomposed into two-particle systems.

2.1.1 Quantum Bits

Up to now we have been concerned with general systems and have not specified any requirements or restrictions to our systems. In theoretical QIP however, only two-level systems are of interest. This reduces complexity and simplifies the involved theory significantly.

In classical information processing the smallest unit carrying information is a bit, a binary digit taking the value 0 or 1. In analogy, a quantum bit is the state vector of a two-level system with the basis states $|0\rangle$ and $|1\rangle$. In contrast to a classical bit a quantum bit, commonly know as qubit, can take values that are in a superposition of the two basis states:

$$|\Psi\rangle = \alpha\,|0\rangle + \beta\,|1\rangle \tag{2.1}$$

The pre-factors α and β can be any complex numbers satisfying $|\alpha|^2 + |\beta|^2 = 1$.

A graphic interpretation of a qubit is the Bloch sphere, which is shown in Fig. (2.1). The state of the qubit is represented by an arrow from the origin to the surface of the unit sphere. The complex nature of the relative phase between α and β accounts for the three axes given by $|0\rangle/|1\rangle$, $|+\rangle/|-\rangle$ and $|R\rangle/|L\rangle$. Here,

$$\begin{aligned} |+\rangle &= \frac{1}{\sqrt{2}}\left(|0\rangle + |1\rangle\right), |-\rangle = \frac{1}{\sqrt{2}}\left(|0\rangle - |1\rangle\right) \textit{and} \\ |R\rangle &= \frac{1}{\sqrt{2}}\left(|0\rangle + i\,|1\rangle\right), |L\rangle = \frac{1}{\sqrt{2}}\left(|0\rangle - i\,|1\rangle\right) \end{aligned} \tag{2.2}$$

are two in QIP commonly used orthonormal bases in addition to the computational basis of $|0\rangle/|1\rangle$. In analogy to the polarization state of light they are often called diagonal ($|+\rangle/|-\rangle$) and circular ($|R\rangle/|L\rangle$) basis, respectively. Note that, for a qubit in a pure state, the state vector always has unit length. However, for a qubit in a mixed state, the length is smaller than unity. For example, the state vector for a completely random qubit is represented by a point at the origin.

2.1.2 Bell-States and Quantum Entanglement

The combined state of two qubits forms a four-dimensional Hilbert space. The most obvious choice for a basis is a generalization of the single qubit computational basis:

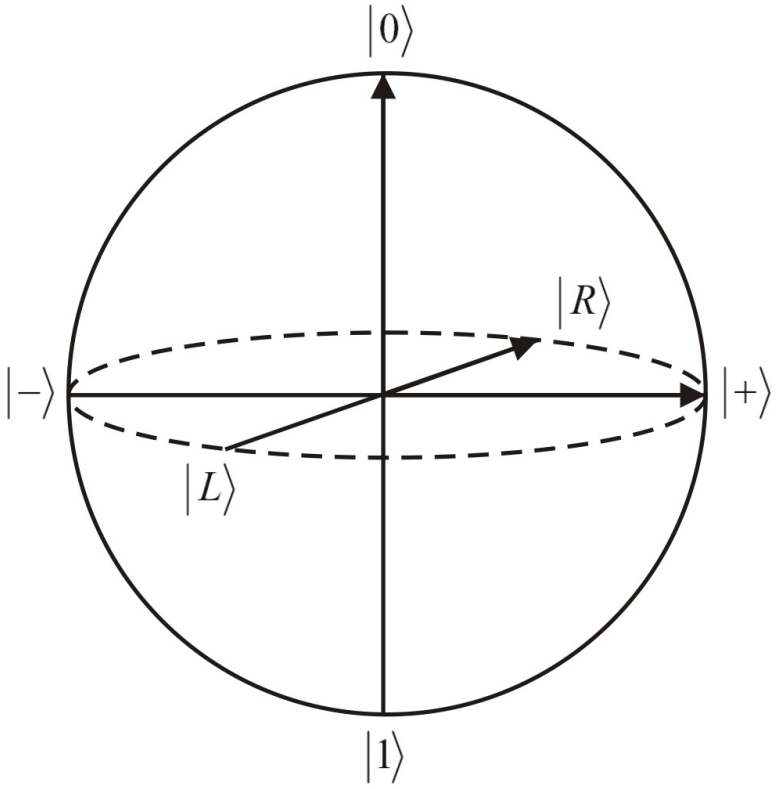

Figure 2.1: *Bloch sphere. An arrow from the origin to the surface of the sphere represents the state of a qubit.* $|0\rangle/|1\rangle$ *are the eigenstates in the computational basis,* $|\pm\rangle = \frac{1}{\sqrt{2}}(|0\rangle \pm |1\rangle)$ *in the diagonal basis, and* $|R\rangle/|L\rangle = \frac{1}{\sqrt{2}}(|0\rangle \pm i|1\rangle)$ *in the circular basis*

$|0\rangle|0\rangle$, $|0\rangle|1\rangle$, $|1\rangle|0\rangle$ and $|1\rangle|1\rangle$. However, in many cases in QIP a different choice will be more suitable:

$$|\Phi^{\pm}\rangle = \frac{1}{\sqrt{2}}(|0\rangle|0\rangle \pm |1\rangle|1\rangle)$$
$$|\Psi^{\pm}\rangle = \frac{1}{\sqrt{2}}(|0\rangle|1\rangle \pm |1\rangle|0\rangle) \tag{2.3}$$

This is known as the Bell basis or the Bell states. In contrast to the states of the computational basis, the Bell states can not be expressed as a product of two single-particle wave functions. Particles in a Bell state are thus non-separable or *entangled*!

Quantum Entanglement

To emphasize the importance of this characteristic we will conduct a little *gedanken-experiment*. Let us assume that two friends, in QIP commonly known as Alice and Bob, choose to share a pair of qubits that are in the entangled Bell state $|\Phi^+\rangle$ (e.g. polarization-entangled photons or spin-entangled electrons). Now Alice chooses to measure her qubit in the computational basis yielding either a $|0\rangle$ or $|1\rangle$ with equal probability. However, since her qubit was originally entangled with Bob's qubit, the combined state collapses to one of the two separable terms of $|\Phi^+\rangle$ ($|0\rangle|0\rangle$ or $|1\rangle|1\rangle$). Therefore, Bob's measurement will now with certainty yield the same result that Alice has obtained. In other words, Alice's measurement has changed the combined state and thereby the state of Bob's qubit.

So far, the same results could have been obtained by simply using a machine that randomly distributes a pair of equal classical bits to Alice and Bob. Then Alice's result is again completely random and is always in a perfect correlation to Bob's result. However, if Alice and Bob are also allowed to measure their qubit in the diagonal basis, things become different. Some measurement results can no longer be explained by classical physics. To understand this, consider the following scenario: Alice and Bob again share a pair of qubits in the state $|\Phi^+\rangle$. They now choose to measure their qubit in the computational or diagonal basis independently of each other. There are thus four possible combinations:

	Alice's choice of basis	Bob's choice of basis	measurement results are
1	$\|0\rangle/\|1\rangle$	$\|0\rangle/\|1\rangle$	correlated
2	$\|0\rangle/\|1\rangle$	$\|+\rangle/\|-\rangle$	not correlated
3	$\|+\rangle/\|-\rangle$	$\|0\rangle/\|1\rangle$	not correlated
4	$\|+\rangle/\|-\rangle$	$\|+\rangle/\|-\rangle$	correlated

(2.4)

The first row describes the case already discussed above. In the second case Alice's measurement again projects the combined state onto $|0\rangle|0\rangle$ or $|1\rangle|1\rangle$. However, since

Bob now decides to measure in the diagonal basis, he obtains $|+\rangle$ or $|-\rangle$ with equal probability. Alice's and his results are thus not correlated. The argument for the third case works analogous. The measurement results in the last case on the other hand are perfectly correlated. This can easily be understood by rewriting $|\Phi^+\rangle$ in the diagonal basis:

$$\left|\Phi^+\right\rangle = \frac{1}{\sqrt{2}}(|+\rangle|+\rangle + |-\rangle|-\rangle) \tag{2.5}$$

Since Alice and Bob both measure in the diagonal basis, this case is identical to the first case up to a simple transformation of basis. However, under no circumstances are we able to construct a classical machine that yields the combined measurement results for the four cases of Table (2.4).

The projection of the combined state by Alice's measurement acts instantaneous and is completely independent of the distance between Alice and Bob. As already mentioned in the introduction chapter, this "spooky action at a distance" has puzzled many physicists. Einstein, Podolsky and Rosen (EPR)[5] argued, that quantum entanglement would contradict *realism* and *locality*. To them a physical property of a system can not be considered *real* if its value is undefined until measured. Einstein once expressed this conception with the words: "Gott würfelt nicht!" (God does not throw the dice). However, in our above example the value of Alice's qubit is undefined until she decides to measure it. Furthermore, they consider the fact unphysical, that an action at point A could have an immediate effect on a system at point B, regardless of the distance between the two *locations*. Again, in our example Alice's measurement forces the combined state to collapse and thereby changes the state of Bob's qubit independently of Bob's *location*. Due to this controversy EPR reasoned that quantum mechanics (QM) must be incomplete.

For many years this effect, known as the EPR paradox, left the physics world puzzled. To solve this problem, local hidden variable theories (LHV) were suggested. The idea is that all properties of a physical system are well defined at all times by a set of variables that is not or not yet accessible to us. Hence, no outcome of a measurement is random, but already predetermined by these variables. In 1964, Bell proposed an experimental test [6] for LHV theories that were considered to complement QM and thus to circumvent its counterintuitive characteristics. He noticed that the expectation values for any LHV and QM differ for specific sets of measurements. More precisely, he formulated an inequality, which holds for any LHV, but is allowed to be violated by QM. This "Bell inequality" was first violated experimentally by Aspect et al. in 1982 [7, 8, 9] and has been tested further under various conditions [10, 11]. Today QM is widely excepted by physicists.

We would like to point out that some loopholes of the experimental Bell tests still exist, which so far have not been closed simultaneously. However, it is believed that this is due to technological problems and that it is only a question of a few years to close them.

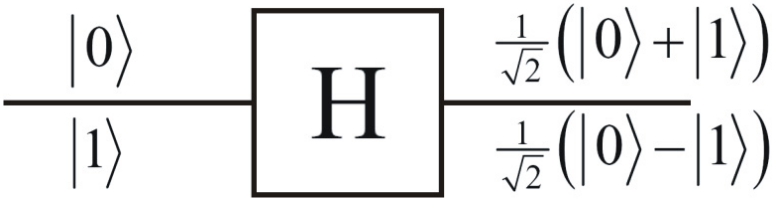

Figure 2.2: *Hadamard gate. The unitary single-qubit gate transforms states from the computational basis to the diagonal basis.*

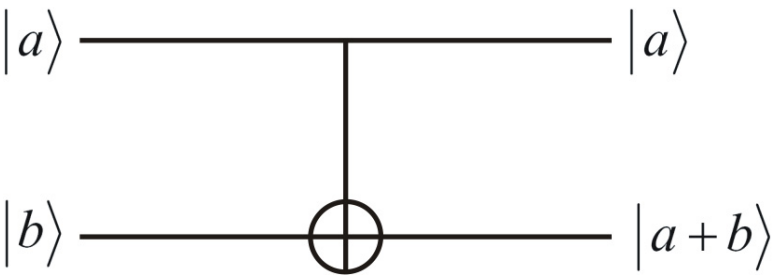

Figure 2.3: *Controlled-NOT (C-NOT) gate. The unitary two-qubit gate flips the second qubit (target) under the condition that the first qubit (control) is a* $|1\rangle$.

Note that despite the violation of realism and locality, quantum entanglement can not be used to contradict special relativity. Since Bob does not know anything about Alice's measurement, super-luminal information transfer is not possible.

Preparation of Bell-States

In many QIP protocols particle pairs in one of the four Bell states are used as an entanglement resource or projective measurements onto the Bell basis are performed to entangle other particles.

Since the properties of the individual qubits are completely undefined, the Bell states are *maximally* entangled. It is therefore not straight forward to prepare or to identify them. A simple quantum circuit consisting of *Hadamard* and *controlled-NOT* gates is needed for this task. The action of a *Hadamard* gate (Fig. 2.2) is equivalent to the following unitary transformation:

$$\begin{aligned} |0\rangle &\rightarrow \frac{1}{\sqrt{2}}(|0\rangle + |1\rangle) \\ |1\rangle &\rightarrow \frac{1}{\sqrt{2}}(|0\rangle - |1\rangle) \end{aligned} \tag{2.6}$$

The *controlled-NOT (C-NOT)* gate (Fig. 2.3) flips the second of two qubits if and

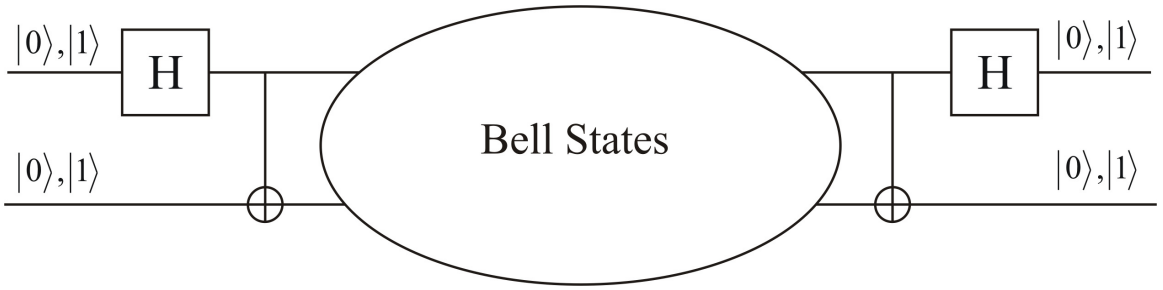

Figure 2.4: *Quantum circuit for generation and detection of Bell states. The inputs and outputs are two qubits in the computational basis, respectively.*

only if the first is $|1\rangle$, namely

$$\begin{aligned} |0\rangle|0\rangle &\rightarrow |0\rangle|0\rangle \\ |0\rangle|1\rangle &\rightarrow |0\rangle|1\rangle \\ |1\rangle|0\rangle &\rightarrow |1\rangle|1\rangle \\ |1\rangle|1\rangle &\rightarrow |1\rangle|0\rangle. \end{aligned} \tag{2.7}$$

Now consider the network shown in Fig. (2.4). Under the action of the gates on the left-hand side of the network, the input two-qubit states will undergo a series of unitary transformations. For example, after passing through the two gates the input state $|0\rangle|0\rangle$, will be transformed into:

$$\begin{aligned} |0\rangle|0\rangle \quad &\overset{Hadmard}{- - - \longrightarrow} \quad \tfrac{1}{\sqrt{2}}\left(|0\rangle|0\rangle + |1\rangle|0\rangle\right) \\ &\overset{C-NOT}{- - - \longrightarrow} \quad \tfrac{1}{\sqrt{2}}\left(|0\rangle|0\rangle| + |1\rangle|1\rangle\right) \quad = \quad |\Phi^+\rangle \end{aligned} \tag{2.8}$$

We have thus been able to create one of the four Bell states. Correspondingly, the network can prepare the two qubits in one of the remaining three Bell states:

$$\begin{aligned} |1\rangle|0\rangle &\longrightarrow \frac{1}{\sqrt{2}}\left(|0\rangle|0\rangle| - |1\rangle|1\rangle\right) = \left|\Phi^-\right\rangle \\ |0\rangle|1\rangle &\longrightarrow \frac{1}{\sqrt{2}}\left(|0\rangle|1\rangle| + |1\rangle|0\rangle\right) = \left|\Psi^+\right\rangle \\ |1\rangle|1\rangle &\longrightarrow \frac{1}{\sqrt{2}}\left(|0\rangle|1\rangle| - |1\rangle|0\rangle\right) = \left|\Psi^-\right\rangle \end{aligned} \tag{2.9}$$

The right-hand side of the network reverses the action of Eq. (2.8) and Eq. (2.9) and can be used to implement the so-called *Bell State Measurement* (BSM) on the two qubits by disentangling the Bell states. In this way, the BSM is reduced to two single-qubit measurements.

Finally, we would like to emphasize that, in general, any measurement on any number of qubits can be implemented using only single-qubit operations and the quantum C-NOT gates.

This follows from the fact that the quantum C-NOT gate, together with simple single-qubit operations, forms an adequate set of quantum gates, i.e. the set from which any unitary operation may be built [38, 39]. Thus, if we want to measure observable A pertaining to n qubits, we could construct a compensating unitary transformation U that maps 2^n states of the form $|a_1\rangle|a_2\rangle...|a_n\rangle$ (where $a_i = 0, 1$) into the eigenstates of A. This allows both to prepare the eigenstates of A, which in general can be highly entangled, and to reduce the measurement described by A to n simple, single-qubit measurements.

2.1.3 Quantum Teleportation

There are several fundamental concepts, procedures and algorithms that constitute the frame of QIP. Quantum teleportation - the transfer of a quantum state between two distant locations - is certainly one of those cornerstones of QIP. It is central to a number of QIP protocols [23, 40, 29, 41]. Since it lays at the heart of the work performed within the framework of this thesis, we will give a detailed introduction and description of this concept. Furthermore, it serves as an example for the application of a bipartite entangled state and demonstrates a fascinating feature of quantum entanglement.

Humanity has always dreamed to be able to travel by simply disappearing and then reappearing at some distant location. An object to be transferred or *teleported* can be fully characterized by its properties, which in classical physics can be determined by measurement. To create a copy of that object at a distant location one does not need the original parts and pieces; all that is needed is to send the scanned information so that it can be used for reconstructing the object. But how precisely can this be a indistinguishable copy of the original? What if the parts and pieces are electrons, atoms and molecules? What happens to their individual quantum properties, which according to Heisenberg's uncertainty principle cannot be measured with arbitrary precision?

Bennett et al. [35] have suggested that it is possible to transfer the quantum state of a particle onto another particle - the process of quantum teleportation - provided one does not get any information about the state in the course of this transformation. This requirement can be fulfilled by using quantum entanglement.

The possibility of transferring quantum information is one of the keystones of the emerging field of QIP [13]. As we will see below and in the following chapters, quantum teleportation is indeed not only a critical component of quantum computation and communication, its experimental realization also allows new studies of the fundamentals of quantum theory.

To make the problem of transferring quantum information clearer, suppose that

Alice has some particle in a certain quantum state $|\Psi\rangle$ and she wants Bob, at a distant location, to have a particle in that same state. There is certainly the possibility to send Bob the particle directly. But suppose that the communication channel between Alice and Bob is not good enough at the time of the procedure to preserve the necessary quantum coherence or suppose that this would take too much time, which could easily be the case if $|\Psi\rangle$ is the state of a more complicated or massive object. Then, what strategy can Alice and Bob pursue?

As mentioned above, no measurement that Alice can perform on $|\Psi\rangle$ will be sufficient for Bob to reconstruct the state because the state of a quantum system cannot be fully determined by measurements. Quantum systems are so evasive since they can be in a superposition of several states at the same time. A measurement on the quantum system will force it into only one of these states. Similar to the scenario of Alice and Bob in the above section, we can illustrate this important quantum feature by taking a single photon, which can be horizontally or vertically polarized, indicated by the states $|H\rangle$ and $|V\rangle$. It can even be polarized in the general superposition of these two states

$$|\Psi\rangle = \alpha|H\rangle + \beta|V\rangle \tag{2.10}$$

were again α and β are two complex numbers satisfying $|\alpha|^2+|\beta|^2 = 1$ as in Eq. (2.1).

If a photon in the state $|\Psi\rangle$ passes through a polarizing beam splitter (PBS), a device that transmits (reflects) horizontally (vertically) polarized photons (Fig. 2.9), it will be found in the transmitted (reflected) beam with probability $|\alpha|^2$ ($|\beta|^2$). Then the general state $|\Psi\rangle$ has been projected either onto $|H\rangle$ or onto $|V\rangle$ by the action of the measurement. We conclude that the rules of quantum mechanics, in particular the projection postulate, make it impossible for Alice to perform a measurement on $|\Psi\rangle$ by which she would obtain all the information necessary to reconstruct the state.

Theory of Quantum Teleportation

Although the projection postulate in quantum mechanics seems to bring Alice's attempts to provide Bob with the state $|\Psi\rangle$ to a halt, it was realized by Bennett et al. [35] that precisely this projection postulate enables teleportation of $|\Psi\rangle$ from Alice to Bob. During the teleportation Alice will destroy the quantum state at hand while Bob receives the quantum state, with neither Alice nor Bob obtaining information about the state $|\Psi\rangle$. A key role in the teleportation scheme is played by an entangled ancillary pair of particles, which is initially shared by Alice and Bob.

Suppose particle 1, which Alice wants to teleport, is in the initial state ($|\Psi\rangle_1 = \alpha\,|0\rangle_1 + \beta\,|1\rangle_1$) (Fig. 2.5). The ancillary pair of particles 2 and 3 shared by Alice and Bob is in a maximally entangled Bell state:

$$\left|\Phi^+\right\rangle_{23} = \frac{1}{\sqrt{2}}(|0\rangle_2\,|0\rangle_3 + |1\rangle_2\,|1\rangle_3). \tag{2.11}$$

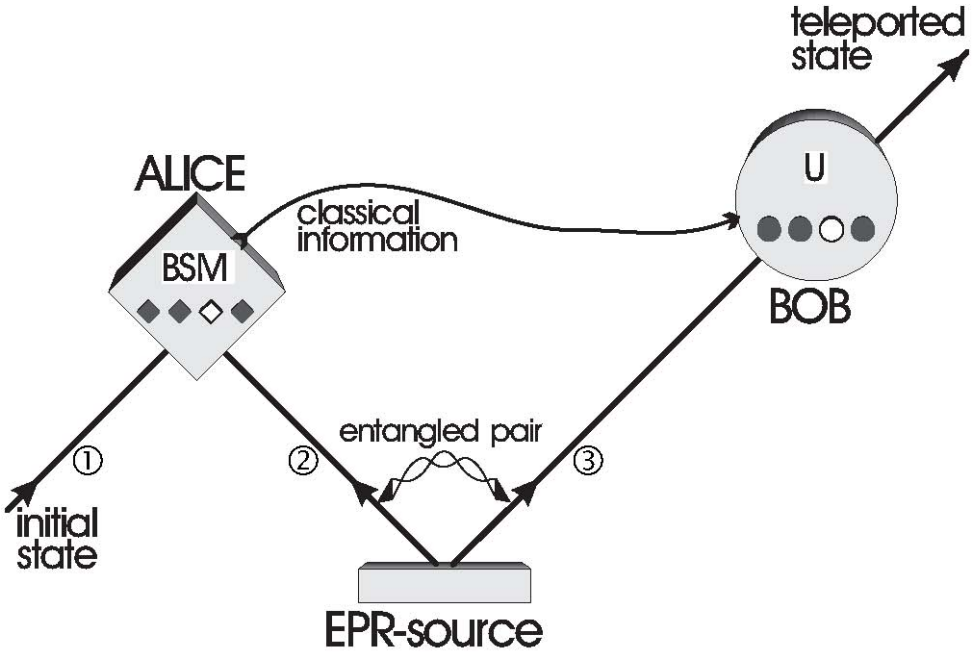

Figure 2.5: *Scheme showing the principle of quantum teleportation. Alice has a quantum system, particle 1, in an initial state, which she wants to teleport to Bob. Alice and Bob also share an ancillary entangled pair of particles 2 and 3 emitted by an Einstein-Podolsky-Rosen (EPR) source. Alice then performs a joint Bell-state measurement (BSM) on the initial particle and one of the ancillaries, projecting them also onto an entangled state. After she has sent the result of her measurement as classical information to Bob, he can perform a unitary transformation (U) on the other ancillary particle resulting in it being in the state of the original particle.*

This entangled pair, emitted by an *EPR source*, is a single quantum system in an equal superposition of the states $|0\rangle_2|0\rangle_3$ and $|1\rangle_2|1\rangle_3$. As described in the above section, the entangled state contains no information on the individual particles; it only indicates that the two particles will be in opposite states. As a tribute to Einstein, Podolsky and Rosen, these pairs are often called *EPR pairs*.

The scheme of quantum teleportation works as follows. Alice starts with 'her' particle 1, initially in the state $|\Psi\rangle_1$, and the ancillary particle 2, which is entangled with the other ancillary particle 3 in the hands of Bob. Although this establishes the possibility of nonclassical correlations between Alice and Bob, the entangled pair at this stage contains no information about $|\Psi\rangle_1$. Indeed the entire system, comprising Alice's unknown particle 1 and the entangled pair is in a pure product state, $|\Psi\rangle_1 |\Phi^+\rangle_{23}$, involving neither classical correlation nor quantum entanglement between the unknown particle and the entangled pair. Therefore no measurement on either member of the entangled pair, or both together, can yield any information about $|\Psi\rangle_1$.

The essential point to achieve teleportation is to perform a joint BSM on particles 1 and 2 which projects them onto one of the four Bell states of Eq's. (2.3). The complete state of the three particles before Alice's measurement is

$$\begin{aligned} |\Psi\rangle_{123} \;=\; |\Psi\rangle_1|\Phi^+\rangle_{23} \;=\; & \tfrac{\alpha}{\sqrt{2}}\left(|0\rangle_1|0\rangle_2|0\rangle_3 + |0\rangle_1|1\rangle_2|1\rangle_3\right) \\ + \; & \tfrac{\beta}{\sqrt{2}}\left(|1\rangle_1|0\rangle_2|0\rangle_3 + |1\rangle_1|1\rangle_2|1\rangle_3\right). \end{aligned} \tag{2.12}$$

In the above equation particles 1 and 2 are represented in the computational basis. However, we can express the combined state in the Bell basis and can thus rewrite Eq. (2.12) as:

$$\begin{aligned} |\Psi\rangle_{123} \;=\; & \tfrac{1}{2}|\Phi^+\rangle_{12}\left(\alpha|0\rangle_3 + \beta|1\rangle_3\right) \\ & + \tfrac{1}{2}|\Phi^-\rangle_{12}\left(\alpha|0\rangle_3 - \beta|1\rangle_3\right) \\ & + \tfrac{1}{2}|\Psi^+\rangle_{12}\left(\alpha|1\rangle_3 + \beta|0\rangle_3\right) \\ & + \tfrac{1}{2}|\Psi^-\rangle_{12}\left(\alpha|1\rangle_3 - \beta|0\rangle_3\right) \end{aligned} \tag{2.13}$$

Note that particle 1 is still completely separable from particles 2 and 3, since the state in Eq. (2.13) is still the same as in Eq. (2.12), just in a different notation.

However, Eq. (2.13) implies that, regardless of the unknown state $|\Psi\rangle_1$, the four BSM outcomes are equally likely, each occurring with probability 1/4. Quantum physics predicts that once particles 1 and 2 are projected into one of the four entangled states, particle 3 is instantaneously projected into one of the four pure states superposed in Eq. (2.13). Denoting $|0\rangle_3$ by the vector $\begin{pmatrix} 1 \\ 0 \end{pmatrix}$ and $|1\rangle_3$ by $\begin{pmatrix} 0 \\ 1 \end{pmatrix}$,

they are thus, respectively,

$$\begin{array}{cc} \begin{pmatrix} 1 & 0 \\ 0 & 1 \end{pmatrix} \left(\alpha \begin{pmatrix} 1 \\ 0 \end{pmatrix} + \beta \begin{pmatrix} 0 \\ 1 \end{pmatrix} \right), & \begin{pmatrix} 1 & 0 \\ 0 & -1 \end{pmatrix} \left(\alpha \begin{pmatrix} 1 \\ 0 \end{pmatrix} + \beta \begin{pmatrix} 0 \\ 1 \end{pmatrix} \right), \\ \begin{pmatrix} 0 & 1 \\ 1 & 0 \end{pmatrix} \left(\alpha \begin{pmatrix} 1 \\ 0 \end{pmatrix} + \beta \begin{pmatrix} 0 \\ 1 \end{pmatrix} \right), & \begin{pmatrix} 0 & -1 \\ 1 & 0 \end{pmatrix} \left(\alpha \begin{pmatrix} 1 \\ 0 \end{pmatrix} + \beta \begin{pmatrix} 0 \\ 1 \end{pmatrix} \right). \end{array} \tag{2.14}$$

with the identity operator and the well known Pauli matrices $(\hat{I}, \hat{\sigma}_x, \hat{\sigma}_y, \hat{\sigma}_z)$, this can be expressed as:

$$\begin{array}{cc} \hat{I} \left|\Psi\right\rangle_3, & \hat{\sigma}_z \left|\Psi\right\rangle_3, \\ \hat{\sigma}_x \left|\Psi\right\rangle_3, & i\hat{\sigma}_y \left|\Psi\right\rangle_3 \end{array} \tag{2.15}$$

where $\left|\Psi\right\rangle_3 = \alpha \left|0\right\rangle_3 + \beta \left|1\right\rangle_3$. Each of these possible resultant states for Bob's EPR particle 3 is related in a simple way to the original state $\left|\Psi\right\rangle_1$ which Alice sought to teleport. In the case of the first outcome ($\left|\Phi^+\right\rangle$) the state of particle 3 is the same as the initial state of particle 1, so Bob needs do nothing further to produce a replica of Alice's unknown state. In the other three cases, Bob could accordingly apply one of the unitary Pauli transformations in Eq. (2.15) to convert the state of particle 3 into the original state of particle 1, after receiving via a classical communication channel the information which one of the four BSM results was obtained by Alice. After Bob's unitary operation, the final state of particle 3 is therefore

$$\left|\Psi\right\rangle_3 = \alpha \left|0\right\rangle_3 + \beta \left|1\right\rangle_3 . \tag{2.16}$$

Note that during the BSM particle 1 loses its identity because it becomes entangled with particle 2. Therefore the state $\left|\Psi\right\rangle_1$ is destroyed on Alice's side during teleportation.

The result in Eq. (2.16) deserves some further comments. The transfer of quantum information from particle 1 to particle 3 can happen over arbitrary distances, hence the name teleportation. Experimentally, quantum entanglement has been shown to survive over a distance of 144 km [19]. We note that in the teleportation scheme it is not necessary for Alice to know where Bob is. Furthermore, the initial state of particle 1 can be completely unknown not only to Alice but to anyone. It could even be quantum mechanically completely undefined at the time the Bell-state measurement takes place. This is the case when, as already remarked by Bennett et al. [35], particle 1 itself is a member of an entangled pair and therefore has no well-defined properties on its own. This ultimately leads to entanglement swapping [42, 43] and the teleportation of composite systems, which will be discussed in more detail in chapters 3 to 5.

It is also important to notice that the BSM does not reveal any information on the properties of any of the particles. This is the very reason why quantum teleportation using coherent two-particle superpositions works, while any measurement on one-particle superpositions would fail. The fact that no information whatsoever on

either particle is gained is also the reason why quantum teleportation escapes the verdict of the no-cloning theorem [44]. After successful teleportation particle 1 is not available in its original state anymore, and therefore particle 3 is not a clone but really the result of teleportation.

2.2 Multipartite Entanglement

Multipartite entanglement is genuinely different from entanglement in quantum systems consisting of two parts. The prefix *multi* may in general refer to quantum systems composed of a macroscopic number of subsystems, such as the parts of an interacting many-body system, or it may merely mean *three*. In contrast to bipartite systems, multipartite systems may contain different types of entanglement. To illustrate this difference, let us consider a quantum system that is composed of several qubits. Each of the qubits is thought to be held by a separated party, respectively. It may come as quite a surprise that depending on the type of entanglement between the qubits, a single party may or may not be able to destroy the entanglement of the entire system with a single measurement. The different kinds of entanglement may differ for various characteristics such as robustness against de-coherence, connectivity or violation of classical physics.

Tests of quantum mechanics that are conceptually different from standard bipartite Bell tests become possible with multipartite entanglement. For example *all-versus-nothing* tests with tripartite systems do not violate any inequalities but yield expectation values that are genuinely different for quantum and classical physics [45, 46]. In the experiment several different settings are measured, where each outcome is either a 1 or -1. The expectation value for the product of these measurements by classical physics is 1, whereas quantum mechanics predicts a -1, the exact opposite.

Besides the interest in fundamental physics, multipartite entanglement attracts a lot of research as it is the most important resource for many quantum computation algorithms and protocols such as the Deutsch-Jozsa algorithm [22], Grover's search algorithm for unsorted databases [20], the quantum fourier transform and closely connected Shor's algorithm for factoring large numbers [21].

2.2.1 Classes of Multipartite Entangled States

The complexity of a physical system grows exponentially with the number of its dimensions or degrees of freedom. A multipartite system can be any in between highly entangled and fully separable. However, many multipartite entangled states feature almost exactly the same characteristics and as a matter of fact can be categorized to posses the same *class of entanglement*.

To see this, let us consider a pair of qubits, shared by Alice and Bob, which is in

one of the four Bell states of Eq. (2.3):

$$\left|\Phi^{\pm}\right\rangle = \frac{1}{\sqrt{2}}(|0\rangle|0\rangle \pm |1\rangle|1\rangle)$$
$$\left|\Psi^{\pm}\right\rangle = \frac{1}{\sqrt{2}}(|0\rangle|1\rangle \pm |1\rangle|0\rangle)$$

Either one of Alice and Bob can change the combined state from one Bell state to another. If, for example, Alice wants to change the state from $|\Phi^+\rangle$ to $|\Phi^-\rangle$, all she needs to do, is to apply a unitary $\hat{\sigma}_z$ Pauli operation to her qubit. Likewise, she can transform the state into the other two Bell states by applying a $\hat{\sigma}_x$ or $\hat{\sigma}_y$ operation, respectively. Alice can transform the combined system to another Bell state without any help or even knowledge of Bob, just by local (only at her side) unitary operations (LU). The Bell states are thus equivalent under LU.

Consider now a more general case:

$$|\Psi\rangle = \sin\vartheta|0\rangle_1|0\rangle_2 + \cos\vartheta|1\rangle_1|1\rangle_2 \tag{2.17}$$

Here ϑ is a free variable that parameterizes the degree of entanglement in the two-qubit system. For the general case we are not able to transform $|\Psi\rangle$ into a maximally entangled Bell state with the help of LU. However, if we have many copies of $|\Psi\rangle$, we are able to distill a smaller number of copies of maximally entangled states by entanglement purification [47, 48, 49]. This means that two distant parties can generate any bipartite entangled state form another one only by local operations assisted with classical communication (LOCC). All bipartite entangled states are thus equivalent - are in the same class of entanglement - under LOCC.

The smallest number of dimensions for a physical system to feature more than one class of entanglement is three [50]. Any genuinely tripartite entangled state can be converted, by means of LOCC, into one of two standard forms, namely either a so called *Greenberger-Horn-Zeilinger* (GHZ) state [45]

$$|GHZ\rangle = \frac{1}{\sqrt{2}}(|0\rangle_1|0\rangle_2|0\rangle_3 + |1\rangle_1|1\rangle_2|1\rangle_3) \tag{2.18}$$

or else a second (W) state

$$|W\rangle = \frac{1}{\sqrt{3}}(|0\rangle_1|0\rangle_2|1\rangle_3 + |0\rangle_1|1\rangle_2|0\rangle_3) + |1\rangle_1|0\rangle_2|0\rangle_3). \tag{2.19}$$

If a state $|\Psi\rangle$ can be converted into the state $|GHZ\rangle$ of Eq. (2.18) under LOCC and another state $|\Phi\rangle$ can be converted into the state $|W\rangle$ of Eq. (2.19), then it is not possible to transform, even with only a very small probability of success, $|\Psi\rangle$ into $|\Phi\rangle$ nor the other way round. There are thus two classes of entanglement for genuinely tripartite entangled states. Note, that there are more classes of entanglement for tripartite systems, namely states that contain only bipartite entanglement and are otherwise separable such as

$$|\varphi\rangle = \frac{1}{\sqrt{2}}|0\rangle_1(|0\rangle_2|0\rangle_3 + |1\rangle_2|1\rangle_3) \tag{2.20}$$

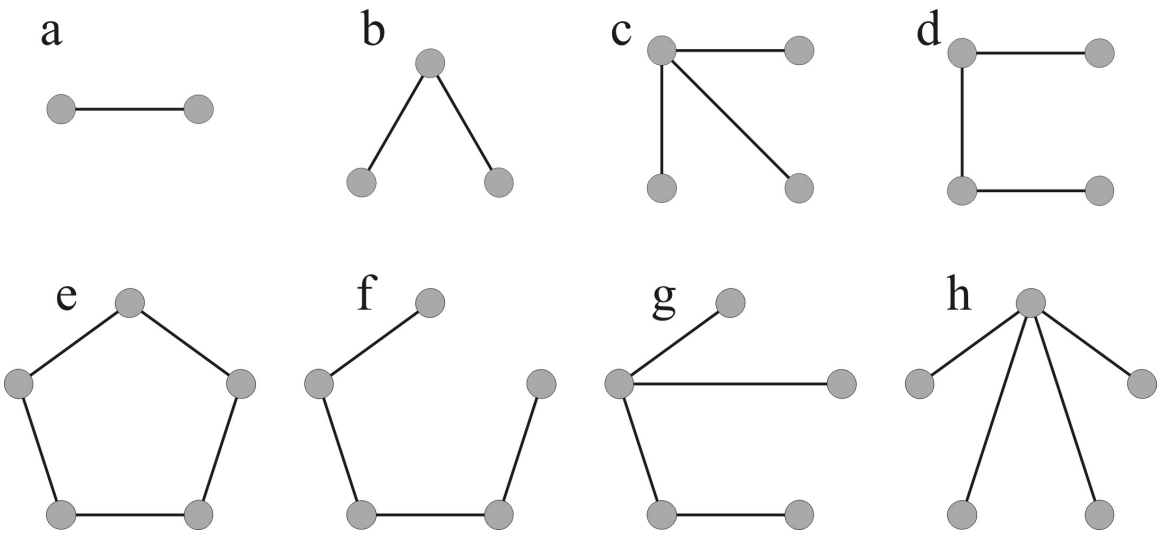

Figure 2.6: *Graphs representing multipartite states - graph states. Each vertex corresponds to a qubit prepared in the state $|+\rangle$ and each edge represents a C-phase gate having been applied between the two connected qubits. The list shows all connected graphs with up to five vertices that are not equivalent under LU transformations.*

where particles 2 and 3 are entangled, but completely separable from particle 1. A n-partite pure state $|\Psi\rangle$ is called *biseparable*, whenever a grouping of the n particles into two groups G_A and G_B can be found, such that the resulting state is a product state, as in Eq. (2.20), otherwise it is a genuine multipartite entangled state.

The *GHZ-class* and *W-class* states feature fundamentally different behaviors. On the one hand, states of the GHZ-class can demonstrate much stronger violations of locality and realism than states of the W-class [51]. On the other hand, the W-class is much more robust against de-coherence and the loss of a qubit. If in a three-qubit system prepared in a W (GHZ) state one of the qubits is traced out then the remaining two qubits are entangled (completely unentangled). Indeed, from a single copy of the reduced density matrix for any two qubits belonging to a state form the W-class, one can always obtain a state which is arbitrarily close to a Bell state by means of a filtering measurement [52]. This means that, if one of the parties sharing the system prepared in a W (GHZ) state decides not to cooperate with the other two, or if for some reason the information about one of the qubits is lost, then the remaining two parties still can (cannot) use entanglement resources to perform communication tasks.

Graph-States

The number of entanglement classes that are equivalent under LOCC increases for higher dimensions. It is quite difficult to characterize them or to even find the exact

number of classes for a given dimension. However, groups of entanglement classes exist that reoccur in all systems regardless of the dimensions. In recent years, a special group of states has become the center of attention. They are commonly known as *graph-states*, since many entanglement properties of graph states are closely related to their graphic representations [53, 54, 55].

Graph-states can be associated with graphs of vertices and edges. Each vertex represents a qubit prepared in the state

$$|+\rangle = \frac{1}{\sqrt{2}}(|0\rangle + |1\rangle) \tag{2.21}$$

and each edge represents a *controlled-phase* (C-phase) gate having been applied between the two connected qubits. A C-phase gate flips the sign of the state if and only if both qubits are $|1\rangle$, namely:

$$\begin{array}{rcl} |0\rangle|0\rangle & \rightarrow & |0\rangle|0\rangle \\ |0\rangle|1\rangle & \rightarrow & |0\rangle|1\rangle \\ |1\rangle|0\rangle & \rightarrow & |1\rangle|0\rangle \\ |1\rangle|1\rangle & \rightarrow & -|1\rangle|1\rangle \end{array} \tag{2.22}$$

and thus entangles two qubits initially prepared in the state $|+\rangle$ of Eq. (2.21).

For a given number of dimensions there exists a finite (large) number of possibilities for different graph states. However, two different graphs may correspond to states that are equivalent under LOCC. We will demonstrate such a case in the next section. Fig. (2.6) shows all connected graphs with up to five vertices that are not equivalent under LU transformations.

Fig. (2.6b) is the graphic representation of the GHZ state of Eq. (2.18). Let us now define a generalization of the GHZ state for n dimensions [56] as

$$|GHZ_n\rangle = \frac{1}{\sqrt{2}}(|a_1\rangle_1|a_2\rangle_2...|a_n\rangle_n + |\bar{a}_1\rangle_1|\bar{a}_2\rangle_2...|\bar{a}_n\rangle_n) \tag{2.23}$$

with $a_i = [0, 1]$ and $\bar{a}_i = NOT(a_i)$. Such a GHZ state can always be associated with a star graph. For example, four and five qubit GHZ states are represented by Fig. (2.6c) and Fig. (2.6h), respectively.

Besides the thought-provoking theoretical structure of graph states, they have also provided new insights into studies of non-locality [57, 58, 10, 59] and decoherence [60]. Most of all, a subclass of graph states known as *cluster states* can serve as an essential resource for various quantum information tasks [55], most prominently as the exceptionally universal resource for one-way quantum computation [61], which we will discuss in the following section.

2.2.2 One-Way Quantum Computation

The promise that quantum computers can dramatically outperform their classical counterparts for some computational tasks has initiated a lot of effort to implement

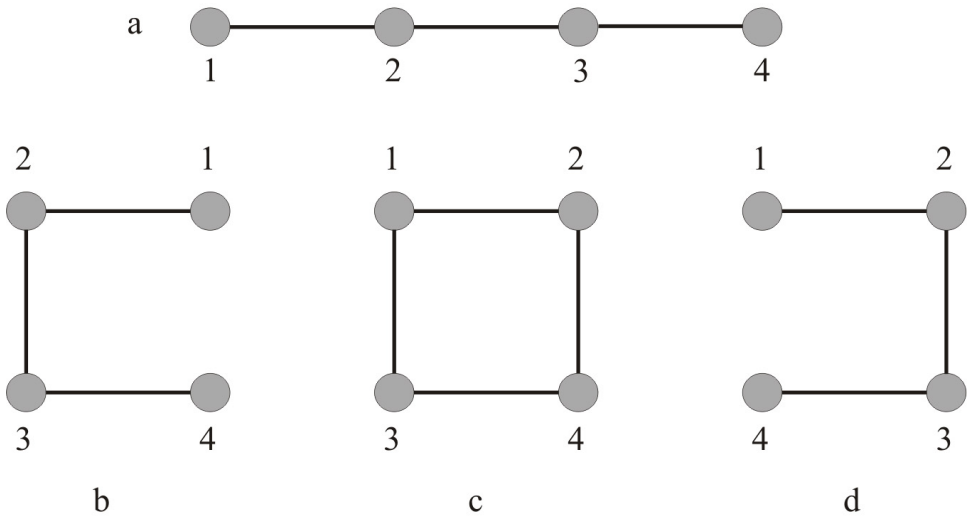

Figure 2.7: *Four-qubit cluster states. Cluster states are graph states represented by a one or two-dimensional quadratic lattice, where the entangling connection, represented by an edge between two vertices, can only be applied between two neighboring qubits. Although all four cluster states are equivalent under LU transformations, they correspond each to a different quantum circuit and thus a different quantum algorithm.* ***a)*** *linear cluster* ***b)*** *horseshoe cluster* ***c)*** *box cluster* ***d)*** *horseshoe cluster (rotated by* 180°*)*

quantum computers. The first theoretical schemes based on the idea to process physical qubits by performing quantum logic gates on them and to subsequently measure the output. However, the realization of two-qubit gates (or higher number of qubits) has proven to be quite difficult in the experiment. They can be achieved for example with optical elements and/or ancilla particles via projective measurements. But the intrinsic randomness of these measurements only allows for probabilistic gate operations, i.e. the gate operations are successful only in a small fraction of the time. The other times the outcomes need to be discarded. Although the gate success probability increases with additional resources, such schemes achieve nearly deterministic gate operations only in the asymptotic regime of infinite resources, which is experimentally infeasible.

The one-way quantum computation model [61, 62] is an exciting alternative approach to the original proposals and allows the resource for the quantum computation to be prepared *off-line* prior to any logical operations. The computational resource is a highly entangled *cluster state* mentioned in the above section. Once the cluster state is prepared, the computation proceeds deterministically, i.e. every measurement produces a meaningful result, requiring only single qubit measurements and feed-forward of the measurement result. Feed-forward is the essential feature that makes one-way quantum computation deterministic and can be seen as an active correction of errors introduced by the randomness of measurement outcomes.

A cluster state, the computational resource, is a graph state represented by a one or two-dimensional quadratic lattice, where the entangling connection, represented by an edge between two vertices, can only be applied between two neighboring qubits (Fig. 2.7). It constitutes a universal state for quantum computing, meaning that any quantum logic operation can be carried out on a sufficiently large and appropriately structured cluster state. Moreover the entanglement of cluster state has been shown to be robust against de-coherence [63] and persistent against loss of qubits [54]. Recent experiments succeeded in creating cluster states with various methods [64, 59, 65, 66].

Single qubit measurements are essential in cluster state quantum computing. The shape of the cluster state and the nature of these measurements, i.e. the order of measurements and the individual measurement bases are determined by the desired algorithm. The four-qubit cluster states corresponding to the graphs of Fig. (2.7) are all equivalent under LU transformations, e.g. the box cluster **(c)** can be obtained from the line cluster **(a)** by Hadamard rotations and by swapping (relabeling) qubits 2 and 3. However, with the convention that measurements are performed in the order form left to right right all four cases correspond to different quantum circuits, respectively.

The input state $|\psi_{in}\rangle$ is always initialized as $|+\rangle$. It is important to note that the entire information of the input state is initially stored in the multi-particle correlations of the cluster, with the individual physical qubits being completely undefined and therefore not carrying any information about the input state. The cluster state is thus a maximally entangled state, simple examples are the 2-qubit Bell states (Eq. 2.3) and 3-qubit GHZ states (Eq. 2.18). Single qubit measurements on the cluster processes the encoded input from one qubit to another analogous to remote state preparation. In principle, two basic types of single-particle measurements suffice to operate the one-way quantum computer. Measurements in the computational basis ($|0\rangle_j/|1\rangle_j$) have the effect of disentangling, i.e. removing the physical qubit j from the cluster. This leaves a smaller cluster state and thus gives the ability to shape the cluster to the specific algorithm. The measurements which perform the actual QIP are made in the basis $B(\alpha) = \{|\alpha_+\rangle, |\alpha_-\rangle\}$, where

$$|\alpha_\pm\rangle = \frac{1}{\sqrt{2}}(|0\rangle \pm e^{-i\alpha}|1\rangle) \tag{2.24}$$

and α can be any real number between 0 and 2π. We will give a detailed discussion on single-qubit gate operations, i.e. measurements on linear cluster states such as in Fig. (2.7a) and then proceed to a simple two-qubit gate (Fig. 2.7b). The argument can be generalized to an entire quantum algorithm in a straight-forward manner [64].

The choice of measurement basis determines the single-qubit rotation, $\hat{R}_z(\alpha) = \exp(-i\alpha\hat{\sigma}_z/2)$, followed by a Hadamard operation $\hat{H}$, on the input state.

$$\hat{H}\hat{R}_z(\alpha)|\psi_{in}\rangle \quad \Rightarrow \quad |\psi_{in}\rangle \text{ ——} \boxed{\hat{R}_z^{(\alpha)}} \text{—} \boxed{H} \text{—} |\psi_{out}\rangle \tag{2.25}$$

The order and choices of these measurements determine the unitary gates that are implemented and therefore the algorithm that is computed. Remember that input states are by construction always $|\psi_{in}\rangle = |+\rangle$ unless the cluster is part of a larger cluster state. Rotations around the z-axis can be implemented through the identity $\hat{H}\hat{R}_z(\alpha)\hat{H} = \hat{R}_x(\alpha)$ so that two consecutive measurements on a linear 3-qubit cluster can rotate the input state to any arbitrary output state on the Bloch sphere (Fig. 2.1):

$$\begin{aligned} &\hat{H}\hat{R}_z(\beta)\hat{H}\hat{R}_z(\alpha)|\psi_{in}\rangle = \hat{R}_x(\beta)\hat{R}_z(\alpha)|\psi_{in}\rangle \\ \Rightarrow \quad &|\psi_{in}\rangle \text{ —} \boxed{\hat{R}_z^{(\alpha)}} \text{—} \boxed{\hat{R}_x^{(\beta)}} \text{—} |\psi_{out}\rangle \end{aligned} \tag{2.26}$$

Up until now, we have not incorporated the actual measurement result in our analysis. Eq. (2.25) only holds if the outcome of the measurement s yields $|\alpha_+\rangle$. We denote this case as $s = 0$ and the other case of $|\alpha_-\rangle$ as $s = 1$. Due to the intrinsic randomness of the quantum measurement, it happens with equal probability that the measurement yields the result $s = 1$. In that case, a Pauli-error ($\hat{\sigma}_x = $ —$\boxed{X}$—) is introduced in the computation, so that the single measurement in basis $B_j(\alpha)$ rotates the qubit to:

$$\hat{\sigma}_x\hat{H}\hat{R}_z(\alpha)|\psi_{in}\rangle \quad \Rightarrow \quad |\psi_{in}\rangle \text{ —} \boxed{\hat{R}_z^{(\alpha)}} \text{—} \boxed{H} \text{—} \boxed{X} \text{—} |\psi_{out}\rangle \tag{2.27}$$

Obviously, by adapting the measurement bases of subsequent measurements, these errors can be eliminated. In the following, let us consider the general case of Eq. (2.26) by taking into account the feed-forward rules. If we thus choose consecutive measurements in bases $B_1(\alpha)$ and $B_2(\beta)$ on the physical qubits 1 and 2 of our 3-qubit cluster, then we rotate the encoded input qubit $|\psi_{in}\rangle$ to the output state

$$|\psi_{out}\rangle = \hat{\sigma}_x^{s_2}\hat{H}\hat{R}_z((-1)^{s_1}\beta)\hat{\sigma}_x^{s_1}\hat{H}\hat{R}_z(\alpha)|\psi_{in}\rangle = \hat{\sigma}_x^{s_2}\hat{\sigma}_z^{s_1}\hat{R}_x((-1)^{s_1}\beta)\hat{R}_z(\alpha)|\psi_{in}\rangle \tag{2.28}$$

which is stored on qubit 3. The measurement outcome, $s_i = \{0, 1\}$, on the physical qubit i determines the measurement basis for the succeeding qubit and indicates any introduced Pauli errors that have to be compensated for. This idea can schematically be depicted as a circuit diagram:

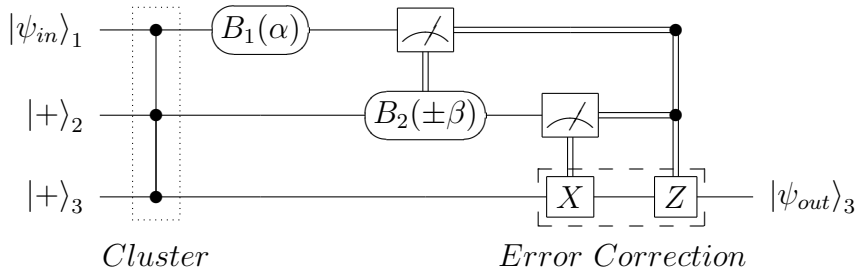

(2.29)

Single wires represent quantum channels, while double lines denote classical communication. The circles in front of the measurement meters show the measurement basis. No error correction is required for the specific case where the outcomes of the first

and second qubit are $s_1 = s_2 = 0$ and hence, as expected, $|\psi_{out}\rangle = \hat{R}_x(\beta)\hat{R}_z(\alpha)|\psi_{in}\rangle$. However, if the outcome of the first qubit is $s_1 = 1$ ($s_2 = 0$) the measurement basis for the second qubit has to be changed from $B_2(\beta)$ to $B_2(-\beta)$ and finalized by a Pauli error correction, i.e. $\hat{\sigma}_z$ on the third (output) qubit, to get the desired output of the computation. This yields $|\psi_{out}\rangle = \hat{\sigma}_z\hat{R}_x(-\beta)\hat{R}_z(\alpha)|\psi_{in}\rangle$ Similar corrections are required in the cases when the third qubit's outcome is $s_2 = 1$ ($s_1 = 0$) and hence $|\psi_{out}\rangle = \hat{\sigma}_z\hat{R}_x(\beta)\hat{R}_z(\alpha)|\psi_{in}\rangle$. Finally, if a projection onto $|\alpha_-\rangle$ occurs to both qubits, ($s_1 = s_2 = 1$), two Pauli errors, $\hat{\sigma}_z$ and $\hat{\sigma}_x$, have to be compensated for on qubit 3 yielding $|\psi_{out}\rangle = \hat{\sigma}_x\hat{\sigma}_z R_x(-\beta)\hat{R}_z(\alpha)|\psi_{in}\rangle$.

Let us now proceed to a two-qubit gate. For simplicity, we will assume that the outcome of all measurements corresponds to $s = 0$, thus making no compensation necessary. However, the correction rules applied in Eq. (2.28) generalize in a straight forward manner. If we choose to perform measurements on the physical qubits 2 and 3 of a four-qubit linear cluster (Fig. 2.7b) in the basis $B_2(\alpha)$ and $B_3(\beta)$, we effectively implement the following circuit

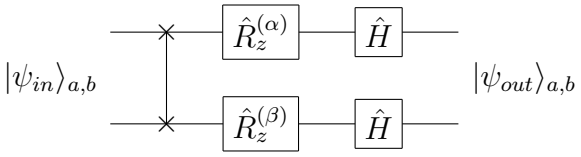

(2.30)

where the connection between logic qubits a and b corresponds to a C-phase gate between them. As mentioned earlier, it is important to understand that the quantum circuit processes the logic qubits a and b, whereas the actual measurements and read out to implement the circuit are performed on the physical qubits 1,2,3 and 4.

The circuit of Eq. (2.30) performs a C-phase gate followed by the usual single qubit rotation and Hadamard gate for both qubits, respectively:

$$|\psi_{out}\rangle_{a,b} = \hat{H}^a\hat{R}_z^a(\alpha)\hat{H}^b\hat{R}_z^b(\beta)\hat{U}^{a,b}_{C-phase}|\psi_{in}\rangle_{a,b} \tag{2.31}$$

For an input state of $|\psi_{in}\rangle_{a,b} = |+\rangle_a|+\rangle_b$ the circuit generates entanglement between logic qubits a and b.

This concludes our brief introduction to one-way quantum computation. The introduced single qubit rotation and the two-qubit C-phase gate are a sufficient basis for universal quantum computation. It is important to understand that we are able to process our quantum circuit and thereby our quantum algorithm deterministically, even though only local measurements and classical feed-forward procedures are employed, which are well within technological reach. The major difficulty is left to produce the highly entangled cluster state. However, since it is prepared before the actual computation, we can generate it off-line, i.e. we can use as many trials as we need to make sure we have succeeded with our task.

Considerable efforts have been stepped towards generating and characterizing cluster states in linear optics [67, 59, 10, 64, 68, 69, 66]. Recently the principal feasibility of the one-way quantum computing model has been experimentally demonstrated through a four-photon cluster state [64, 69, 70].

For the far future one might think of relatively simple quantum computers at many different locations, which can perform the local measurement algorithms. The necessary cluster state resources can then be downloaded from a sophisticated source via a *quantum internet*.

2.2.3 Verification of Multipartite Entanglement

In the above sections, we have discussed several aspects of quantum entanglement and QIP. We have silently assumed that we are able to generate perfectly pure states with certainty. In the experiment, however, this is not the case. We are only able to generate mixed states that resemble the desired pure states up to a certain degree. *Quantum fidelity* is a measure for this purity and is defined as

$$F = Tr[\hat{\rho}|\Psi\rangle\langle\Psi|] \tag{2.32}$$

where $\hat{\rho}$ is the density matrix of the generated mixed state and $|\Psi\rangle$ is the state vector of the desired pure state. The fidelity can take values between 1, the generated state is perfectly equal to the desired state, and 0, the generated state contains no parts of the desired state.

For all procedures in QIP there exists a certain threshold that marks the minimum fidelity for which a task can still be accomplished. It is thus necessary to obtain knowledge of the quality of the generated states. Complete knowledge of the density matrix gives in principle all information about the state of a system. Even though it might still be a extremely difficult theoretical task to determine certain properties from it such as the entanglement of formation [71, 72], the density matrix yields most of the information needed, directly.

If we are able to subsequently produce many identical copies of our state, we can reconstruct every entry of the density matrix $\rho_{i,j} = \langle i|\hat{\rho}|j\rangle$ from the measured expectation values of all pauli matrix combinations $\langle\hat{\sigma}_i^1\hat{\sigma}_i^2\hat{\sigma}_i^3...\hat{\sigma}_i^n\rangle$. Here, i identifies one of the Pauli matrices or the identity $[x, y, z, I]$ and n is the number of qubits in the system. This procedure is known as *quantum state tomography*. By increasing statistics it can be as accurate as desired. However, the number of measurements needed for quantum state tomography grows exponentially with n, which can result in a very long measurement time and is thus unpractical for various experimental applications.

For many experiments, though, it is sufficient to proof the presence of genuine multipartite entanglement. *Quantum witness* is a recently developed approach to proof this presence in a system with only a minimum number of measurements involved [73]. We will try to introduce the basic idea:

A quantum witness of genuine n-partite entanglement is an observable which has a positive expectation value on states with $(n-1)$-partite entanglement and a negative expectation value on some n-partite entangled states. The latter states and their entanglement, respectively, are said to be detected by $\hat{\mathcal{W}}$. Witnesses

provide sufficient criteria for entanglement and for distinguishing the various classes of genuine entangled states.

A witness operator $\hat{\mathcal{W}}$ that detects genuine multipartite entanglement of a pure state $|\Psi\rangle$ (and of states that are close to $|\Psi\rangle$) is given by

$$\hat{\mathcal{W}} = \alpha \hat{\mathrm{I}} - |\Psi\rangle\langle\Psi| \tag{2.33}$$

where $\hat{\mathrm{I}}$ is the identity operator and

$$\alpha = \max_{|\Phi\rangle \epsilon \mathrm{B}} |\langle\Phi|\Psi\rangle|^2 \tag{2.34}$$

with B denoting the set of bi-separable states. This construction guarantees that

$$Tr\left[\hat{\mathcal{W}}\hat{\rho}_B\right] \geq 0 \tag{2.35}$$

for all bi-separable states $\hat{\rho}_B$, and that

$$Tr\left[\hat{\mathcal{W}}|\Psi\rangle\langle\Psi|\right] < 0. \tag{2.36}$$

Thus a negative expectation value of the observable $\hat{\mathcal{W}}$ clearly proofs the presence of multipartite entanglement in the state $|\Psi\rangle$. The determination of α and thus the construction of $\hat{\mathcal{W}}$ can be a difficult task and depends largely on the respective problem. A construction of witnesses to detect six-partite entanglement will be discussed with the experiment introduced in chapter 6.

2.3 Manipulation of Multi-Photon-Entanglement with linear optics

One of the exciting aspects of quantum information science is that there are several candidates of quite different physical systems that can in principle be used to implement QIP and it doesn't look like the race between them will be decided anytime soon. Promising candidates are, but not limited to, ion traps [25], nuclear magnetic resonance [26], quantum dots [27], super-conducting devices (Josephson junction) [28] and photons [29].

We try to implement QIP with photons and linear optics for various reasons such as very strong robustness against de-coherence, extremely fast and accurate implementations of universal single qubit operations and the vast availability of already existing electro-optic devices.

In this section, we will describe the process of spontaneous parametric down-conversion, the source of entangled photons used throughout all experiments of this thesis and will discuss in detail the implementation of a Bell-state analyzer as an example for the application of linear optics.

2.3.1 Spontaneous Parametric Down-Conversion

Remarkable effort has been dedicated to the implementation of single photon sources and subsequent entanglement procedures [74]. However, at the moment the process of spontaneous parametric down-conversion (SPDC) is still the best source for entangled photon pairs. It provides mechanisms where such pairs can be produced with sufficient intensity and in good purity. In SPDC, one uses a non-centrosymmetric crystal with nonlinear electric susceptibility. In such a medium, an incoming photon can decay with relatively small probability into two photons in a way that energy and momentum inside the crystal are conserved.

In the following we will describe a simple technique to produce polarization-entangled photon pairs using the process of non-collinear type-II parametric down-conversion [30]. In the experiment, the desired polarization-entangled state is produced directly out of a single nonlinear crystal [BBO (β-barium-borate)]. In that process, the two photons are emitted with different polarizations (Fig. 2.8). Calculating the emission direction of the photons [75, 30], one notices that photons of each polarization are emitted into one cone in such a way that momenta of two photons always add up to the momentum of the pump photon. Thus, the emission direction of each individual photon is completely uncertain within the cone, but once one photon is registered, and thus its emission direction is defined, the other photon is found just exactly opposite from the pump beam on the other cone. The total quantum mechanical state is therefore extremely rich and is a superposition of all such pairs of emission modes.

The interesting point is now that the crystal can be cut and arranged such that the two cones intersect, as shown in Fig. (2.8). Then, along the lines of intersection, the polarization of neither photon is defined, but what is defined is the fact that the two photons have to have different polarizations. This contains all the necessary features of entanglement in a nutshell. Measurement on each of the photons separately is totally random and gives with equal probability vertical or horizontal polarization. But once one photon, for example photon A, is measured, the polarization of the other photon B is orthogonal! Choosing an appropriate basis, e.g. $|H\rangle$ and $|V\rangle$ (see Eq. 2.10), the state emerging through the two arms A and B is thus a superposition of $|H\rangle|V\rangle$ and $|V\rangle|H\rangle$, say

$$\frac{1}{\sqrt{2}}(|H\rangle_A|V\rangle_B + e^{i\alpha}|V\rangle_A|H\rangle_B) \tag{2.37}$$

where the relative phase α arises from the crystal birefringence, and an overall phase shift is omitted.

Using an additional birefringent phase shifter (or even slightly rotating the down-conversion crystal itself), the value of α can be set as desired, e.g. to the values 0 or π. Somewhat surprisingly, a net phase shift of π may be obtained by a 90° rotation of a quarter wave plate in one of the paths. Similarly, a half wave plate in one path can be used to change horizontal polarization to vertical and vice versa. One can

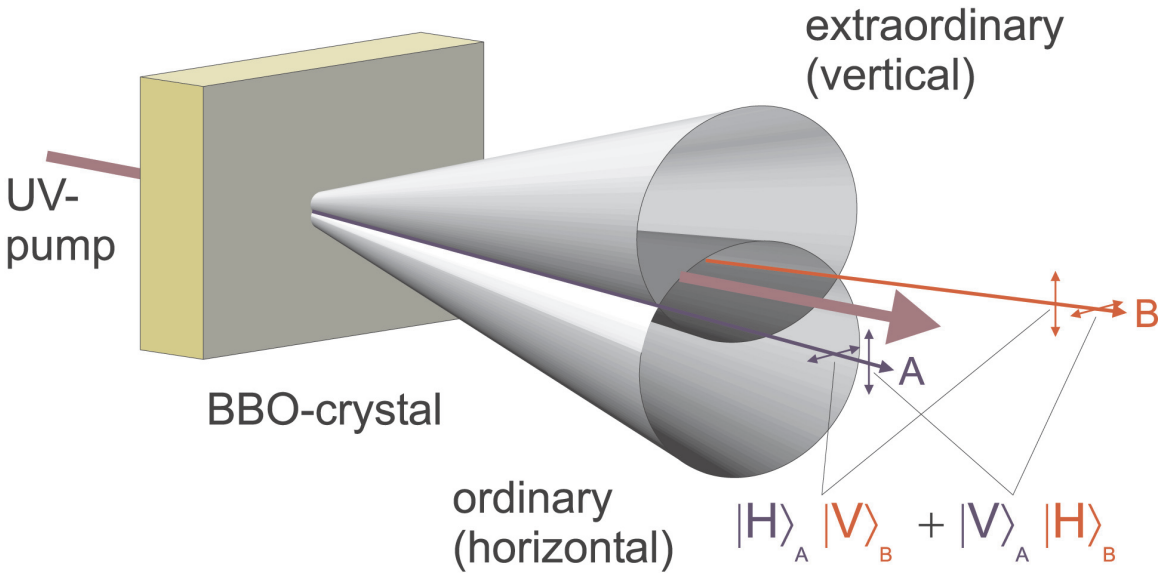

Figure 2.8: *Principle of type-II parametric down-conversion. Inside a nonlinear crystal (here, BBO), an incoming pump photon can decay spontaneously into two photons. Two down-converted photons arise polarized orthogonally to each other. Each photon is emitted into a cone. The photon of the top cone is vertically polarized while its exactly opposite partner in the bottom cone is horizontally polarized. Along the directions where the two cones intersect, their polarizations are undefined; all that is known is that they have to be different, which results in polarization entanglement between the two photons in arms A and B.*

thus very easily produce any of the four Bell states of Eq's. (2.3).

The birefringent nature of the down-conversion crystal complicates the actual entangled state produced, since the ordinary and extraordinary photons have different velocities inside the crystal, and propagate along different directions even though they become collinear outside the crystal (an effect well known from calcite prisms, for example). The resulting longitudinal and transverse walk-offs between the two terms in the state of Eq. (2.37) are maximal for pairs created near the entrance face, which consequently acquire a relative time delay $\delta T = L(1/u_o - 1/u_e)$ (L is the crystal length, and u_o and u_e are the ordinary and extraordinary group velocities, respectively) and a relative lateral displacement $d = L \tan \rho$ (ρ is the angle between the ordinary and extraordinary beams inside the crystal). If $\delta T \geq \tau_c$, the coherence time of the down-conversion light, then the terms in Eq. (2.37) become, in principle, distinguishable by the order in which the detectors would fire, and no interference will be observable. Similarly, if d is larger than the coherence width, the terms can become partially labeled by their spatial location.

Because the photons are produced coherently along the entire length of the crystal, one can completely compensate for the longitudinal walk-off [76]—after compensation, interference occurs pairwise between processes where the photon pair is created at distances $\pm x$ from the middle of the crystal. The ideal compensation is therefore to use two crystals, one in each path, which are identical to the down-conversion crystal, but only half as long. If the polarization of the light is first rotated by 90° (e.g. with a half wave plate), the retardation between the o and e components is exchanged and complete temporal indistinguishability is restored ($\delta T = 0$). The same method provides optimal compensation for the transverse walk-off effect as well. Here, the compensation crystals were oriented along the same direction as that of the down-conversion crystal. In the following experiments we always slightly rotate the orientation of one of the compensation crystals to tune the relative phase $\alpha = \pi$.

The BBO crystal used in our experiments is 2.0mm long and was cut at $\theta_{pm} = 43.5°$ (the angle between the crystal optic axis and the pump). To optimize the coupling efficiency, the cones have to intersect with orthogonal tangents, which was the case if the cone-overlap directions, selected by irises before the detectors, were separated by 6°. The transverse walk-off d (0.2mm) was small compared to the coherent pump beam width (2mm), so the associated labeling effect was minimal. However, it was necessary to compensate for longitudinal walk-off, since our 2.0mm BBO crystal produced $\delta T = 260$fs, while τ_c [determined by the collection irises and interference filters (centered at 780nm, 3.2nm FWHM)] was at about of the same order. As discussed above, we used an additional BBO crystal (1.0mm thickness, $\theta_{pm} = 43.5°$) in each of the paths, preceded by a half wave plate to exchange the roles of the horizontal and vertical polarizations.

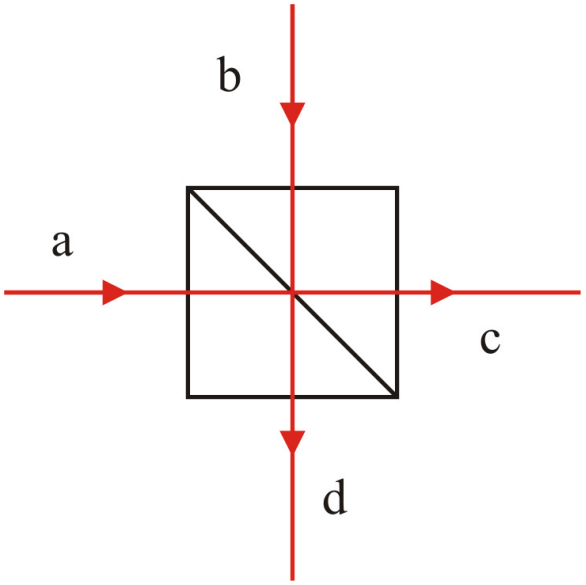

Figure 2.9: *Polarizing beam splitter (PBS). A PBS has two input modes a and b and two output modes c and d. It perfectly transmits (reflects) horizontally (vertically) polarized light. If a photon in the state* $|\Psi\rangle = \alpha|H\rangle + \beta|V\rangle$ *passes through a PBS, it will be found in the transmitted (reflected) beam with probability* $|\alpha|^2$ *(*$|\beta|^2$*).*

2.3.2 Bell-State Analyzer

The Bell state measurement (BSM) is a fundamental procedure in QIP, as it is an essential component in many protocols such as quantum teleportation. In the following we will describe the implementation of a Bell state analyzer with linear optics as we have used it in the experiments described in the following chapters.

The Bell state analyzer is based on the two-photon interference effect at a standard cube polarizing beam splitter (PBS). A PBS has two spatial input modes a and b and two output modes c and d (Fig. 2.9). If a photonic-qubit in the general state $|\Psi\rangle = \alpha|H\rangle + \beta|V\rangle$ (compare Eq. 2.10) is directed onto a PBS in mode a or b, the $|H\rangle$ and $|V\rangle$ terms are split into the two output modes c and d:

$$\begin{aligned} (\alpha|H\rangle + \beta|V\rangle)\,|a\rangle &\rightarrow \alpha|H\rangle|c\rangle + i\beta|V\rangle|d\rangle \\ (\alpha|H\rangle + \beta|V\rangle)\,|b\rangle &\rightarrow i\beta|V\rangle|c\rangle + \alpha|H\rangle|d\rangle \end{aligned} \tag{2.38}$$

where, e.g. $|a\rangle$ describes the spatial quantum state of the photon in input beam a. The PBS perfectly transmits (reflects) horizontally (vertically) polarized light. Here the factor i in front of the reflected term is a consequence of unity. It corresponds physically to a phase jump upon reflection at the semi-transparent mirror [77].

Let us now consider the PBS with two incident photons, 1 and 2, photon 1 in input mode a, and photon 2 in input mode b. Suppose that photon 1 is in the state $\alpha|H\rangle+\beta|V\rangle$, and photon 2 is in the state $\gamma|H\rangle+\delta|V\rangle$ ($|\alpha|^2+|\beta|^2 = 1$, $|\gamma|^2+|\delta|^2 = 1$). For this general case, four different possibilities arise: (1) both particles are reflected,

(2) both particles are transmitted, (3) the first particle is reflected and the second one is transmitted, and (4) the first one is transmitted and the second one is reflected. If the two photons have the same frequency and arrive at the PBS simultaneously, we have to consider coherent superpositions of the amplitudes for these different possibilities.

To show how the Bell state analyzer works, consider the general input state of photons 1 and 2 in input modes a and b, respectively:

$$|\Psi_{in}\rangle = \left(\alpha|\Phi^+\rangle_{12} + \beta|\Phi^-\rangle_{12} + \gamma|\Psi^+\rangle_{12} + \delta|\Psi^-\rangle_{12}\right)|a\rangle_1|b\rangle_2 \tag{2.39}$$

Here, we have used the Bell basis (see chapter 2.3) for illustrative reasons, which will become apparent later on ($|\alpha|^2 + |\beta|^2 + |\gamma|^2 + |\delta|^2 = 1$). We can rewrite Eq. (2.39) in the computational basis:

$$\begin{aligned} |\Psi_{in}\rangle = \; & \tfrac{1}{\sqrt{2}}[(\alpha+\beta)|H\rangle_1|H\rangle_2 + (\gamma+\delta)|H\rangle_1|V\rangle_2 \\ & +(\gamma-\delta)|V\rangle_1|H\rangle_2 + (\alpha-\beta)|V\rangle_1|V\rangle_2] \quad |a\rangle_1|b\rangle_2 \end{aligned} \tag{2.40}$$

As shown in Eq. (2.38), for photons 1 and 2 passing through the PBS their spatial modes will undergo a corresponding unitary transformation. The two-photon state thus evolves into:

$$\begin{aligned} |\Psi_f\rangle_{12} = \tfrac{1}{\sqrt{2}} \quad & [(\alpha+\beta)|H\rangle_1|c\rangle_1|H\rangle_2|d\rangle_2 + i(\gamma+\delta)|H\rangle_1|c\rangle_1|V\rangle_2|c\rangle_2 \\ & +i(\gamma-\delta)|V\rangle_1|d\rangle_1|H\rangle_2|d\rangle_2 + (\alpha-\beta)|V\rangle_1|d\rangle_1|V\rangle_2|c\rangle_2] \end{aligned} \tag{2.41}$$

We now proceed by placing a half-wave plate (HWP) into spatial modes c and d, respectively. The fast axis of the HWP is set to an angle of 22.5° to the horizontal axis. By this, the HWPs essentially implement Hadamard gates and the state of Eq. (2.41) evolves to:

$$\begin{aligned} |\Psi_f\rangle_{12} = \tfrac{1}{2\sqrt{2}}\{ \quad & (\alpha+\beta)[|H\rangle_1|H\rangle_2 + |H\rangle_1|V\rangle_2 + |V\rangle_1|H\rangle_2 + |V\rangle_1|V\rangle_2]|c\rangle_1|d\rangle_2 \\ & +i(\gamma+\delta)[|H\rangle_1|H\rangle_2 - |H\rangle_1|V\rangle_2 + |V\rangle_1|H\rangle_2 - |V\rangle_1|V\rangle_2]|c\rangle_1|c\rangle_2 \\ & +i(\gamma-\delta)[|H\rangle_1|H\rangle_2 + |H\rangle_1|V\rangle_2 - |V\rangle_1|H\rangle_2 - |V\rangle_1|V\rangle_2]|d\rangle_1|d\rangle_2 \\ & -(\alpha-\beta)[|H\rangle_1|H\rangle_2 - |H\rangle_1|V\rangle_2 - |V\rangle_1|H\rangle_2 + |V\rangle_1|V\rangle_2]|d\rangle_1|c\rangle_2\} \end{aligned} \tag{2.42}$$

To complete the Bell state analyzer, we have to direct the output modes c and d onto two additional PBSs. The entire setup is shown in Fig. (2.10). Just like in Eq. (2.41) the photons in modes c and d will undergo corresponding unitary transformations:

$$\begin{aligned} |\Psi_f\rangle_{12} = \tfrac{1}{2\sqrt{2}}\{ \quad & (\alpha+\beta) \quad [|H\rangle_1|e\rangle_1|H\rangle_2|h\rangle_2 + i|H\rangle_1|e\rangle_1|V\rangle_2|g\rangle_2 \\ & \qquad +i|V\rangle_1|f\rangle_1|H\rangle_2|h\rangle_2 - |V\rangle_1|f\rangle_1|V\rangle_2|g\rangle_2] \\ & +i(\gamma+\delta) \quad [|H\rangle_1|e\rangle_1|H\rangle_2|e\rangle_2 - i|H\rangle_1|e\rangle_1|V\rangle_2|f\rangle_2 \\ & \qquad +i|V\rangle_1|f\rangle_1|H\rangle_2|e\rangle_2 + |V\rangle_1|f\rangle_1|V\rangle_2|f\rangle_2] \\ & +i(\gamma-\delta) \quad [|H\rangle_1|h\rangle_1|H\rangle_2|h\rangle_2 + i|H\rangle_1|h\rangle_1|V\rangle_2|g\rangle_2 \\ & \qquad -i|V\rangle_1|g\rangle_1|H\rangle_2|h\rangle_2 + |V\rangle_1|g\rangle_1|V\rangle_2|g\rangle_2] \\ & -(\alpha-\beta) \quad [|H\rangle_1|h\rangle_1|H\rangle_2|e\rangle_2 - i|H\rangle_1|h\rangle_1|V\rangle_2|f\rangle_2 \\ & \qquad -i|V\rangle_1|g\rangle_1|H\rangle_2|e\rangle_2 - |V\rangle_1|g\rangle_1|V\rangle_2|f\rangle_2]\} \end{aligned} \tag{2.43}$$

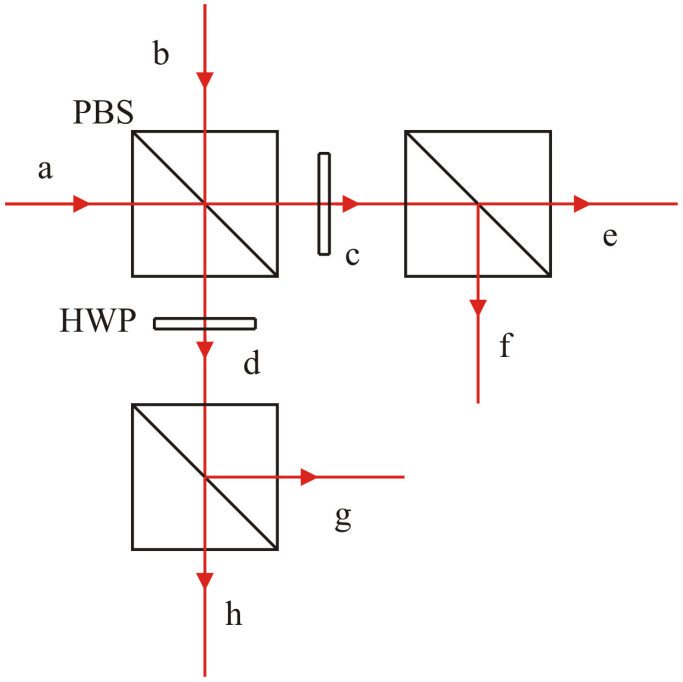

Figure 2.10: *Bell state analyzer. Two photons in input modes a and b are interfered on the first PBS. The two output modes c and d are analyzed with a half-wave plate (HWP) and a second PBS, respectively. A coincidence detection of photons in modes e+h or f+g corresponds to a* $|\Phi^-\rangle$ *detection, whereas a e+g or f+h coincidence corresponds to a* $|\Phi^+\rangle$ *detection.*

After photons 1 and 2 have passed through the setup of Fig. (2.10) it is not possible to distinguish them any more. The total two-photon state including both the spatial and the polarization part, therefore, has to obey bosonic quantum statistics. This implies that the outgoing physical state must be symmetric under the exchange of labels 1 and 2. To do so, one should symmetrize the state $|\Psi_f\rangle_{12}$, i.e. also include its exchange wave function $|\Psi_f\rangle_{21}$. The final outgoing state therefore reads

$$|\Psi_f\rangle = \frac{1}{\sqrt{2}}\left(|\Psi_f\rangle_{12} + |\Psi_f\rangle_{21}\right), \tag{2.44}$$

and consequently we have

$$\begin{aligned} |\Psi_f\rangle = \tfrac{1}{2}\{ \quad & \beta \quad && [|H\rangle_1|H\rangle_2(|e\rangle_1|h\rangle_2 + |h\rangle_1|e\rangle_2) \\ & && -|V\rangle_1|V\rangle_2(|f\rangle_1|g\rangle_2 + |g\rangle_1|f\rangle_2)] \\ & +i\alpha \quad && [|H\rangle_1|V\rangle_2(|e\rangle_1|g\rangle_2 + |h\rangle_1|f\rangle_2) \\ & && +|V\rangle_1|H\rangle_2(|g\rangle_1|e\rangle_2 + |f\rangle_1|h\rangle_2)] \\ & +i(\gamma+\delta) \quad && [|H\rangle_1|H\rangle_2|e\rangle_1|e\rangle_2 + |V\rangle_1|V\rangle_2|f\rangle_1|f\rangle_2] \\ & +i(\gamma-\delta) \quad && [|H\rangle_1|H\rangle_2|h\rangle_1|h\rangle_2 + |V\rangle_1|V\rangle_2|g\rangle_1|g\rangle_2]\} \end{aligned} \tag{2.45}$$

Close inspection of Eq. (2.45) shows that we can identify two out of the four Bell states. The probability to find a photon each in output modes e and h is exactly $|\beta|^2/2$. The same probability arises for a coincidence detection of photons in modes f and g. The overall probability for these two cases is thus $|\beta|^2$. Comparison with our original input state in Eq. (2.39) shows that this is exactly the probability for photons 1 and 2 to be in the Bell state $|\Phi^-\rangle_{12}$, i.e. for $\beta = 1$ ($\beta = 0$) we know with certainty that the photons will (never) jointly emerge either from modes e and h or modes f and g. Since our system only consists of two particles, we are forced to conclude that a coincidence detection of photons in modes e+h or f+g projects photons 1 and 2 onto the state $|\Phi^-\rangle_{12}$. Correspondingly, we are able to identify the state $|\Phi^+\rangle_{12}$ by registering a coincidence in modes e+g or f+h (probability = $|\alpha|^2$). Note, that we are not able to distinguish between the states $|\Psi^+\rangle_{12}$ and $|\Psi^-\rangle_{12}$ since no coincidence configuration can be genuinely associated with either one of them. With the help of our Bell state analyzer we are thus able to identify two out of the four Bell states via two-fold coincidence analysis and *post selection*. We want to mention that a similar setup with a non-polarizing 50:50 beam splitter instead of the interference PBS can be used to identify the states $|\Psi^+\rangle_{12}$ and $|\Psi^-\rangle_{12}$.

Chapter 3

Quantum Teleportation of a Two-Qubit Composite System

3.1 Introduction

The concept of quantum teleportation of a single-qubit and its importance in QIP was described in chapter (2.1.3). Experimental demonstrations thereof have been implemented with photons [36, 78, 79] and ions [80, 81]. Very recently long-distance teleportation [82, 83] and open-destination teleportation [84] have also been realized. However, the teleportation of single qubits is insufficient for a large-scale realization of quantum communication and computation [23, 40, 29, 41]. The teleportation of a composite system containing two or more qubits has thus been seen as a long-standing goal in quantum information science.

In this chapter we will discuss the first experimental demonstration of a two-photon quantum teleportation. In the experiment, we develop and exploit a six-photon interferometer to teleport an arbitrary polarization state of two photons. Not only does our six-photon interferometer provide an important step towards teleportation of a complex system, it will also enable future experimental investigations on a number of fundamental quantum communication and computation protocols [40, 85, 86, 61]. The concept of two-qubit teleportation and the experimental six-photon setup described in this chapter furthermore constitute the basis for the experiments of the following chapters (4,5,6).

3.2 Teleportation of a Two-Qubit System

Although there exist other ways to achieve teleportation of a composite system [87, 88], our experimental scheme [29, 89] closely follows the original proposal for teleportation of single qubits (chapter 2.1.3). In the two-qubit teleportation, the sender, Alice, wants to send an unknown state of a system composed of qubits 1 and

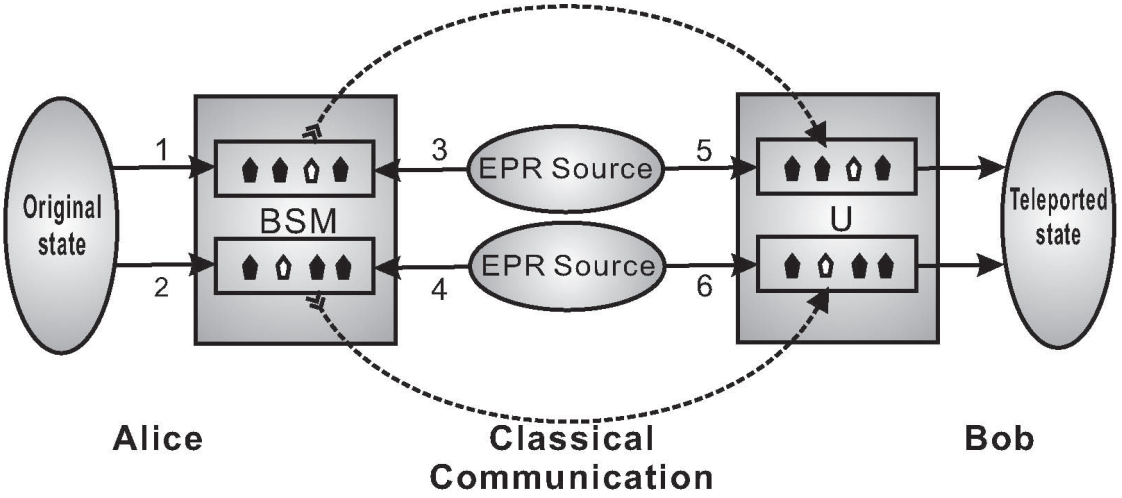

Figure 3.1: *Schematic diagram showing the principle of two-qubit teleportation. Alice wants to teleport an unknown state of a system composed of photon 1 and 2 to Bob. To do so, Alice and Bob first share two entangled photon pairs (EPR source), photon pairs 3-5 and 4-6. Alice then carries out a joint Bell-state measurement (BSM) both on photons 1 and 3 and on photons 2 and 4, respectively. On receiving Alice's BSM results via classical communication, Bob can then carry out a corresponding unitary transformation (*U*) on both photons 5 and 6 to convert them into the original state of photons 1 and 2.*

2,

$$|\chi\rangle_{12} = \alpha\,|H\rangle_1\,|H\rangle_2 + \beta\,|H\rangle_1\,|V\rangle_2 + \gamma\,|V\rangle_1\,|H\rangle_2 + \delta\,|V\rangle_1\,|V\rangle_2\,, \tag{3.1}$$

where α, β, γ and δ are four arbitrary complex numbers satisfying $|\alpha|^2+|\beta|^2+|\gamma|^2+|\delta|^2=1$, to a distant receiver, Bob (Fig. 3.1). In order to achieve teleportation, Alice and Bob first have to share two ancillary entangled photon pairs (photon pairs 3-5 and 4-6) which are prepared in the Bell state $|\Phi^+\rangle$ (see Eq. 2.3). The two-qubit teleportation scheme then works as follows.

Alice first teleports the state of photon 1 to photon 5 following the standard teleportation protocol. In terms of the four Bell-states of photons 1 and 3,

$$\begin{aligned} |\Phi^\pm\rangle_{13} &= \frac{1}{\sqrt{2}}(|H\rangle_1|H\rangle_3 \pm |V\rangle_1|V\rangle_3) \\ |\Psi^\pm\rangle_{13} &= \frac{1}{\sqrt{2}}(|H\rangle_1|V\rangle_3 \pm |V\rangle_1|H\rangle_3), \end{aligned} \tag{3.2}$$

the combined state of photons 1, 2, 3 and 5 can be rewritten as

$$\begin{aligned} |\chi\rangle_{12}|\Phi^+\rangle_{35} =& \frac{1}{2}(|\Phi^+\rangle_{13}|\chi\rangle_{52} + |\Phi^-\rangle_{13}\hat{\sigma}_{5z}|\chi\rangle_{52} \\ &+ |\Psi^+\rangle_{13}\hat{\sigma}_{5x}|\chi\rangle_{52} + |\Psi^-\rangle_{13}(-i\hat{\sigma}_{5y})|\chi\rangle_{52}), \end{aligned} \tag{3.3}$$

where $\hat{\sigma}_x$, $\hat{\sigma}_y$ and $\hat{\sigma}_z$ are the well-known Pauli operators. Eq. (3.3) implies, that by performing a joint Bell state measurement (BSM) on qubits 1 and 3, Alice projects the state of qubits 5 and 2 onto one of the four corresponding states. After she has told Bob her BSM result via a classical communication channel, Bob can convert the state of qubits 5 and 2 into the original state $|\chi\rangle_{52}$ by applying to photon 5 a corresponding local unitary transformation ($\hat{I}$, $\hat{\sigma}_x$, $\hat{\sigma}_y$, $\hat{\sigma}_z$), independent of the original state.

Similarly, the combined state of photons 2, 4, 5 and 6 can be rewritten in terms of the four Bell-states of photons 2 and 4 as

$$\begin{aligned}|\chi\rangle_{52}|\Phi^+\rangle_{46} =& \frac{1}{2}(|\Phi^+\rangle_{24}|\chi\rangle_{56} + |\Phi^-\rangle_{24}\hat{\sigma}_{6Z}|\chi\rangle_{56} \\ &+ \left|\Psi^+\right\rangle_{24}\hat{\sigma}_{6X}\,|\chi\rangle_{56} + \left|\Psi^-\right\rangle_{24}(-i\hat{\sigma}_{6Y})\,|\chi\rangle_{56}).\end{aligned} \tag{3.4}$$

Following the above procedure, Alice can also teleport the state of photon 2 to photon 6. First, Alice performs a joint BSM on photons 2 and 4 and sends the BSM result to Bob. Upon the BSM result received, by applying to photon 6 a corresponding local unitary transformation ($\hat{I}$, $\hat{\sigma}_x$, $\hat{\sigma}_y$, $\hat{\sigma}_z$), Bob can convert the state of qubits 5 and 6 into the original state

$$|\chi\rangle_{56} = \alpha|H\rangle_5|H\rangle_6 + \beta|H\rangle_5|V\rangle_6 + \gamma|V\rangle_5|H\rangle_6 + \delta|V\rangle_5|V\rangle_6 \tag{3.5}$$

to accomplish the task of the most general two-qubit teleportation.

The above scheme has a remarkable feature: it teleports the two photonic qubits, 1 and individually. This way, neither the two original qubits nor the teleported qubits have to be in the same place. Such a flexibility is desired in distributed quantum information processing, such as quantum telecomputation [41] and quantum secret sharing [90, 91]. Moreover, the above method of teleporting each qubit of a composite system individually can be easily generalized to teleport a N-qubit complex system.

3.3 A Stable High-Intensity Entangled Photon Source

Although significant experimental advances have been achieved in teleportation of single qubits (photons and ions), the realization of teleportation of a composite system containing two or more qubits has remained a real experimental challenge. This is because, on the one hand recent photonic experiments [82, 83, 84] would have a too low six-photon coincidence rate. On the other hand, the experiments with trapped ions [81, 80] are limited by the finite life time of ion qubits due to de-coherence and the non-ideal fidelity of quantum logic operations between ion qubits. As photons are robust against de-coherence and high precision unitary transformations for photons can be carried out with linear optical devices, in the present experiment we still chose to use polarization-entangled photon pairs via parametric down-conversion [30] as the main resource while various efforts have been made to greatly improve the brightness and stability of the entangled photon sources.

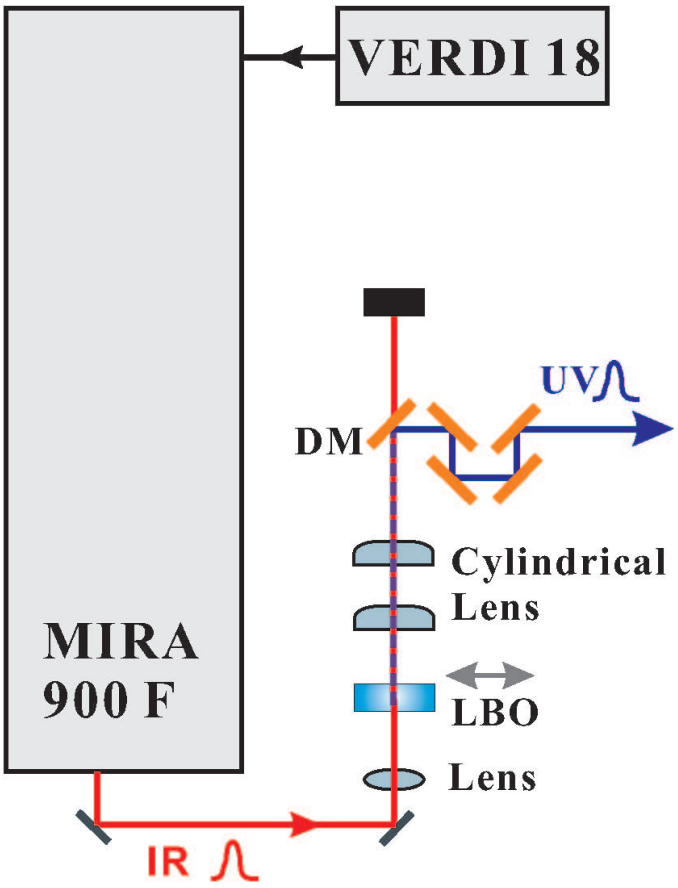

Figure 3.2: *Method to increase the power of the ultraviolet light. A modified mode-locked Ti:sapphire laser (MIRA), pumped with an all-solid-state CW laser Verdi-V18 (operating at 14W), is used to produce high-intensity ultra-fast infrared light pulses. The infrared light pulse passes through the LBO crystal to generate via up-conversion the ultraviolet pulse necessary for parametric down-conversion. Behind the LBO, two cylindrical lenses with orthogonal axes, (one horizontal and one vertical) are used to shape and focus the ultraviolet beam and five dichroic mirrors (DM) are used to separate the ultraviolet from the infrared light.*

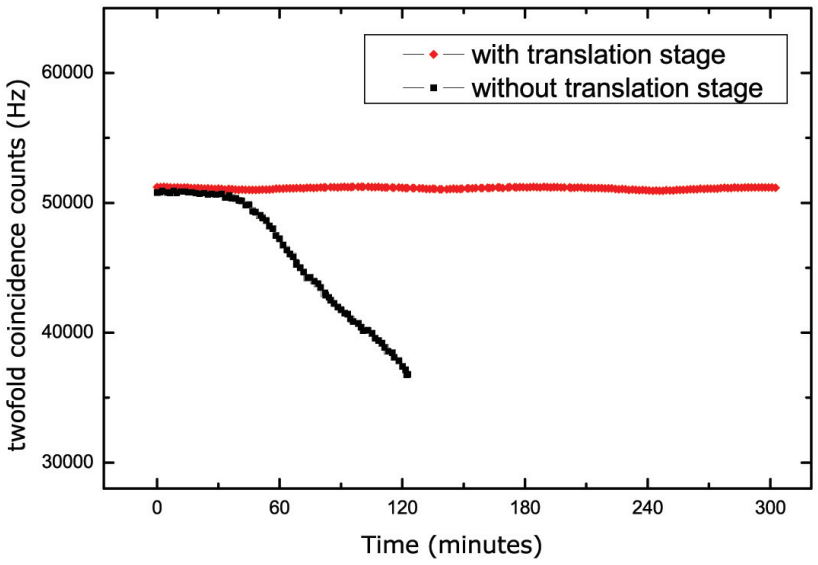

Figure 3.3: *Performance of the LBO crystal. Measured two-fold coincidences with and without moving the translation stage of the LBO up-conversion crystal over time.*

A natural way to obtain a brighter entangled photon source is to increase the power of the ultraviolet light necessary for parametric down-conversion. To significantly increase the ultraviolet power, we would need a more powerful ultra-fast infrared laser system for the up-conversion process. To achieve this, we have used an all-solid-state CW laser Verdi-V18 instead of Verdi-V10 to pump a modified mode-locked Ti:sapphire laser system Mira900-F (Mira) as is shown in Fig. (3.2). Unfortunately, the conversion efficiency of the Ti:sapphire crystal will drop greatly when the pump power is beyond a certain threshold, typically 10 in the commercial Mira. This is because the pump laser Verdi-V18 will bring more heat to the Ti:sapphire crystal. To solve this problem, a better cooling cycle system around the Ti:sapphire crystal is used. Moreover, a brighter pump laser in the Mira cavity will make the output infrared pulse unstable. A new output coupler with higher transmission efficiency is used in the cavity to stabilize the output laser. After these innovations, we achieved an ultra fast infrared pulse with an output power of about 2.9W with the Verdi-V18 operated at 14W,which is almost twice as high as before.

The high power infrared pulse was properly focused on a LiB_3O_5 (LBO) crystal to achieve the best up-conversion efficiency. To avoid damage to the LBO, caused by the focused laser beam, the LBO is mounted on a motorized translation stage and will be moved by a distance of 10 μm to another point once the reference - single count rate of detector D5H (see Fig. 3.4) - is below a certain threshold. To

demonstrate the advantage of this technique, we measure the two-fold coincidence count rates over time, first without and then with moving the translation stage of the LBO. As can be observed in Fig. (3.3), our feedback control system greatly improves the stability of the down-conversion rates. Since back-reflection of the LBO into the Mira system can destroy the mode-lock condition, perfect control of the LBO motion is crucial. Due to the brighter infrared pulse, much more noise (i.e. infrared light) is introduced to the ultraviolet light during the up-conversion process. To compensate for this, two additional dichroic mirrors (to have a total of seven) are added in comparison to former experiments to further separate the ultraviolet light with the infrared noise.

To have a better collection efficiency of entangled photon pairs, we significantly shortened the distance between the BBOs and the fiber couplers to make our setup more compact. Besides the improvement in collection efficiency, a compact setup also helps to significantly improve the stability of the whole six-photon interferometer. To optimize the collection efficiency for all three entangled photon pairs, we chose a 10 cm focus lens between the two BBOs and a 20 cm radius concave mirror behind the second BBO to refocus the ultraviolet pulse such that it has the same beam size in all three BBO pumping processes. With these modifications, we achieved a stable high-intensity entangled photon source.

3.4 Experimental Setup

A schematic diagram of our experimental setup is shown in Fig. (3.4). The developed high-intensity ultraviolet laser successively passes through two BBO crystals to generate three polarization-entangled photon pairs [30]. The ultraviolet laser beam is circularized and has a central wavelength of 390 nm, a pulse duration of 180 fs, a repetition rate of 76 MHz and an average power of 1.0 W. All three photon pairs are originally prepared in the Bell state $|\Phi^+\rangle = (|HH\rangle + |VV\rangle)/\sqrt{2}$. Following the efforts described in the above section, we managed to observe on average 10^5 photon pairs per second from each source. This is almost five times brighter than the source achieved in a recent teleportation experiment [84]. With this high-intensity entangled photon source we could obtain in total 10 six-photon events per minute. This is two orders of magnitude higher than any former photonic teleportation experiment could have achieved.

With the help of wave plates and polarizers, we prepared photon pair 1-2 in the desired two-qubit state $|\chi\rangle_{12}$ that is to be teleported. Photon pairs 3-5 and 4-6, which are in the state $|\Phi^+\rangle$, are used as the two ancillary pairs.

To implement two-qubit teleportation, it is necessary to perform a joint BSM on photons 1 and 3 and photons 2 and 4, respectively. To demonstrate the working principle of two-qubit teleportation it is sufficient to identify one of the four Bell-states in both BSMs, although this will result in a reduced efficiency - the fraction of success - of 1/16. In the experiment, we decide to analyze the Bell-state $|\Phi^+\rangle$ (see

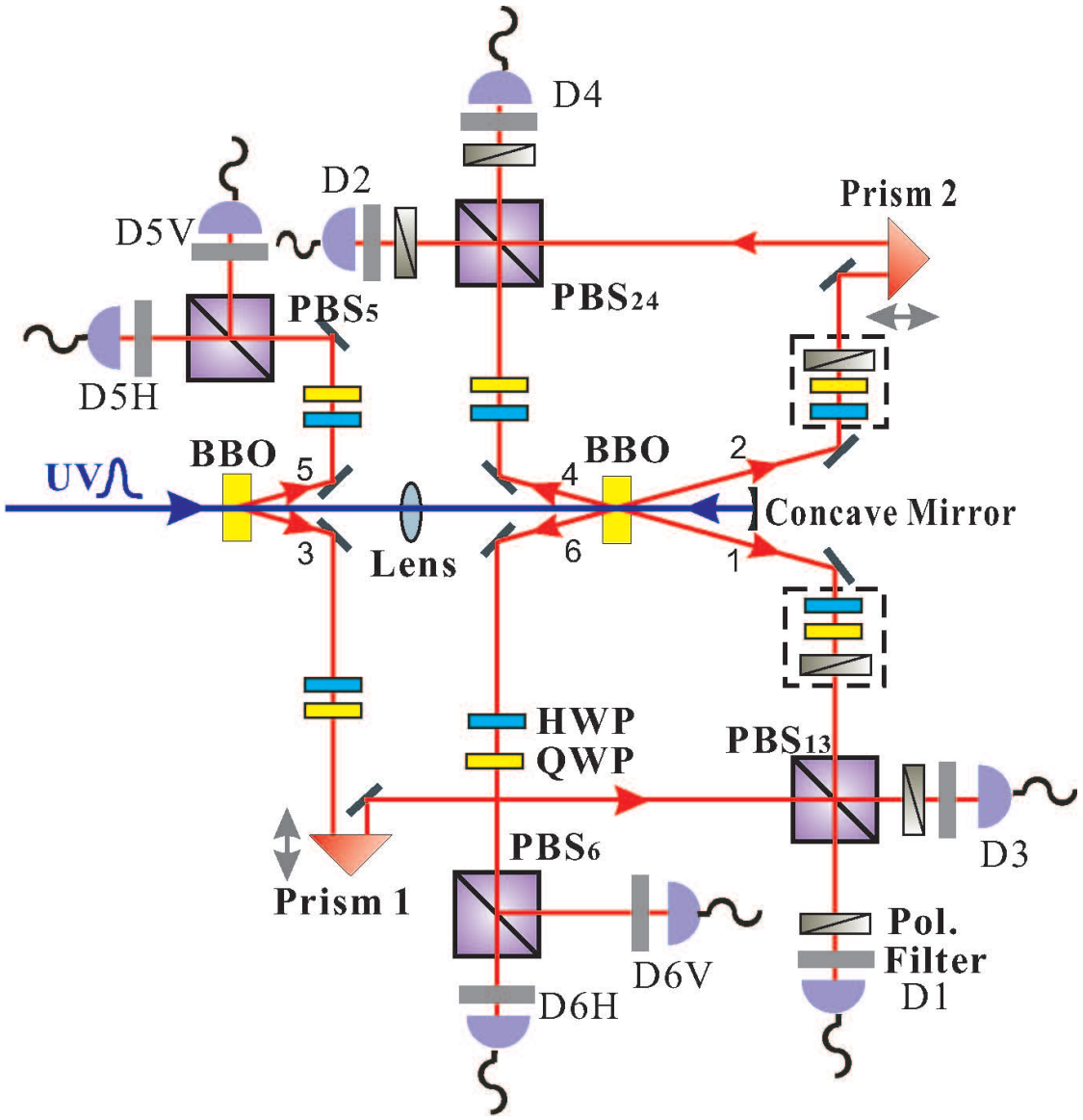

Figure 3.4: *A schematic diagram of the experimental setup. The ultraviolet pulse passes through a BBO crystal to generate a polarization-entangled photon pair in modes 3 and 5 (i.e. the first ancillary entangled photon pair). After the first BBO, a 10-cm-focus lens is introduced to refocus the ultraviolet pulse onto the second BBO to produce another entangled photon pair in modes 1 and 2 (to prepare the two qubits to be teleported). Reflected by a concave mirror, the ultraviolet pulse pumps once more into the second BBO and generates the third entangled photon pair in modes 4 and 6 (that is, the second ancillary photon pair). Prisms 1 and 2, both mounted on step motors, are used to compensate the time delay for the interference on polarizing beam splitters PBS13 and PBS24, respectively. PBS5 and PBS6 are used to verify the teleported state with the help of wave plates in front of them. The photons are all detected by silicon avalanched single-photon detectors. Coincidences are recorded with a coincidence unit clocked by the infrared laser pulses. Pol. are linear polarizers and Filter labels the narrow band filter with* $\Delta\lambda_{FWHM} = 2.8nm$.

chapter 2.3.2). This is achieved by interfering photons 1 and 3 and photons 2 and 4 on the polarizing beam-splitters, PBS_{13} and PBS_{24}, respectively. To interfere photons 1 and 3 (photons 2 and 4) on the PBS_{13} (PBS_{24}), it has to be guaranteed that the two photons have good spatial and temporal overlap at the PBS such that they are indistinguishable. To achieve this, the two outputs of the PBSs are spectrally filtered ($\Delta\lambda_{FWHM} = 2.8nm$) and monitored by fiber-coupled single-photon detectors [92]. Moreover, perfect temporal overlap is accomplished by adjusting the path length of photon 3 (photon 2) by a delay prism 1 (prism 2) to observe "Shih-Alley-Hong-Ou-Mandel"-type interference fringes (HOM) [93, 94] behind the PBS_{13} (PBS_{24}) in the diagonal ($|+\rangle/|-\rangle$) basis [95]. A typical interference of the *HOM-dip* kind is shown in Fig. (3.5), where we use photons 2 and 5 (1 and 6) as a trigger to reduce noise contributions. These interferometers are sensitive only to length changes on the order of the coherence length of the detected photons ($\sim$110 μm) and stay stable for weeks. With the help of polarizers at 45°, the required projection of photons 1 and 3 (2 and 4) onto $|\Phi^+\rangle$ can then be achieved by detecting behind PBS_{13} (PBS_{24}) a $|+\rangle|+\rangle$ or $|-\rangle|-\rangle$ coincidence between detectors D1 and D3 (D2 and D 4) [95], as we have described in detail in chapter (2.3.2). Note that, in the experiment, only the $|+\rangle|+\rangle$ coincidence is registered, which further reduces the teleportation efficiency to 1/64. However, by inserting one PBS and two detectors behind each output of PBS13 and PBS24, respectively, both $|\Phi^+\rangle$ (by detecting a $|+\rangle|+\rangle$ or $|-\rangle|-\rangle$ coincidence) and $|\phi^-\rangle$ (by detecting a $|+\rangle|-\rangle$ or $|-\rangle|+\rangle$ coincidence) can be identified and thus the efficiency can be increased up to 1/4 [96].

As shown in Eq. (3.3) and Eq. (3.4), the projection measurements onto $|\Phi^+\rangle_{13}$ and $|\Phi^+\rangle_{24}$ leave photons 5 and 6 in the state $|\chi\rangle_{56}$, i.e. the original state of photons 1 and 2. To demonstrate that our two-qubit teleportation protocol works for a general unknown polarization state of photons 1 and 2, we decide to teleport three different initial states:

$$\begin{aligned} |\chi\rangle_A &= |H\rangle_1|V\rangle_2 \\ |\chi\rangle_B &= \tfrac{1}{2}\left(|H\rangle_1 + |V\rangle_1\right)\left(|H\rangle_2 - i|V\rangle_2\right) \\ |\chi\rangle_C &= \tfrac{1}{\sqrt{2}}\left(|H\rangle_1|V\rangle_2 - |V\rangle_1|H\rangle_2\right) \end{aligned} \tag{3.6}$$

$|\chi\rangle_A$ is simply one of the four computational basis vectors in the two-qubit Bloch sphere (Fig. 2.1); $|\chi\rangle_B$ is composed of a linear polarization state and a circular polarization state, which is also a superposition of all the four computational basis vectors; and $|\chi\rangle_C$ is a maximally entangled Bell state.

3.5 Experimental Results

We quantify the quality of our teleportation experiment by looking at the fidelity of the teleported state as defined in Eq. (2.32). To measure the fidelity of two-qubit teleportation, two PBSs (PBS_5 and PBS_6) and corresponding wave plates (HWP

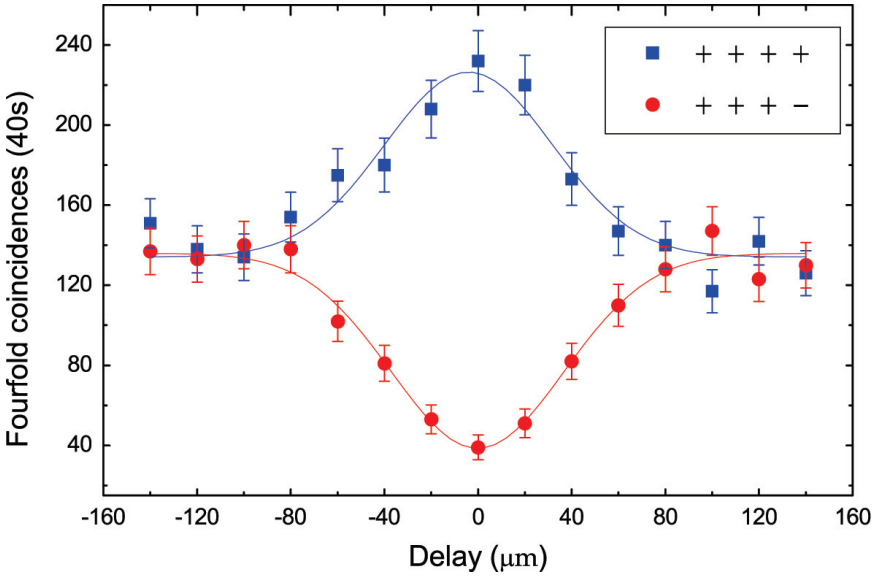

Figure 3.5: *Two-photon interference of "Hong-Ou-Mandel-dip " kind. Two photons, each from a pair in the Bell state $|\Phi^+\rangle$ are interfered on a PBS and detected in the diagonal basis. The remaining two photons are used as triggers to reduce noise contributions. The data points are fitted with Gaussian curves to guide the eye. Outside the coherence length there is no interference because of the temporal distinguishability. Maximum interference occurs at zero delay between the two photons at the interference PBS.*

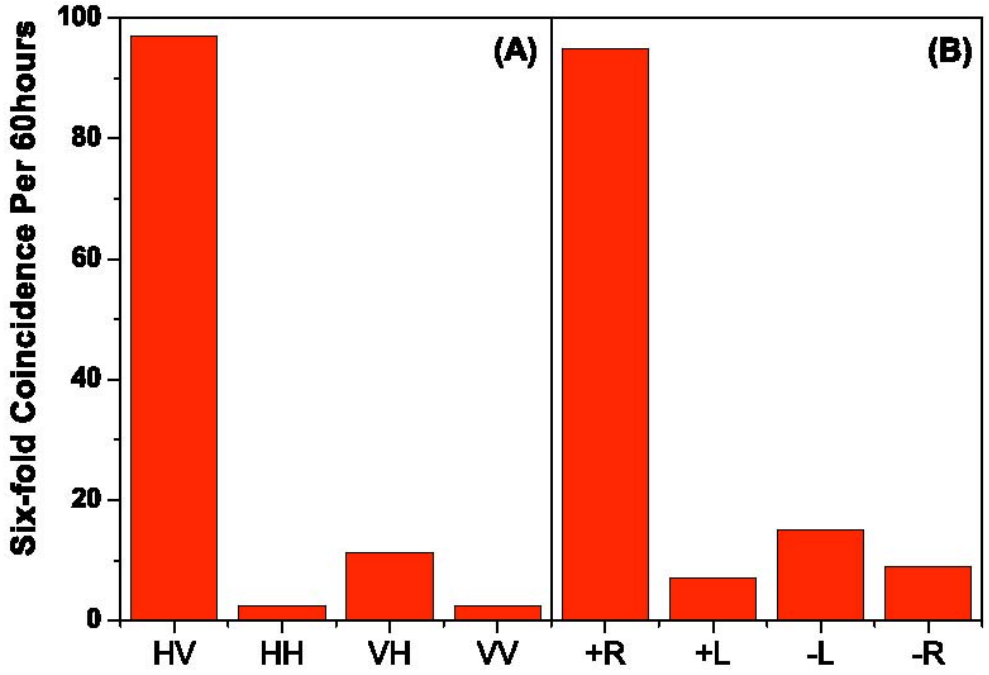

Figure 3.6: *Experimental results for the teleportation of the $|\chi\rangle_A$ state and the $|\chi\rangle_B$ state. Each measurement took 60 h.* ***(A)*** *The $|\chi\rangle_A$ state. We measured photon 5 and 6 in the computational basis.* ***(B)*** *The $|\chi\rangle_B$ state. We measured photon 5 in the diagonal and photon 6 in the circular basis. The fraction of $|H\rangle|V\rangle$ ($|+\rangle|R\rangle$) to the sum of all counts shows the fidelity for the teleportation of the $|\chi\rangle_A$ ($|\chi\rangle_B$) state in A (B).*

and QWP), as shown in Fig. (3.4), are combined properly to analyze the teleported state of photons 5 and 6.

The fidelity measurements for the $|\chi\rangle_A$ and $|\chi\rangle_B$ teleportation are straight forward. Conditioned on detecting a $|+\rangle|+\rangle$ coincidence between D1 and D3, D2 and D4, respectively, we analyze the teleported state of photons 5 and 6 in the computational basis for the $|\chi\rangle_A$ teleportation; whereas we analyze photon 5 in the diagonal basis and photon 6 in the circular basis for the $|\chi\rangle_B$ teleportation. As the above state analysis only involves orthogonal measurements on individual qubits, the fidelity of the teleported state is directly given by the fraction of observing a $|\chi\rangle_A$ or $|\chi\rangle_B$ state at detectors D5 and D6. The measurement results are shown in Fig. (3.6). The experimental integration time for each fidelity measurement was about 60 hours

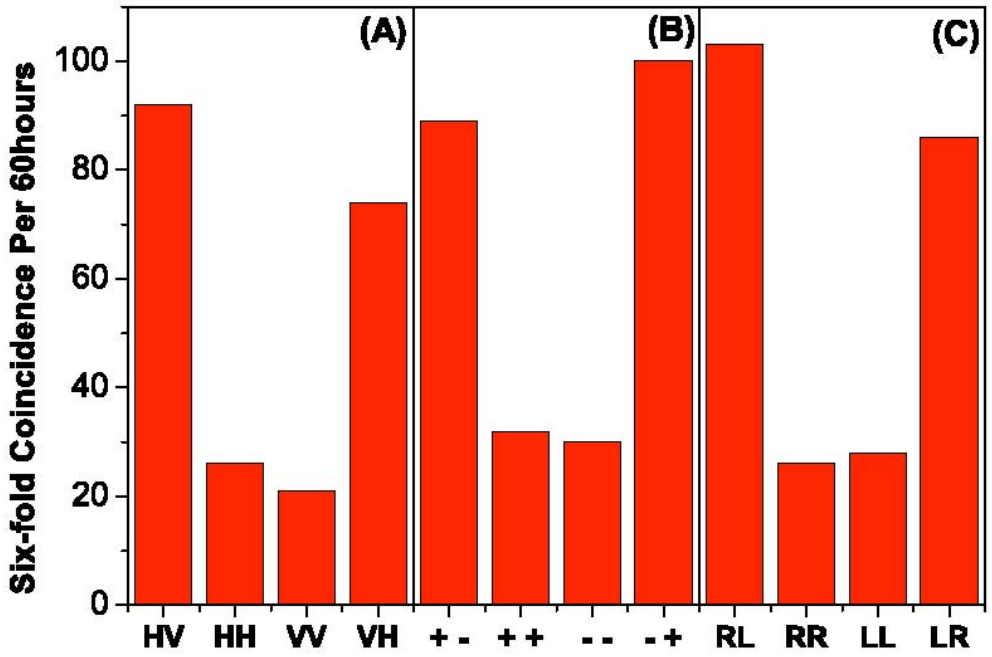

Figure 3.7: *Experimental results for the $|\chi\rangle_C$ teleportation. Three complementary bases were used: (**A**) computational, (**B**) diagonal and (**C**) circular basis, corresponding to the three different local measurements $\langle\hat{\sigma}_x\hat{\sigma}_x\rangle$, $\langle\hat{\sigma}_y\hat{\sigma}_y\rangle$ and $\langle\hat{\sigma}_z\hat{\sigma}_z\rangle$. Each measurements took 60 hours. In A whenever there is a $|H\rangle|H\rangle$ or $|V\rangle|V\rangle$ coincidence, the result of $\hat{\sigma}_x\hat{\sigma}_x$ is $+1$, whereas $|H\rangle|V\rangle$ or $|V\rangle|H\rangle$ represents -1. In B, $|+\rangle|+\rangle$ or $|-\rangle|-\rangle$ represents $+1$, whereas $|+\rangle|-\rangle$ or $|-\rangle|+\rangle$ represents -1. In C, $|R\rangle|R\rangle$ or $|L\rangle|L\rangle$ displaces $+1$, whereas $|R\rangle|L\rangle$ or $|L\rangle|R\rangle$ displaces -1.*

Original States	Fidelities	Fidelities after subtraction of noise
$\|H\rangle\|V\rangle$	0.86 ± 0.03	0.97 ± 0.03
$(\|H+V\rangle\|H-iV\rangle)/2$	0.75 ± 0.02	0.83 ± 0.02
$(\|H\rangle\|V\rangle - \|V\rangle\|H\rangle)/\sqrt{2}$	0.65 ± 0.03	0.77 ± 0.03
Average	0.75 ± 0.03	0.86 ± 0.03

Table 3.1: Fidelities of quantum teleportation of a two-qubit composite system.

and we recorded about 100 desired two-qubit teleportation events. The integration time is slightly longer than would be expected from the original source rate, due to the additional losses at the interference PBSs. On the basis of our original data, we conclude that the fidelity for $|\chi\rangle_A$ and $|\chi\rangle_B$ is 0.86 ± 0.03 and 0.75 ± 0.02, respectively.

The measurement on the fidelity of the $|\chi\rangle_C$ teleportation is a bit more complex, since a complete Bell state analysis on photons 5 and 6 usually requires nonlinear interaction between them. Fortunately, the fidelity can still be determined by local measurements on individual qubits. To see this, we write the density matrix of $|\chi\rangle_C$ in terms of the Pauli matrices:

$$|\chi\rangle_{CC}\langle\chi| = |\Psi^-\rangle\langle\Psi^-| = \frac{1}{4}\left(\hat{I} - \hat{\sigma}_x\hat{\sigma}_x - \hat{\sigma}_y\hat{\sigma}_y - \hat{\sigma}_z\hat{\sigma}_z\right) \tag{3.7}$$

By Eq. (2.32), we have:

$$F = Tr\left(\hat{\rho}|\Psi^-\rangle\langle\Psi^-|\right) = \frac{1}{4}Tr\left[\hat{\rho}\left(\hat{I} - \hat{\sigma}_x\hat{\sigma}_x - \hat{\sigma}_y\hat{\sigma}_y - \hat{\sigma}_z\hat{\sigma}_z\right)\right] \tag{3.8}$$

This implies that we can obtain the fidelity of the $|\chi\rangle_C$ teleportation by consecutively carrying out three local measurements $\langle\hat{\sigma}_x\hat{\sigma}_x\rangle$, $\langle\hat{\sigma}_y\hat{\sigma}_y\rangle$ and $\langle\hat{\sigma}_z\hat{\sigma}_z\langle$ on the two teleported qubits. The measurement results for the three operators are shown in Fig. (3.7), each of which took about 60 hours. Using Eq. (3.8) we determine an experimental fidelity of 0.65 ± 0.03.

3.6 Discussion

As can be seen from the above experimental results, all the teleportation fidelities are well beyond the state estimation limit of 0.40 for a two-qubit composite system [97], hence successfully demonstrating quantum teleportation of a two-qubit composite system. The imperfection of the fidelities is mainly due to the noise caused by emission of two pairs of down-converted photons by a single source [36]. In our experiment, this noise contributes around 10 spurious six-fold coincidences in 60 hours and was not subtracted in the fidelity estimation. Table (3.1) clearly shows that by subtracting this noise, as it was done in a previous experiment [36], the fidelities improve strongly. Besides the double pair emission, the limited interference

visibility and imperfect entangled state also reduce our teleportation fidelities. We notice that the fidelities of $|\chi\rangle_B$ and $|\chi\rangle_C$ teleportation are worse than those of $|\chi\rangle_A$. This is because the fidelities of $|\chi\rangle_B$ and $|\chi\rangle_C$ teleportation depend on the interference visibility on PBS13 and PBS24, while the $|\chi\rangle_A$ teleportation fidelity does not. Moreover, as the quality of the initial entangled state $|\chi\rangle_C$ is not as good as for the disentangled states $|\chi\rangle_A$ and $|\chi\rangle_B$, the fidelity of $|\chi\rangle_C$ teleportation is worse than that of the other two.

In this chapter, we have discussed the development and exploration of a six-photon interferometer to report the first experimental demonstration of a two-qubit composite system. Not only does our experiment present an important step towards teleportation of a complex system, the techniques developed also enable immediate experimental investigations on novel quantum communication and computation protocols, which will become more apparent in the following chapters.

Chapter 4

Multistage Entanglement Swapping

4.1 Introduction

Entanglement swapping is arguably one of the most important ingredients for quantum repeaters and quantum relays, which lay at the heart of quantum communication [42, 23, 24, 85, 98, 99]. For photonic quantum communication, the distance is largely limited due to de-coherence from coupling to the environment and an increasing loss of photons in a quantum channel. This leads to an exponential fidelity decay of quantum information. This drawback can eventually be overcome by subdividing larger distances into smaller sections over which entanglement or quantum states can be distributed. The sections are then bridged by entanglement swapping processes [23, 24, 85, 98]. The swapping procedure therefore constitutes one of the key elements for a quantum relay, and a full quantum repeater if combined with quantum purification [100, 101, 48, 49] and quantum memory [102, 103, 104]. As a result, quantum communication becomes feasible despite of realistic noise and imperfections. At the same time, the overhead for the used resources and communication time only increase polynomially with the distance [23, 24, 85, 98, 99].

When dividing a quantum channel into many segments, with the length of each segment comparable to the channel loss length, one can achieve reliable and robust long-distance quantum communication by connecting two adjacent segments through entanglement swapping. Experimentally, photonic entanglement swapping has so far successfully been achieved for the case of discrete variables [79, 105, 106], and for continuous variables [107, 108, 109], both via a single stage process. However, only after successful multiple swapping, we are able to have a fully functional quantum repeater. In fact, there are additional advantages utilizing a multiple swapping process. For a quantum relay with many segments, it is equivalent to significantly lower the dark-count rate, which is a substantial factor limiting the transmission distance of successful quantum communication [85, 98]. For quantum information

carriers possessing mass, multiple swapping processes can speed up the distribution of entanglement by a factor that is proportional to the number of segments used [43]. Moreover, multistage entanglement swapping can improve the protection of quantum states against noise suffered from amplitude errors [43].

In this chapter we discuss an experimental demonstration of a multiple entanglement swapping over two stages. This is achieved by utilizing three highly bright and spatially independent pairs of polarization entangled photons, and performing BSMs among the three segments between the two communication parties. Two successful BSMs yield a final maximally entanglement pair distributed between the two parties. To quantitatively evaluate the performance, we have observed the quality of the output state by the characterization of an entanglement witness, which confirms genuine entanglement generation. Our experiment implements an entanglement distribution over two distant stations which are initially independent of each other and have never physically interacted in the past. This proof-of-principle demonstration constitutes an important step towards robust long-distance quantum relays, quantum repeaters and related quantum protocols based on multiple entanglement swapping.

4.2 Multistage Entanglement Swapping

The principle for multistage entanglement swapping is sketched in Fig. (4.1). Consider three independent stations, simultaneously emitting each a pair of maximally entangled photons (EPR pair). In anticipation of our experiments we assume that these are polarization entangled photons in the state

$$|\Psi\rangle_{123456} = |\Psi^-\rangle_{12} \times |\Psi^-\rangle_{34} \times |\Psi^-\rangle_{56}, \tag{4.1}$$

where $|\Psi^-\rangle_{ij}$ is one of the four maximally entangled Bell states of Eq. (2.3). Note that photon pairs 1-2, 3-4 and 5-6 are entangled in the antisymmetric polarization state, respectively. However, the states of the three pairs are factorizable from each other, namely there is no entanglement among any photons from different pairs.

As a first step we perform a joint BSM on photons 2 and 3, i.e. photons 2 and 3 are projected onto one of the four Bell states. Moreover, this measurement also projects photons 1 and 4 onto a Bell state, in a form depending on the result of the BSM of photons 2 and 3. Close inspection shows that for the initial state given in Eq. (4.1), the emerging state of photons 1 and 4 is identical to the one that photons 2 and 3 collapse into. This is a consequence of the fact that the state of Eq. (4.1) can be rewritten as

$$\begin{aligned} |\Psi\rangle_{123456} \quad = \quad & \tfrac{1}{2}[|\Psi^+\rangle_{14}|\Psi^+\rangle_{23} - |\Psi^-\rangle_{14}|\Psi^-\rangle_{23} \\ & -|\Phi^+\rangle_{14}|\Phi^+\rangle_{23} + |\Phi^-\rangle_{14}|\Phi^-\rangle_{23}] \\ & \times|\Psi^-\rangle_{56} \end{aligned} \tag{4.2}$$

In all cases photons 1 and 4 emerge entangled despite the fact that they never interacted with one another in the past. After the joint measurement of photons 2

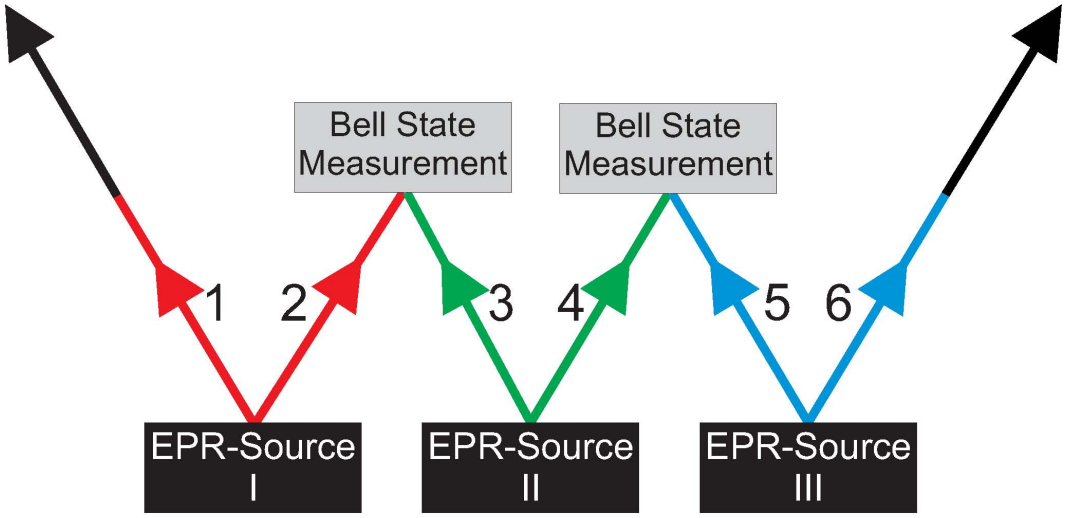

Figure 4.1: *Principle of multistage entanglement swapping. Three Einstein Podolsky Rosen (EPR) sources produce pairs of entangled photons 1-2, 3-4 and 5-6. Photon 2 from the inial state and photon 3 from the first ancillary pair are subjected to a joint BSM, and so are photon 4 from the first ancillary and photon 5 from the second ancillary pair. The two BSMs project outgoing photons 1 and 6 onto an entangled state. Thus the entanglement of the initial pair is swapped to an entanglement between photons 1 and 6.*

and 3 one knows immediately about the entanglement type between photons 1 and 4.

Without loss of generality, we assume in the first step that photons 2 and 3 have collapsed into the state $|\Phi^+\rangle_{23}$ as a result of the first BSM. The remaining four-photon state is then of the form

$$\begin{aligned} |\Psi\rangle_{1456} \quad = \quad & \tfrac{1}{2}\,[|\Psi^+\rangle_{16}|\Phi^-\rangle_{45} + |\Psi^-\rangle_{16}|\Phi^+\rangle_{45} \\ & -|\Phi^+\rangle_{16}|\Psi^-\rangle_{45} - |\Phi^-\rangle_{16}|\Psi^+\rangle_{45}] \end{aligned} \tag{4.3}$$

In a similar manner we perform a second BSM on photons 4 and 5. Again a detection of the state $|\Phi^+\rangle_{45}$ results in projecting the remaining photons 1 and 6 onto the Bell state

$$|\Psi^-\rangle_{16} = \frac{1}{\sqrt{2}}(|H\rangle_1|V\rangle_6 - |V\rangle_1|H\rangle_6) \tag{4.4}$$

4.3 Experimental Setup

A schematic diagram of our setup for multistage entanglement swapping is illustrated in Fig. (4.2). The used setup is very similar to the one used in the previous chapter (3). The pulsed high-intensity ultraviolet (UV) beam successively passes through three β-Barium-Borate (BBO) crystals to generate three polarization entangled photon pairs via type-II parametric down conversion [30]. For the joint BSM

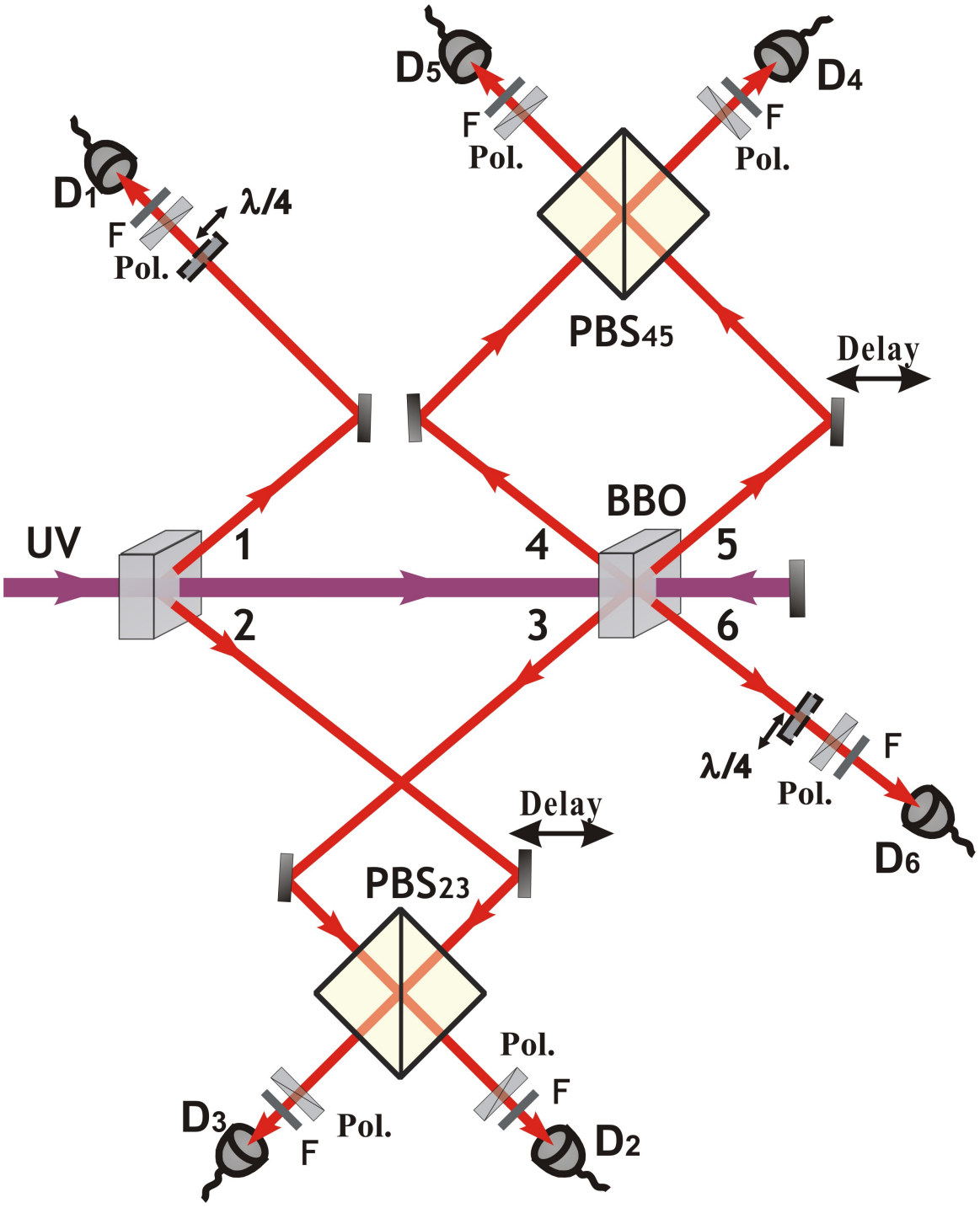

Figure 4.2: *A schematic diagram of the experimental setup. The focused ultraviolet laser beam passes through the first BBO generating photon pair 1-2. Refocussed, it passes through the second BBO generating the ancillary pair 3-4. After reflection it again passes through the second BBO generating pair 5-6. In order to perform a BSM of photons 2 and 3 (4 and 5), they are interfered at PBS23 (PBS45) and analyzed with polarizers at 45°. PBS1 and PBS6 are polarization analyzers for the swapped entangled state.*

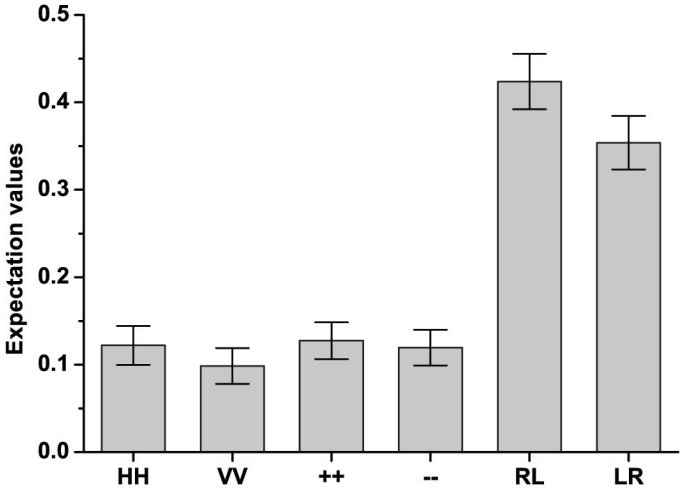

Figure 4.3: *Experimental expectation values for every correlation function of the entanglement witness for the swapped state. The results are derived by twofold coincidence measurements along three complementary common bases* ***(a)*** $|H\rangle|V\rangle$, ***(b)*** $|+\rangle|-\rangle$ *and* ***(c)*** $|R\rangle|L\rangle$, *conditioned on a fourfold coincidence event in* $|++++\rangle$ *for detectors D2-D3-D4-D5 which ensures two successful Bell state measurements.*

of photons 2 and 3 (photons 4 and 5), we choose to analyze the case of detecting the projection onto a $|\Phi^+\rangle$ state. Using once again the method of chapter (2.3.2) the Bell state analyzer allows the projection of photons 2 and 3 (4 and 5) onto the state $|\Phi^+\rangle$ upon the detection of a $|+\rangle|+\rangle$ or $|-\rangle|-\rangle$ coincidence at detectors D2 and D3 (D4 and D5). Again, only the $|+\rangle|+\rangle$ coincidences are registered, which yields an overall success efficiency of 1/64. The resulting state of photons 1 and 6 is polarization analyzed behind PBS1 and PBS6, respectively.

4.4 Experimental Results

As shown in equations Eq. (4.2, 4.3, 4.4) the projection measurements onto $|\Phi^+_{23}\rangle$ and $|\Phi^+_{45}\rangle$ leave photons 1 and 6 in the maximally entangled state $|\Psi^-_{16}\rangle$. In contrast to quantum state tomography, the measurement of witness operators does not provide a complete reconstruction of the original quantum state, it however allows to check with a minimal number of local measurements for an entanglement character of a quantum state (see section 2.2.3). To verify that the two photons really result in an entangled state, and thus the swapping operation is successful, the expectation value of the corresponding witness operator [110, 111] is expected to take a value between -1 and 0. In our case, the applied witness operator W is the most efficient one since it involves only the minimal number of local measurements [110]. It can

be measured locally by choosing correlated measurement settings, that involve only the simultaneous detection of linear, diagonal and circular polarizations for both photons. We have performed local measurements on the outgoing state of photons 1 and 6 in the three complementary bases; linear (computational) ($|H\rangle/|V\rangle$), diagonal ($|+\rangle/|-\rangle$) and circular ($|R\rangle/|L\rangle$).

The entanglement witness is given by

$$\begin{aligned}\hat{\mathcal{W}} \;=\; & \tfrac{1}{2}\,(|HH\rangle\langle HH| + |VV\rangle\langle VV| + |++\rangle\langle ++| \\ & +|--\rangle\langle --| - |RL\rangle\langle RL| - |LR\rangle\langle LR|).\end{aligned} \tag{4.5}$$

In the experiment, we perform measurements for each correlation function of the entanglement witness. The expectation values are shown in Fig. (4.3). Experimental integration time for each local measurement took about 60 hours and we recorded about 180 events of desired two-qubit coincidences. Every expectation value for a correlation function is obtained by making a von Neumann measurement along a specific basis and compute the probability over all the possible events. For example, for a HH correlation $\mathrm{Tr}(\hat{\rho}|HH\rangle\langle HH|)$, we perform measurements along the linear (computational) basis. Then its value is given by the number of coincidence counts of HH over the sum of all coincidence counts of HH, HV, VH and VV. We proceed likewise for the other correlation settings. The witness can then directly be evaluated to

$$\mathrm{Tr}(\hat{\rho}\hat{\mathcal{W}}) = -0.16 \pm 0.03. \tag{4.6}$$

The negativity of the measured witness implies clearly that the original entanglement has indeed been swapped. The imperfection of our data is due to the non-ideal quality of entangled states generated from the high power UV beam, as well as the partial distinguishability of independent photons at PBS23 and PBS45, which leads to non-perfect interferences and a degrading of the entanglement output quality [112, 113]. Moreover, double pair emission by a single source causes noise of an order of 10 spurious six-fold coincidences in 60 hours and was not subtracted in calculating the expectation value of the witness operator.

To ensure that there is no entanglement between photons 1 and 6 before neither of the entanglement swapping process, we have performed a complete quantum state tomography of the combined state. The experimental expectation values for various bases are illustrated in Fig. (4.4). Concurrence [72] is a monotone function of entanglement, ranging from 0 for a separable state to 1 for a maximally entangled state. In terms of concurrence, we can thus quantify the degree of entanglement through a reconstructed density matrix ρ_{init} for the initial combined state from the data shown in Fig. (4.4). The concurrence C_{init} derived from ρ_{init} is $C_{init} = \max(0, -0.39 \pm 0.01) = 0$. As expected, the concurrence C is exactly 0, which shows that photons 1 and 6 were independent and did not reveal any entanglement whatsoever before the swapping. Ideally, for a completely mixed state the expectation value for all local measurements should be 0, except for the unity operator,

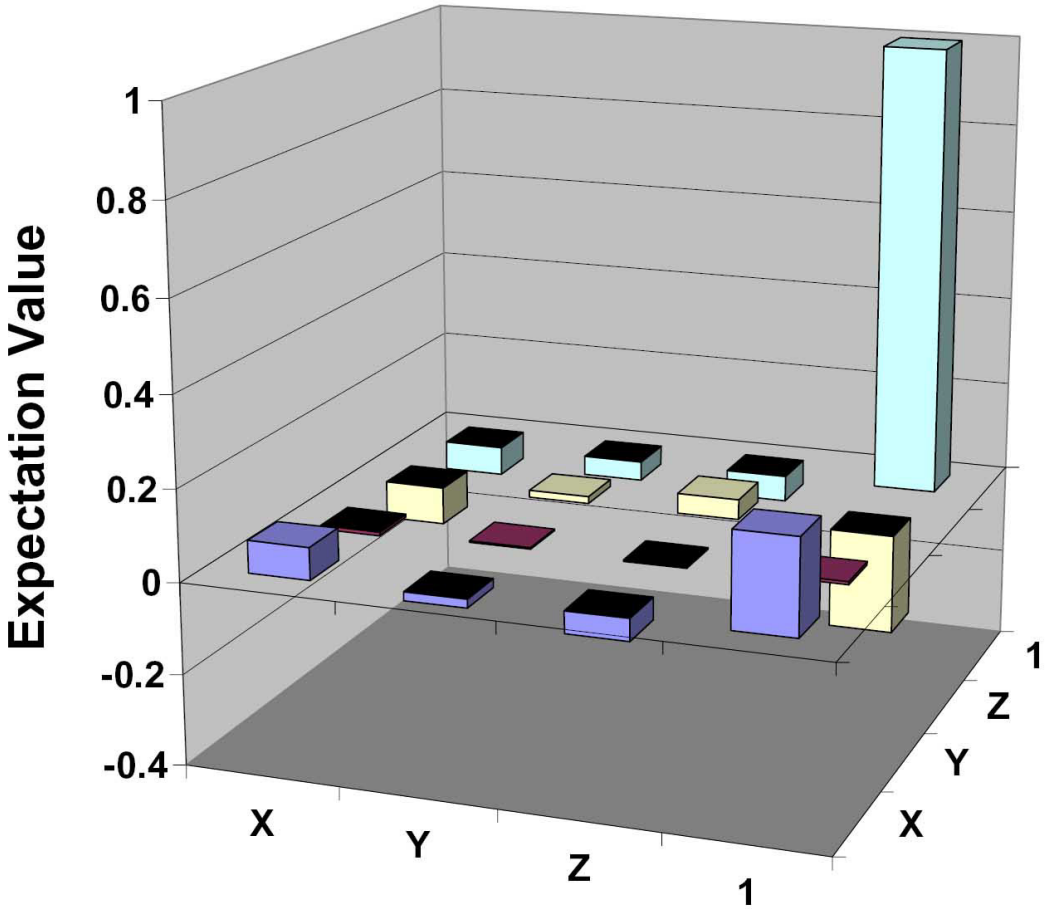

Figure 4.4: *Complete quantum state tomography on photons 1 and 6 before entanglement swapping. Label X corresponds to measurement setting $\hat{\sigma}_x$, while Y and Z are for $\hat{\sigma}_y$ and $\hat{\sigma}_z$, respectively. The result shows that the photons didn't reveal any entanglement whatsoever before the swapping operation.*

which should be 1. The contributions of the measurement settings other than the unity operator are mainly due to noise caused by scattered light of the UV beam at the BBO crystal. After the two-stage entanglement swapping, entanglement arises as unambiguously confirmed by the witness measurement of Eq. (4.6).

4.5 Discussion

In this chapter, we have discussed the first demonstration of a proof-of-principle implementation of a two-stage entanglement swapping using photonic qubits. The feasibility and effectiveness of this process has been verified by a successful distribution of genuine entanglement after two simultaneously independent swapping processes. This result yields the possibility of immediate near-future applications of various practical QIP tasks. If combined with narrow-band entanglement sources, the implementation of quantum relays (without quantum memory) and quantum repeaters (with quantum memory) for either free space or fiber-based entanglement distribution could become within current reach, as well as quantum state transfer and quantum cryptography networks in a more efficient way and over much larger distances of around hundreds of kilometers. Our demonstration also allows for the possibility of utilizing multi-party, multiple stages entanglement swapping to achieve global quantum communication networks, though with significant challenges ahead [43].

Chapter 5

Teleportation-Based Controlled-NOT Gate for Fault-Tolerant Quantum Computation

5.1 Introduction

Quantum computers promise dramatic speed ups for many computational tasks [21, 20] and the ability to simulate nature at the micro scale, which is not possible with conventional computers. For large scale quantum computation however, the coupling of physical qubits to the environment imposes a major challenge for a real-life implementation [114, 115, 116]. The teleportation-based scheme offers a way for scalable quantum computing. Most attractively, this architecture allows for realizations of universal quantum gates in a fault-tolerant manner as shown by Gottesman and Chuang [40], and in fact serves as an important basis for measurement-based quantum computing. In this chapter we discuss the first implementation of a proof-of-principle experiment of this architecture by demonstrating a teleportation-based two-qubit controlled-NOT (C-NOT) gate through linear optics with our six-photon interferometer. We prepare a two-photon input, which can be in a completely random state together with a four-photon cluster state used as the working base. The information of the input-qubits is then transferred onto the cluster state via two separate Bell-state measurements (BSM). The two-photon output is ready to use and is verified by measurements in three orthogonal basis. The obtained results clearly proof the involved working principles and the entangling capability of the gate. Our experiment could represent an important mile stone towards the feasibility of realistic quantum computers and could trigger many further applications in linear quantum optics.

5.2 Fault-Tolerant Quantum Gates

Any system in nature couples to its environment. In quantum computation this can lead to errors among the processed qubits making quantum error correction schemes necessary. Several algorithms to encode a logic qubit onto a number of physical qubits have been developed [117, 118, 86, 119]. These codes are able to correct for any single qubit error, as long as maximally one of the physical qubits has been altered. After decryption one is able to recover the unaltered, original logic qubit. The minimal number of physical qubits that can be used to correct for one error is five [100, 120]. A next problem arises once we want to perform quantum gates, i.e. to perform logic operations on the protected data. Since the logic qubit has been encoded, we need to perform corresponding operations on the physical qubits. Depending on the characteristics of the chosen code and gate (in particular conditional gates), errors may then not only propagate between blocks of encoded qubits but also within them. This can compromise the code's ability to correct for these errors. The solution are so called "fault-tolerant quantum gates". A procedure is fault-tolerant if its failing components (this includes the input) do not spread more errors in the block of encoded output qubits than the code can correct.

In 1999, Gottesman and Chuang introduced a protocol to implement any quantum gate needed for quantum computation in a fault-tolerant manner [40]. Their work has opened doors to new ideas and has triggered several important protocols in theoretical quantum information processing, such as the "One-way quantum computer" [121] (see chapter 2.2.2) or the KLM scheme [29]. However, not even an in-principle implementation of a teleportation-based quantum gate, as suggested by Gottesman and Chuang, has been realized up to now, which could demonstrate the experimental possibility of fault-tolerant quantum computation.

In the following, we discuss the first non-trivial realization of the scheme. We exploit our six photon interferometer described in chapter (3) to combine the techniques of quantum teleportation of a composite system [122] and the creation of a four-qubit photon cluster state [59]. We chose to implement a C-NOT gate, since together with very easy to implement single qubit operations, a C-NOT gate is sufficient to perform all logic operations needed for quantum computation [29].

The approach of Gottesman and Chuang, a generalization of quantum teleportation [35, 36] (see chapters 2.1.3, 3.2), is straight forward and requires only a minimum of resources. A key element of their work is the C-NOT gate, which acts on two qubits, a control and a target qubit. The logic table of the C-NOT operation (U^{C-NOT}) is given by (see chapter 2.1.2) $|H\rangle_1|H\rangle_2 \rightarrow |H\rangle_1|H\rangle_2$, $|H\rangle_1|V\rangle_2 \rightarrow |V\rangle_1|V\rangle_2$, $|V\rangle_1|H\rangle_2 \rightarrow |V\rangle_1|H\rangle_2$ and $|V\rangle_1|V\rangle_2 \rightarrow |H\rangle_1|V\rangle_2$, where we have used the photon polarization degree of freedom to encode our qubits. A schematic diagram of the procedure can be observed in Fig. (5.1a). In the following, we will first present a rather conceptual approach to the scheme and then discuss it in more detail.

One starts with the two input qubits $|T\rangle_1$ (target) and $|C\rangle_2$ (control). Instead of

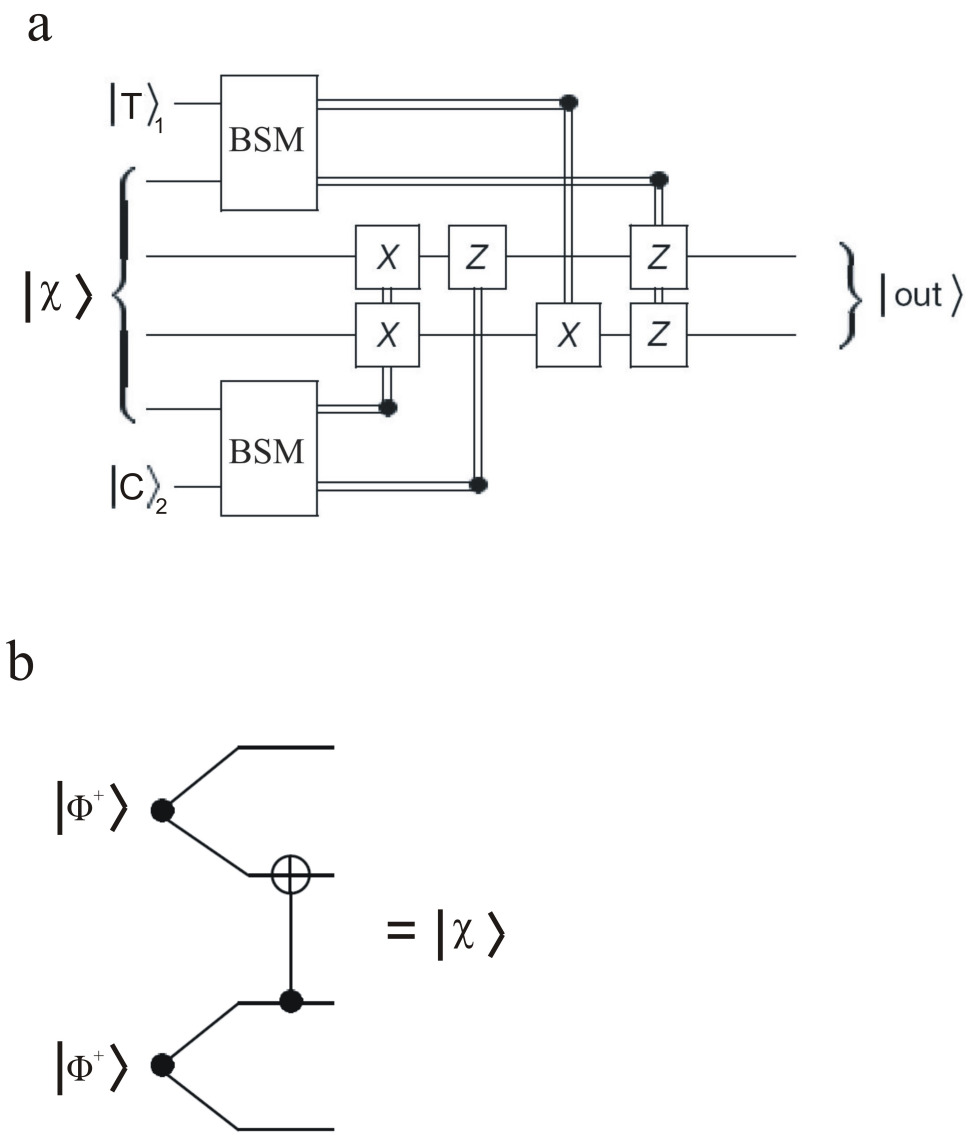

Figure 5.1: ***(a)*** *Quantum circuit for teleporting two qubits through a C-NOT gate. Time flow is from left to right. The input consisting of the target qubit $|T\rangle_1$ and control qubit $|C\rangle_2$ can be arbitrarily chosen. Bell State Measurements (BSMs) are performed between the input states and the outer qubits of the special entangled state $|\chi\rangle$. Depending on the outcome of the BSMs, local unitary operations (X, Z) are conducted on the remaining qubits of $|\chi\rangle$, which then form the output $|out\rangle = U^{C-NOT}|T\rangle_1|C\rangle_2$. Single lines correspond to qubits and double lines represent classical bits.* ***(b)*** *The special entangle state $|\chi\rangle$ can be constructed by performing a C-NOT gate on two EPR pairs, with $|\Phi^+\rangle = \frac{1}{\sqrt{2}}(|H\rangle|H\rangle + |V\rangle|V\rangle)$.*

directly performing complicated gate operations on the input qubits, one prepares in forehand a special entangled four-qubit state $|\chi\rangle$. After verification that the creation of $|\chi\rangle$ was successful, one transfers the data of the input qubits onto $|\chi\rangle$ by quantum teleportation. This is done by successively performing a joint "Bell-State-Measurement" (BSM) between the target (control) qubit and an outer qubit of $|\chi\rangle$, i.e. one projects the target (control) qubit and one of the outer qubits of $|\chi\rangle$ onto a joint two-particle "Bell state". As a direct consequence of the projective BSMs and the four-partite entanglement of $|\chi\rangle$, the remaining two (output) qubits already posses the information originally carried by the input qubits, i.e. the input state is teleported onto the four-particle state $|\chi\rangle$. To finish the procedure – just like in the original teleportation scheme (see chapter 3.2) – we need to apply single qubit (Pauli) operations to the output qubits, depending on the outcome of the BSMs.

Due to the special entanglement characteristics of $|\chi\rangle$, the output state is equivalent to the desired unitary transformation of the input state given by

$$|out\rangle = \hat{U}^{C-NOT}|T\rangle_1|C\rangle_2. \tag{5.1}$$

This can be better understood by a closer look at the special entangled state $|\chi\rangle$. It is a four-particle cluster state [121] (see chapter 2.2.2) of the form

$$|\chi\rangle = \frac{1}{2}\left((|H\rangle|H\rangle + |V\rangle|V\rangle)|H\rangle|H\rangle + (|H\rangle|V\rangle + |V\rangle|H\rangle)|V\rangle|V\rangle\right). \tag{5.2}$$

which can be created simply by performing a C-NOT operation on two EPR pairs as can be seen in Fig. (5.1b). This C-NOT operation is the essential difference to the original teleportation scheme and is the reason for the fact that the output state is not identical to the input state, but rather in the desired form of Eq. (5.1).

Let us now have a look at the scheme in more detail: Photons 1 and 2 constitute the input to our C-NOT gate. We assume that they are in a most general input state $|\Psi_{in}\rangle_{12}$, where:

$$|\Psi_{in}\rangle_{ij} = \alpha|H\rangle_i|H\rangle_j + \beta|H\rangle_i|V\rangle_j + \gamma|V\rangle_i|H\rangle_j + \delta|V\rangle_i|V\rangle_j \tag{5.3}$$

The pre-factors α, β, γ and δ are four arbitrary complex numbers satisfying $|\alpha|^2 + |\beta|^2 + |\gamma|^2 + |\delta|^2 = 1$. In this case, Eq. (5.1) takes the form:

$$\begin{aligned} |\Psi_{out}\rangle_{ij} &= \hat{U}^{C-NOT}|\Psi_{in}\rangle_{ij} \\ &= \alpha|H\rangle_i|H\rangle_j + \beta|V\rangle_i|V\rangle_j + \gamma|V\rangle_i|H\rangle_j + \delta|H\rangle_i|V\rangle_j \end{aligned} \tag{5.4}$$

The target qubit i is flipped on the condition that the control qubit j is in the state $|V\rangle$.

Together with photons 3, 4, 5 and 6 in the cluster state of Eq. (5.2) we can now express the combined state of all six photons in terms of Bell states for photons 1-3 and 2-5 and in terms of the desired output state $|\Psi_{out}\rangle_{46}$ for photons 4-6 with

corresponding Pauli operations:

$$
\begin{aligned}
|\Psi_{in}\rangle_{12} \otimes |\chi\rangle_{3456} = \\
|\Phi^+\rangle_{13}|\Phi^+\rangle_{25} \quad & |\Psi_{out}\rangle_{46} \quad +|\Phi^+\rangle_{13}|\Phi^-\rangle_{25} \quad \hat{\sigma}_z^6|\Psi_{out}\rangle_{46} \\
+|\Phi^+\rangle_{13}|\Psi^+\rangle_{25} \quad & \hat{\sigma}_x^4\hat{\sigma}_x^6|\Psi_{out}\rangle_{46} \quad +|\Phi^+\rangle_{13}|\Psi^-\rangle_{25} \quad \hat{\sigma}_x^4\hat{\sigma}_x^6\hat{\sigma}_z^6|\Psi_{out}\rangle_{46} \\
+|\Phi^-\rangle_{13}|\Phi^+\rangle_{25} \quad & \hat{\sigma}_z^4\hat{\sigma}_z^6|\Psi_{out}\rangle_{46} \quad +|\Phi^-\rangle_{13}|\Phi^-\rangle_{25} \quad \hat{\sigma}_z^4|\Psi_{out}\rangle_{46} \\
+|\Phi^-\rangle_{13}|\Psi^+\rangle_{25} \quad & \hat{\sigma}_x^4\hat{\sigma}_z^4\hat{\sigma}_x^6\hat{\sigma}_z^6|\Psi_{out}\rangle_{46} \quad +|\Phi^-\rangle_{13}|\Psi^-\rangle_{25} \quad \hat{\sigma}_x^4\hat{\sigma}_z^4\hat{\sigma}_x^6|\Psi_{out}\rangle_{46} \\
+|\Psi^+\rangle_{13}|\Phi^+\rangle_{25} \quad & \hat{\sigma}_x^4|\Psi_{out}\rangle_{46} \quad +|\Psi^+\rangle_{13}|\Phi^-\rangle_{25} \quad \hat{\sigma}_x^4\hat{\sigma}_z^6|\Psi_{out}\rangle_{46} \\
+|\Psi^+\rangle_{13}|\Psi^+\rangle_{25} \quad & \hat{\sigma}_x^6|\Psi_{out}\rangle_{46} \quad +|\Psi^+\rangle_{13}|\Psi^-\rangle_{25} \quad \hat{\sigma}_x^6\hat{\sigma}_z^6|\Psi_{out}\rangle_{46} \\
+|\Psi^-\rangle_{13}|\Phi^+\rangle_{25} \quad & \hat{\sigma}_x^4\hat{\sigma}_z^4\hat{\sigma}_z^6|\Psi_{out}\rangle_{46} \quad +|\Psi^-\rangle_{13}|\Phi^-\rangle_{25} \quad \hat{\sigma}_x^4\hat{\sigma}_z^4|\Psi_{out}\rangle_{46} \\
+|\Psi^-\rangle_{13}|\Psi^+\rangle_{25} \quad & \hat{\sigma}_z^4\hat{\sigma}_x^6\hat{\sigma}_z^6|\Psi_{out}\rangle_{46} \quad +|\Psi^-\rangle_{13}|\Psi^-\rangle_{25} \quad \hat{\sigma}_z^4\hat{\sigma}_x^6|\Psi_{out}\rangle_{46}
\end{aligned}
\tag{5.5}
$$

From this we can directly see, that two BSMs on photons 1-3 and 2-5, project the output photons 4 and 6 onto a state that is directly correlated to the desired final state given in Eq. (5.4). The only thing left to do is to apply corresponding Pauli operations, depending on the outcome of the BSMs.

Note, that in the above scheme all qubits are logic qubits. However, the scheme generalizes in a straight forward manner when we use a larger number of physical qubits to encode our logic qubits. The procedure is then fault-tolerant since all operations are transversal, i.e. qubits of one block of encoded qubits interact only with corresponding qubits in other code blocks. A further advantage is the fact that only classically controlled single-qubit operations and BSMs are needed to perform the actual gate. The resource of the special entangled state $|\chi\rangle$ can be constructed in forehand. If its generation fails nothing is lost by discarding it and trying again until successful generation. We would like to emphasize two aspects: First, the setup can be used to process any unknown input state and second, several other quantum gates can be implemented by this scheme. The choice of gate only depends on the form of the ancillary state $|\chi\rangle$.

5.3 Experimental Setup

A schematic diagram of our experimental setup is shown in Fig. (5.2). We align each β-barium borate (BBO) crystal carefully to produce a pair of polarization entangled photons i and j in the state:

$$|\Psi^+\rangle_{ij} = \frac{1}{\sqrt{2}}\left(|H\rangle_i|H\rangle_j + |V\rangle_i|V\rangle_j\right) \tag{5.6}$$

With the help of wave plates (HWPs) and polarizers, we prepare photon pair 1-2 in the desired two-qubit input state $|\psi\rangle_{12}$. To construct the cluster state $|\chi\rangle$, we use the method described in ref. [59]. Initially, photons 3, 4, 5 and 6 are in the state:

$$
\begin{aligned}
|\Psi^+\rangle_{34} \otimes |\Psi^+\rangle_{56} \quad = \quad & \frac{1}{2}\big(|H\rangle_3|H\rangle_4|H\rangle_5|H\rangle_6 + |H\rangle_3|H\rangle_4|V\rangle_5|V\rangle_6 \\
& +|V\rangle_3|V\rangle_4|H\rangle_5|H\rangle_6 + |V\rangle_3|V\rangle_4|V\rangle_5|V\rangle_6\big)
\end{aligned}
\tag{5.7}
$$

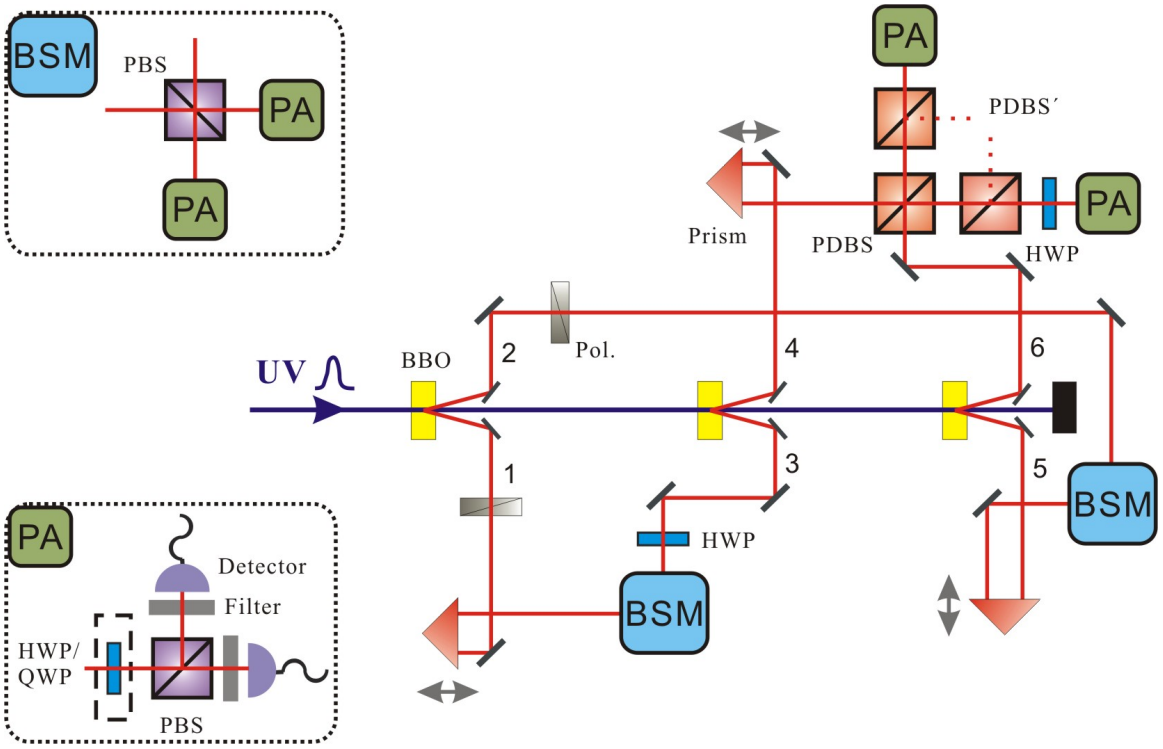

Figure 5.2: *A schematic diagram of the experimental setup. A high-intensity pulsed ultraviolet laser beam (UV) passes through three β-barium borate (BBO) crystals to generate three polarization entangled photon pairs via SPDC (see chapter 2.3.1). At the first BBO the UV generates a photon pair in modes 1 and 2 (that is, the input consisting of the target and control qubit). After the crystal, the UV is refocused onto the second BBO to produce another entangled photon pair in modes 3 and 4 and correspondingly for modes 5 and 6. Photons 4 and 6 are then overlapped at a PDBS and together with photons 3 and 5 constitute the cluster state. Two PDBS' are used for state normalization. The prisms are mounted on step motors and are used to compensate the time delay for the interference at the PDBS and the BSMs. A BSM is performed by overlapping two incoming photons on a PBS and two subsequent polarization analyses (PA). A PA projects the photon onto an unambiguous polarization depending on the basis determined by the choice of HWP or QWP. The photons are detected by silicon avalanched single-photon detectors. Coincidences are recorded with a coincidence unit clocked by the infrared laser pulses. Pol. are polarizers to prepare the input state and Filter label the narrow band filters with* $\Delta_{FWHM} = 3.2$ *nm.*

We direct photons 4 and 6 to the two input modes of a polarization dependent beam splitter (PDBS), respectively. The transmission T_H (T_V) of horizontally (vertically) polarized light at the PDBS is 1 (1/3), and we thus get

$$\begin{aligned}\longrightarrow\quad & \frac{1}{2}\big(|H\rangle_3|H\rangle_{4'}|H\rangle_5|H\rangle_{6'} + \frac{1}{\sqrt{3}}|H\rangle_3|H\rangle_{4'}|V\rangle_5|V\rangle_{6'} \\ & + \frac{1}{\sqrt{3}}|V\rangle_3|V\rangle_{4'}|H\rangle_5|H\rangle_{6'} - \frac{1}{3}|V\rangle_3|V\rangle_{4'}|V\rangle_5|V\rangle_{6'}\big). \end{aligned} \tag{5.8}$$

Here we have neglected terms with more than one photon in a single output mode of the PDBS, since in the experiment we post select only terms that lead to a six-fold coincidence.

In order to symmetrize the state we place a PDBS' ($T_H = 1/3, T_V = 1$) in each output mode of the PDBS and receive

$$\begin{aligned}\longrightarrow\quad & \frac{1}{6}\big(|H\rangle_3|H\rangle_{4''}|H\rangle_5|H\rangle_{6''} + |H\rangle_3|H\rangle_{4''}|V\rangle_5|V\rangle_{6''} \\ & + |V\rangle_3|V\rangle_{4''}|H\rangle_5|H\rangle_{6''} - |V\rangle_3|V\rangle_{4''}|V\rangle_5|V\rangle_{6''}\big). \end{aligned} \tag{5.9}$$

This is already the desired four-qubit cluster state of Eq. (5.2) up to local unitary operations. To bring it to the desired form, we place half-wave plates (HWPs) – with an angle of 22.5° between the fast and the horizontal axis – into arms 3 and 4. This yields

$$\begin{aligned}\longrightarrow\quad & \left(|H\rangle_3|H\rangle_{4''} + |V\rangle_3|V\rangle_{4''}\right)|H\rangle_5|H\rangle_{6''} \\ & + \left(|H\rangle_3|V\rangle_{4''} + |V\rangle_3|H\rangle_{4''}\right)|V\rangle_5|V\rangle_{6''} \quad = |\chi\rangle_{34''56''}, \end{aligned} \tag{5.10}$$

where we have neglected the overall pre-factor 1/6 and we arrive at the desired ancillary four-photon cluster state $|\chi\rangle$ described in ref. [40]. Note, that altogether, the probability of having one photon in each desired output, and thus having successfully created the cluster state, is 1/9.

Teleporting the input data of $|\psi\rangle_{12}$ to $|\chi\rangle_{3456}$ requires joint BSMs on photons 1-3 and photons 2-5. To demonstrate the working principle of the teleportation-based C-NOT gate, it is sufficient to identify one of the four Bell states in both BSMs (see chapter 3.4). However, in the experiment we decide to analyze the two Bell states $|\Phi^+\rangle$ and $|\Phi^-\rangle$ to increase the efficiency - the fraction of success - by a factor of 4. This is achieved by again using the method described in chapter (2.3.2). We interfer photons 1-3 and photons 2-5 on a polarizing beam splitter (PBS) and perform a polarization analysis (PA) on the two outputs [96]. With the help of a HWP, a PBS and fibre-coupled single photon detectors, we are able to project the input photons of the BSM onto $|\Phi^+\rangle$ upon the detection of a $|+\rangle|+\rangle$ or $|-\rangle|-\rangle$ coincidence, and onto $|\Phi^-\rangle$ upon the detection of a $|+\rangle|-\rangle$ or $|-\rangle|+\rangle$ coincidence.

Thus, our projective BSMs leave the remaining photons of the cluster state 4-6 in a state that is identical to the desired output state up to unitary transformations. We thus have to consider four different results of the BSMs:

Result of BSMs	Output state
$\|\Phi^+\rangle_{13}\|\Phi^+\rangle_{25}$	$\|\Psi_{out}\rangle_{46}$
$\|\Phi^+\rangle_{13}\|\Phi^-\rangle_{25}$	$\hat{\sigma}_z^6\|\Psi_{out}\rangle_{46}$
$\|\Phi^-\rangle_{13}\|\Phi^+\rangle_{25}$	$\hat{\sigma}_z^4\hat{\sigma}_z^6\|\Psi_{out}\rangle_{46}$
$\|\Phi^-\rangle_{13}\|\Phi^-\rangle_{25}$	$\hat{\sigma}_z^4\|\Psi_{out}\rangle_{46}$

To receive the desired final state of photons 4 and 6, we have to apply corresponding Pauli operations, depending on the outcome of the BSMs.

To demonstrate that our teleportation-based C-NOT gate protocol works for a general unknown polarization state of photons 1-2, we decide to measure the truth table of our gate. That is, we measure the output for all possible combinations of the two-qubit input in the computational basis. However, that is not sufficient to show the quantum characteristic of a C-NOT gate. The remarkable feature of a C-NOT gate is its capability of entangling two separable qubits. Thus, to fully demonstrate the successful operation of our protocol, we furthermore choose to perform the entangling operation:

$$|H\rangle_T \otimes \frac{1}{\sqrt{2}}(|H\rangle_C + |V\rangle_C) \rightarrow \frac{1}{\sqrt{2}}(|H\rangle_T|H\rangle_C + |V\rangle_C|V\rangle_C) = |\Phi^+\rangle_{TC} \tag{5.11}$$

In the experiment, we observe on average 7×10^4 photon pairs per second from each source. With this high-intensity entangled photon source we obtain in total 3.5 six-photon events per minute. This is less than half the count rate of our previous six-photon experiments of chapters 3 and 4. Since the new scheme is more complex and involves more interferences, the fidelity requirements are more stringent. Thus, we have to reduce the pump power from 1.0 W to 0.8 W in order to reduce noise contributions that arise from the emission of two pairs of down-converted photons by a single source (double-pair-emission).

5.4 Experimental Results

We quantify the quality of our output state by looking at the fidelity as defined in Eq. (2.32). To analyze the operation and to experimentally measure the fidelity of the two-qubit output, we again use PAs. Depending on the measurement setting we use quarter wave plates (QWPs) or HWPs in front of the PBS.

The fidelity measurements for the truth table are straightforward. Conditional on detecting a fourfold coincidence at the two BSMs, we analyze the output photons 4-6 in the computational (H/V) basis. Depending on the type of coincidence at the BSM ($+\rangle|+\rangle$, $|+\rangle|-\rangle$, $|-\rangle|+\rangle$, $|-\rangle|-\rangle$), i.e. is depending onto which Bell state the photons have been projected, we analyze the output by taking into account the corresponding unitary transformation. Since this state analysis only involves

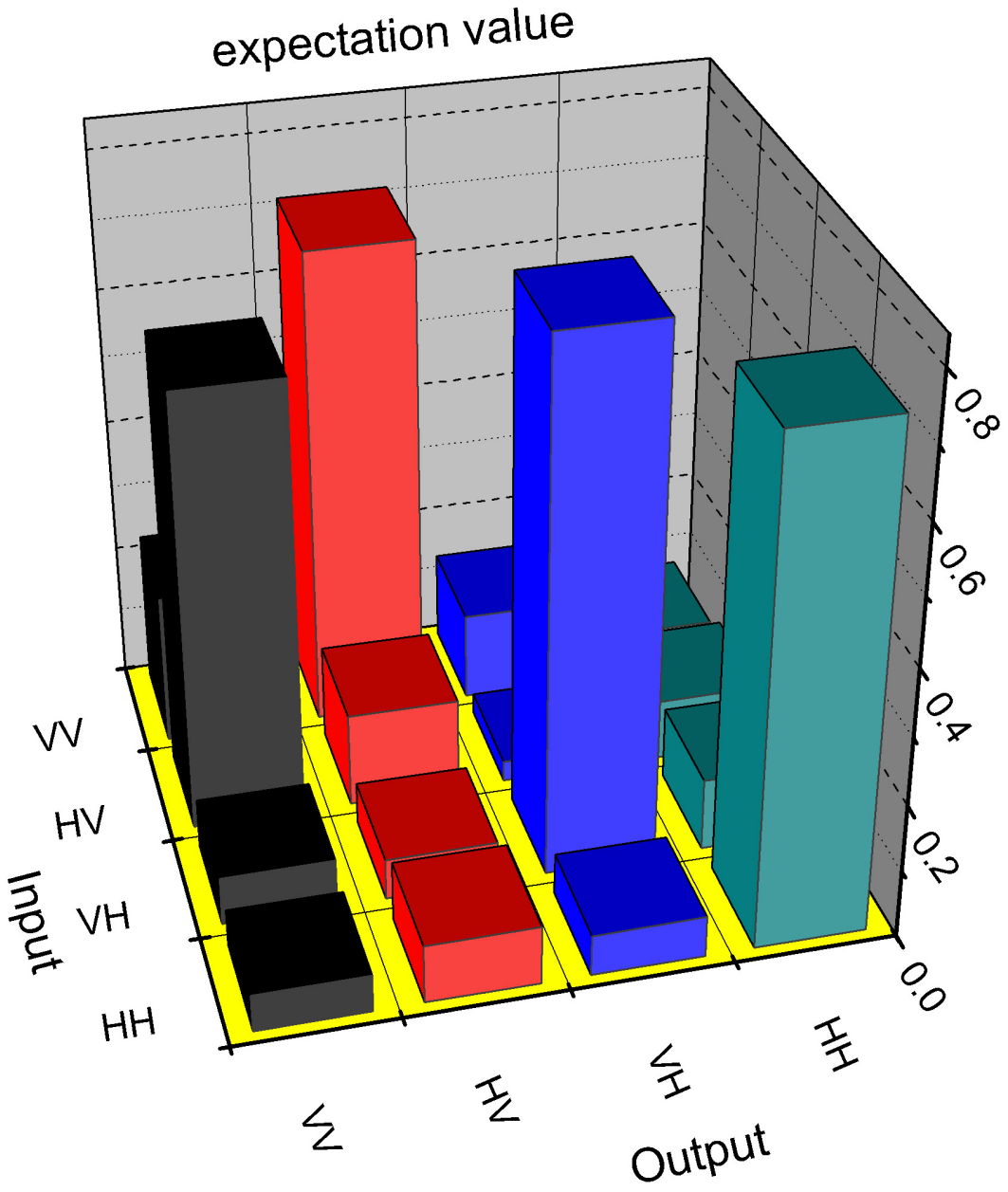

Figure 5.3: *Experimental results for truth table of the C-NOT gate. The first qubit is the target and the second is the control qubit. The average fidelity for the truth table is* 0.72 ± 0.05.

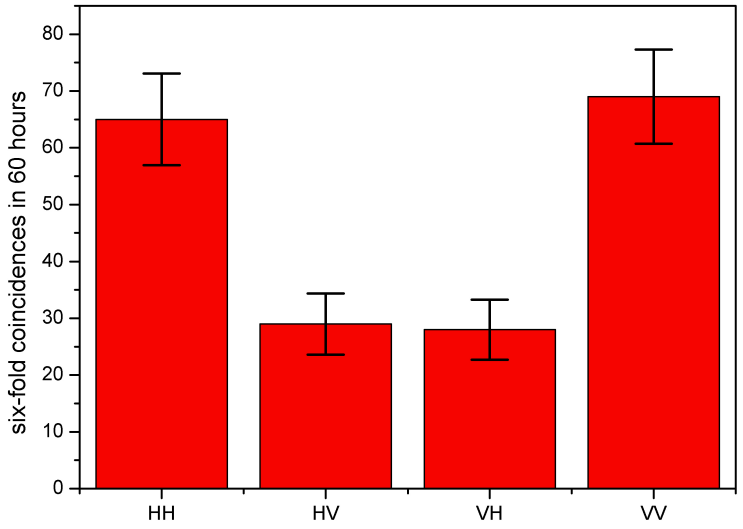

Figure 5.4: *Experimental results for the fidelity measurement of the entangled output state in the* ***computational*** *basis. The measured expectation value for* $\langle\hat{\sigma}_z\hat{\sigma}_z\rangle$ *is* 0.403 ± 0.066.

orthogonal measurements on individual qubits, the fidelity of the output state is directly given by the fraction of observing the desired state. The measurement results are shown in Fig. (5.3). The experimental integration time for each possible combination of the input photons was about 50 hours and we recorded about 120 desired two-qubit events, respectively. The overall count rate is reduced by a factor of 1/72 due to the success probability of creating the cluster state (1/9), the success probability of the BSMs (1/4) and due to the loss by initializing the input state with polarizers (1/2). On the basis of our original data, we conduct that the average fidelity for the two-photon output states of the truth table is 0.72 ± 0.05.

Just like in chapter (3.5), the determination of the entangling capability is a bit more complex. Since the output state is entangled, we are not able to determine its fidelity by a single measurement setting. However, with three successive local measurements on individual qubits we are still able to accomplish our task. This can be seen by a closer look at the fidelity under scrutiny:

$$F = Tr(\hat{\rho}|\Phi^+\rangle\langle\Phi^+|) = \frac{1}{4}Tr\left(\hat{\rho}(\hat{I} + \hat{\sigma}_x\hat{\sigma}_x - \hat{\sigma}_y\hat{\sigma}_y + \hat{\sigma}_z\hat{\sigma}_z)\right) \tag{5.12}$$

This implies that by measuring the expectation values $\langle\hat{\sigma}_x\hat{\sigma}_x\rangle$, $\langle\hat{\sigma}_y\hat{\sigma}_y\rangle$, $\langle\hat{\sigma}_x\hat{\sigma}_x\rangle$ we can directly obtain the fidelity of the entangled output state. The experimental results for the correlated local measurement settings are illustrated in Fig.'s (5.4, 5.5, 5.6). The integration time for the first two settings was about 60 hours and for the third

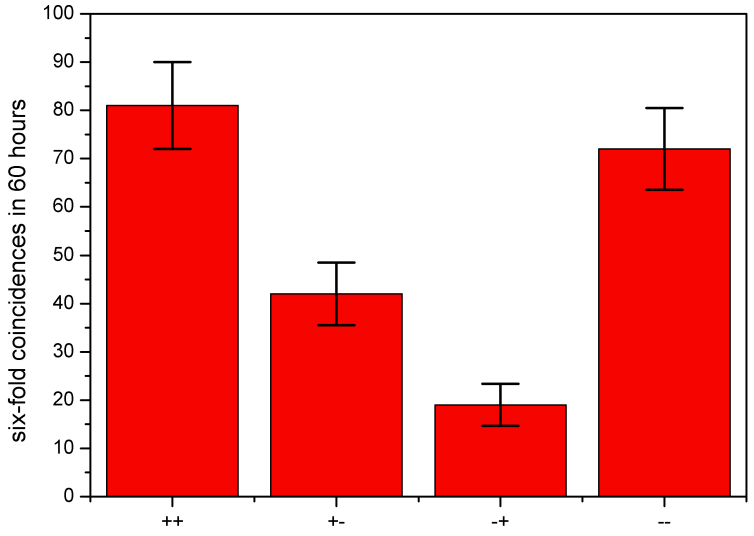

Figure 5.5: *Experimental results for the fidelity measurement of the entangled output state in the* ***diagonal*** *basis. The measured expectation value for* $\langle \hat{\sigma}_x \hat{\sigma}_x \rangle$ *is* 0.462 ± 0.057.

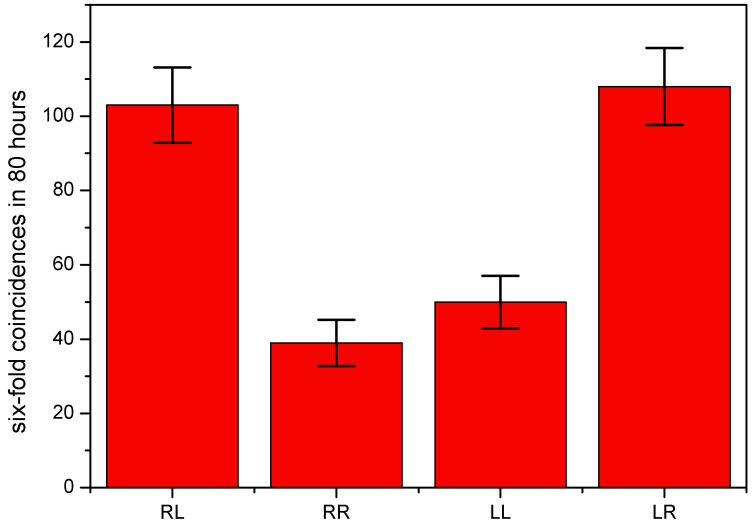

Figure 5.6: *Experimental results for the fidelity measurement of the entangled output state in the* ***circular*** *basis. The measured expectation value for* $\langle \hat{\sigma}_y \hat{\sigma}_y \rangle$ *is* -0.434 ± 0.062.

setting about 80 hours. Using the above equation, we determine from our experimental results an fidelity of 0.575 ± 0.027. This is well beyond the state estimation limit of 0.40 [97]. Furthermore and most importantly, the result proofs genuine entanglement between the two output photons, since it is above the entanglement limit of 0.50.

In addition, we have measured the fidelity of the used four-qubit cluster state $|\chi\rangle_{3456}$ and obtain an experimental result of 0.694 ± 0.003. This measurement has been performed in complete analogy to Kiesel et al. However, at the cost of a bit lower fidelity, we have achieved a count rate that is more than two orders of magnitudes larger. This is necessary in order to be able to perform the six-photon experiment in a reasonable amount of time over which the experimental setup can be kept stable.

5.5 Discussion

All experimental results are calculated directly from the original data and no noise contributions have been subtracted. All errors are of statistical nature and correspond to ± 1 standard deviations. The imperfection of the fidelities is mainly due to double-pair-emission. Furthermore, the limited interference visibility and imperfect input states also reduce the quality of our output states. Note that we achieve a better fidelity for the truth table than for the entangling case. This is because for the latter one the fidelity depends on the interference visibility at the PBS of the BSM.

With our setup we have demonstrated in principle the feasibility of the scheme by Gottesman and Chuang. Note however, that strictly speaking we did not show complete fault-tolerance, since in our experiment we did not encode logic qubits onto a larger number of physical qubits. The principle of the scheme, on the other hand, stays exactly the same and the developed techniques of our setup can be readily extended for the case of a larger number of encoded qubits. Our experiment thus constitutes an important step towards the realization of quantum computation. Along this line, the generation of a large number of qubits, as well as an improvement of the fidelity – needed for realistic quantum computation – still requires extensive efforts in the future.

In this chapter, we have discussed the experimental realization of a C-NOT gate based on quantum teleportation. With our six-photon architecture we have experimentally demonstrated the ability to entangle two separable qubits and have measured the truth table of the gate. This is the a non-trivial proof-of-principle implementation of the protocol introduced by Gottesman and Chuang. The teleportation-based scheme offers an alternative way for scalable quantum computing. Most attractively however, this architecture allows for realizations of universal quantum gates in a fault-tolerant manner, and in fact serves as an important basis for measurement-based quantum computing. Thus, our experimental demonstration of teleportation-

based linear optics quantum computing could serve as an essential basis towards resource-efficient, scalable quantum computation and yielding fault tolerance automatically.

Chapter 6

Entanglement of Six Photons in Graph States

6.1 Introduction

Graph states, as introduced in chapter (2.2.1), are important resources for quantum computation [61], quantum error correction [55], studies of multi-particle entanglement [53] and fundamental tests of non-locality [56, 57, 58] and de-coherence [60]. Many efforts have been undertaken to create multipartite entangled states in different physical systems [84, 64, 123, 25], where maximally up to eight ions have been entangled [25]. Encouraging progress [62, 67, 68, 124, 125, 126, 64] has been achieved in this direction, especially in the linear optics regime. Yet a major challenge ahead lies in the experimental generation of multi-qubit graph states.

In this chapter we discuss the experimental entanglement of six photons and engineering of multi-qubit graph states [62, 67, 68] with our six-photon interferometer (chapters 3, 4, 5). We have created two important examples of graph states, a six-photon GHZ state (see Eq. 2.23), the largest photonic Schrödinger-cat so far, and a six-photon cluster state. With small modifications, our method allows us, in principle, to create various further graph states, and therefore could open the way to experimental tests of, for example, quantum algorithms [61, 124] or loss- and fault-tolerant one-way quantum computation [125, 126].

6.2 Entanglement of Six-Photons in Graph States

Of special interest in the graph-state family are the GHZ states (see Eq. 2.23) and the cluster states (see chapters 2.2.1 and 2.2.2). Experimentally, six-atom GHZ states [123] and four-photon cluster states [64] have been realized. Here, we report the creation of six-photon GHZ states and cluster states with verifiable six-partite entanglement. To do so, we start from three EPR entangled photon pairs (see 2.3.1)

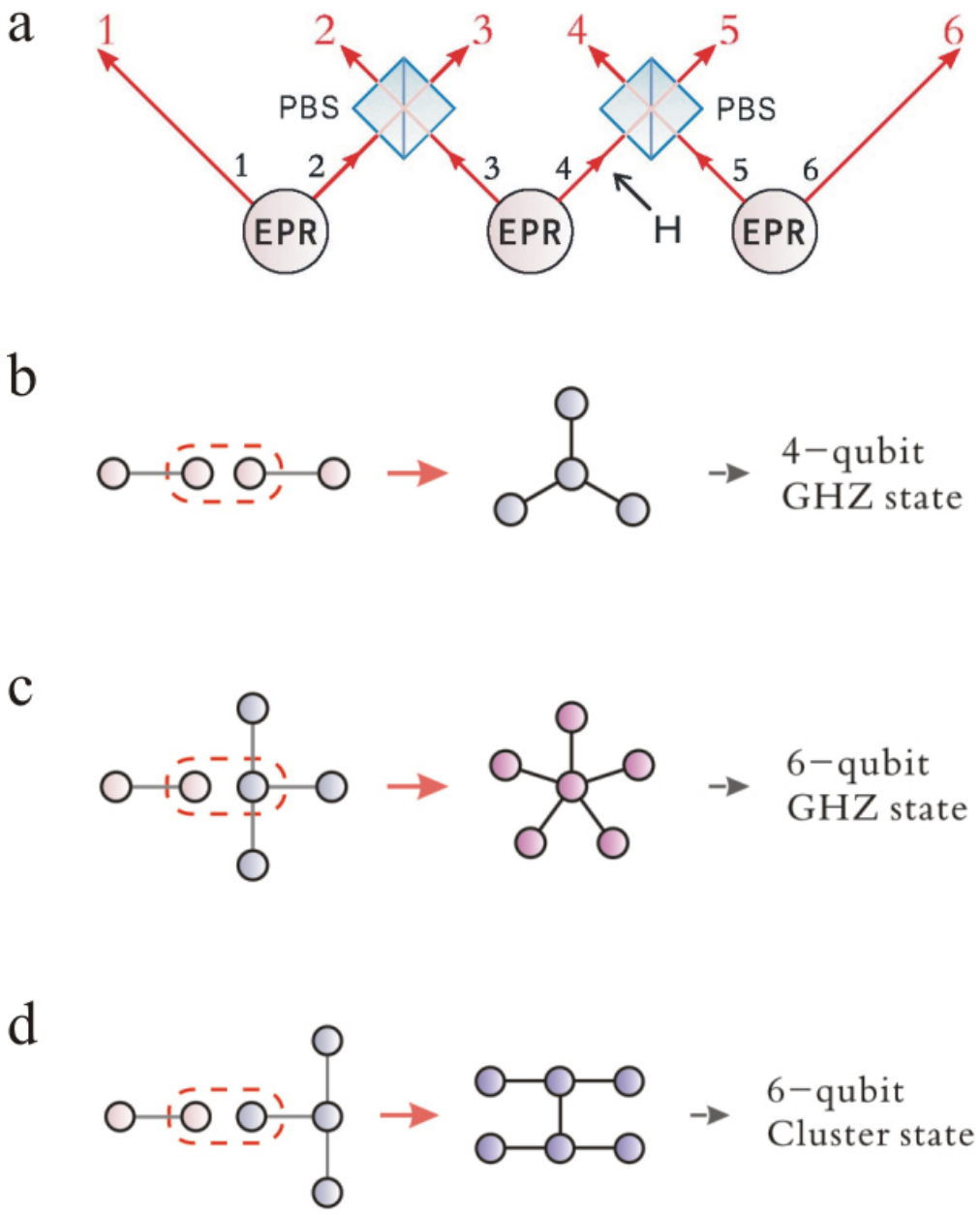

Figure 6.1: *Scheme to generate the six-photon graph states and their representations in the graph-state picture.* ***(a)*** *The six-photon GHZ state (1) and cluster state (2) are created by combining three pairs of entangled photons at PBSs. The Hadamard gate (H) is inserted for generation of the cluster state.* ***(b)-(d)*** *Underlying graphs of the six-photon graph states and how they are created by post-selected fusion operations. The graph state can be thought of as being constructed by first preparing the qubits at each vertex in the state* $|+\rangle$ *and then applying controlled phase gates between pairs of neighbouring qubits. Here, we use the post-selecting fusion operation, that is, combining photons at a PBS, to generate multi-qubit graph states efficiently. In the star graph, we refer to the central node as the root and the others as leaves.*

in the state

$$|\Phi^+\rangle_{ij} = \frac{1}{\sqrt{2}}\left(|H\rangle_i|H\rangle_j + |V\rangle_i|V\rangle_j\right), \tag{6.1}$$

As shown in Fig. (6.1a), we superpose photons in modes 2 and 3 (4 and 5) at polarizing beam splitters (PBSs) (see chapter 2.3.2). As the PBS transmits H and reflects V polarization, only if both incoming photons have the same polarization can they go to different outputs [127, 95]. Thus, a coincidence detection of all six outputs corresponds to the state

$$|G_6\rangle = \frac{1}{\sqrt{2}}\left(|H\rangle_1|H\rangle_2|H\rangle_3|H\rangle_4|H\rangle_5|H\rangle_6 + |V\rangle_1|V\rangle_2|V\rangle_3|V\rangle_4|V\rangle_5|V\rangle_6\right), \tag{6.2}$$

which is a six-photon GHZ state, exhibiting an equal superposition of two maximally different quantum states.

By applying a Hadamard gate on photon 4 before it enters into the PBS (see Fig. 6.1a), the above scheme can be readily modified to generate a six-photon cluster state. It can be considered in two steps: (1) combine photons 2 and 3, such that, on the basis of a coincidence detection, we get a four-photon GHZ state $(|H\rangle_1|H\rangle_2|H\rangle_3|+\rangle_4 + |V\rangle_1|V\rangle_2|V\rangle_3|-\rangle_4)/\sqrt{2}$; (2) combine photons 4 and 5, and by a similar reasoning we obtain what we call here a six-photon cluster state

$$\begin{aligned} |C_6\rangle = \; & \tfrac{1}{2}(|H\rangle_1|H\rangle_2|H\rangle_3|H\rangle_4|H\rangle_5|H\rangle_6 + |H\rangle_1|H\rangle_2|H\rangle_3|V\rangle_4|V\rangle_5|V\rangle_6 \\ & +|V\rangle_1|V\rangle_2|V\rangle_3|H\rangle_4|H\rangle_5|H\rangle_6 + |V\rangle_1|V\rangle_2|V\rangle_3|V\rangle_4|V\rangle_5|V\rangle_6), \end{aligned} \tag{6.3}$$

For an intuitive understanding, in Fig. (6.1) we show the underlying graph of the above states and how they grow from smaller (two-qubit) graph states. Up to local unitary transformations, the GHZ states correspond to star-shaped graphs, and the cluster states to lattice graphs (see chapters 2.2.1 and 2.2.2). The effect of combining two photons at a PBS can be described by the operator $|HH\rangle\langle HH| + |VV\rangle\langle VV|$, leading to the fusion of two separate graph states into a single one [125, 68]. Specifically, Fig. (6.1c) (Fig. (6.1d)) shows that when a two-qubit graph state is combined with the root (leaf) node of a four-qubit star graph, a six-qubit GHZ (cluster) state is produced.

A nice feature of the graph-state representation (see Fig. 2.6 and Fig. 2.7) is that many properties of the graph states and their potential use in QIP can be revealed by their underlying graph. For example, the star-graph states have multiple leaf nodes, which are referred to as micro-clusters in refs [62, 125] and can be used in the so-called parallel fusion for building up large cluster states. The graph of the six-qubit cluster state (Eq. 6.3) forms a standard quantum circuit under the one-way computer model of chapter (2.2.2). Moreover, its geometry embodies a tree-shaped graph, which is the basic building block for loss-tolerant one-way quantum computing [126]. Another interesting feature of the cluster state next to itself, is that even the remaining mixed four-qubit state, after two qubits have been traced out, leads to a GHZ argument for non-locality [57], showing a surprisingly strong entanglement persistency.

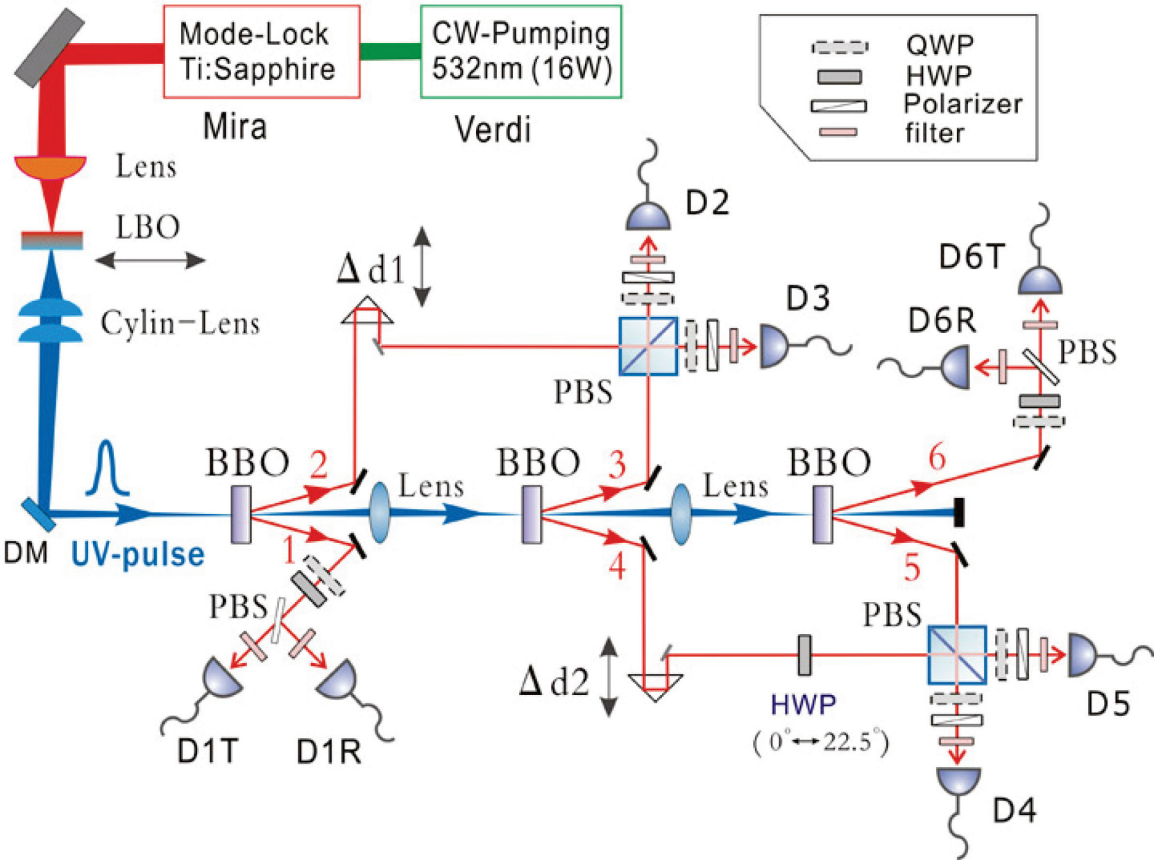

Figure 6.2: *Experimental set-up for the generation of six-photon graph states. The ultraviolet laser beam is circularized and focused on the three BBO crystals to produce three pairs of entangled photons. The entangled photons are spectrally filtered by narrow-band filters and then detected by fibre-coupled single-photon detectors* $(D_{1T}, ..., D_{6R})$*. We use a programmable multichannel coincidence unit to register the multi-fold coincidence events. For polarization analysis, half and quarter-wave plates (HWP, QWP) together with polarizers or PBSs are used. By changing the angle* (θ) *of the HWP at path 4, our set-up is tunable to generate the six-photon GHZ states* $(\theta = 0°)$ *and cluster state* $(\theta = 22.5°)$*.*

6.3 Experimental Setup

Compared to the experiments described in chapters (3, 4, 5) we have slightly changed our setup described in chapter (3.3). The setup is illustrated in Fig. (6.2). Pumped by the continuous-wave green laser, the mode-locked Ti:sapphire laser outputs a pulsed infrared laser with a central wavelength of 788 nm (instead of 780 nm), a pulse duration of 120 fs (instead of 180 nm) and a repetition rate of 76MHz, which passes through the LBO crystal (again mounted on a motorized translation stage) and is up-converted to ultraviolet with a wavelength of $\lambda = 394nm$ (instead of $\lambda = 390nm$). We again use type-II SPDC to produce entangled photons (chapter 2.3.1). The ultraviolet laser pulse successively passes through three BBO crystals to generate entangled photon pairs in spatial modes 1-2, 3-4 and 5-6. We then superpose photons 2 (4) and 3 (5) at a PBS. To ensure that the post-selecting fusion operations have been successfully implemented, we observe interference fringes of four-photon entanglement in mode 1-2-3-4 (3-4-5-6) (similar to Fig. 3.5).

6.4 Experimental Results

We will first discuss to what extent the desired six-photon graph and cluster states were produced and then analyze the presence of genuine multipartite entanglement in these states. The quality of the states can be judged by the fidelity, that is, the overlap of the produced state with the desired one (see chapter 2.2.3). The notion of genuine multipartite entanglement in contrast to biseparability characterizes whether generation of the state requires interaction of all parties (see chapter 2.2.1).

To prove multipartite entanglement, we use the method of entanglement witnesses as described in chapter (2.2.3). A negative expectation value proves the presence of genuine multipartite entanglement. In what follows, we derive efficient entanglement witnesses that are both robust against realistic noise and economical for experimental efforts.

6.4.1 Witness Construction and Detection

For the six-photon GHZ state (Eq. 6.2), we use the witness [73]

$$\hat{\mathcal{W}}_G = \frac{\hat{I}}{2} - |G_6\rangle\langle G_6|, \tag{6.4}$$

where $\hat{I}$ denotes the identity operator. We decompose $|G_6\rangle\langle G_6|$ into locally measurable observables

$$|G_6\rangle\langle G_6| = \frac{1}{2}\left[(|H\rangle\langle H|)^{\otimes 6} + (|V\rangle\langle V|)^{\otimes 6}\right] + \frac{1}{12}\sum_{n=-2}^{3}(-1)^n \hat{M}_{(n)}^{\otimes 6}, \tag{6.5}$$

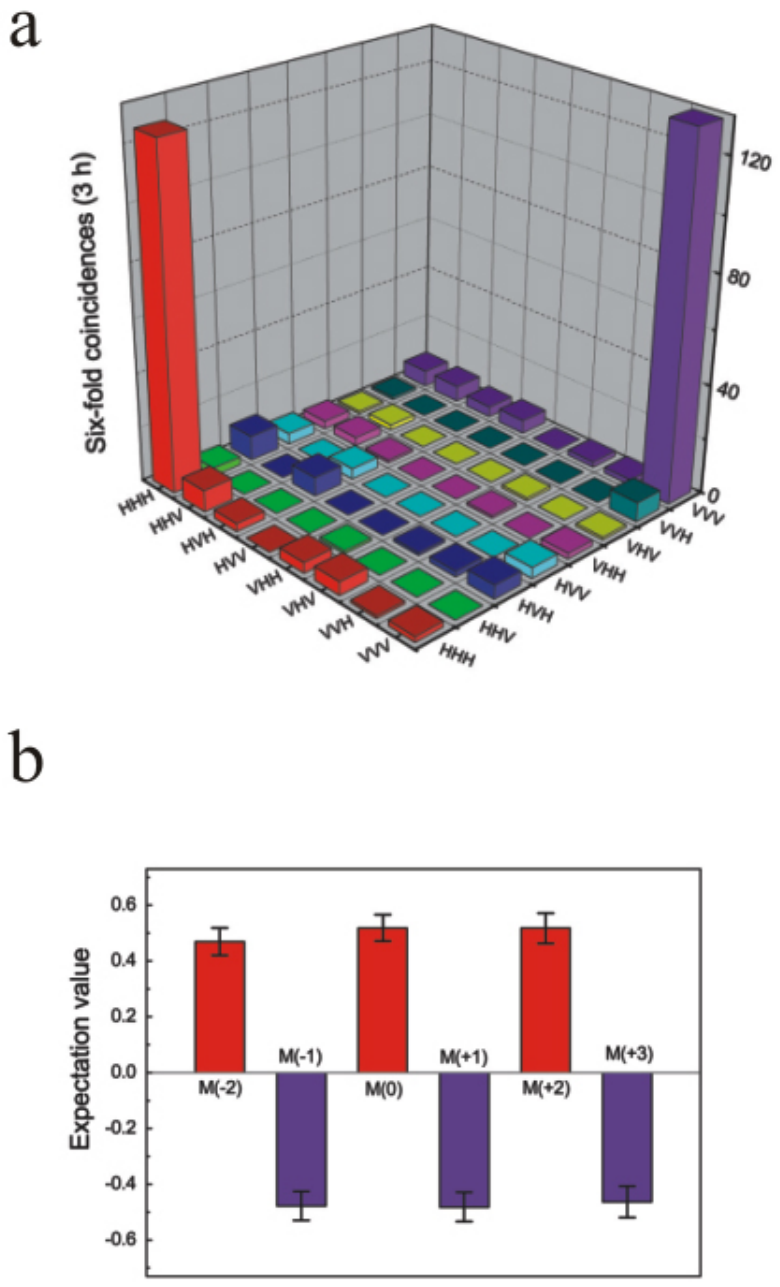

Figure 6.3: *Experimental results for the six-photon GHZ state.* ***(a)*** *Six-fold coincidence counts in the computational basis in 3 hours.* ***(b)*** *The expectation values of* $\hat{M}_{(n)}^{\otimes 6}$*, each derived from a complete set of 64 six-fold coincidence events in 2 hours in the measurement basis* $|H\rangle \pm e^{i\pi/6n}|V\rangle$*. The error bars represent one standard deviation, deduced from propagated poissonian counting statistics of the raw detection events.*

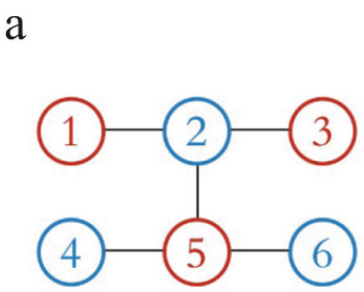

b

$$g_1 = Z_1 Z_2 \mathbb{1}_3 \mathbb{1}_4 \mathbb{1}_5 \mathbb{1}_6$$
$$g_2 = X_1 X_2 X_3 \mathbb{1}_4 Z_5 \mathbb{1}_6$$
$$g_3 = \mathbb{1}_1 Z_2 Z_3 \mathbb{1}_4 \mathbb{1}_5 \mathbb{1}_6$$
$$g_4 = \mathbb{1}_1 \mathbb{1}_2 \mathbb{1}_3 Z_4 Z_5 \mathbb{1}_6$$
$$g_5 = \mathbb{1}_1 Z_2 \mathbb{1}_3 X_4 X_5 X_6$$
$$g_6 = \mathbb{1}_1 \mathbb{1}_2 \mathbb{1}_3 \mathbb{1}_4 Z_5 Z_6$$

Figure 6.4: *The stabilizer operators.* ***(a)*** *The graph corresponds to the cluster state* $|C_6\rangle$ *under* H *transformations on qubits 1, 3, 4 and 6 and* ***(b)*** *its stabilizer operators* $\hat{g}_i$ *where* i *labels the qubits and* $X = \hat{\sigma}_x$, $Y = \hat{\sigma}_y$, $Z = \hat{\sigma}_z$. *The graph state is a common eigenstate of these stabilizer operators, that is,* $\hat{g}_i|C_6\rangle = |C_6\rangle$, *which describe the correlations in the state. The cluster state is the unique state fulfilling this, which allows for an alternative definition of it.*

where

$$\hat{M}_n = \cos(n\pi/6)\hat{\sigma}_x + \sin(n\pi/6)\hat{\sigma}_y \tag{6.6}$$

are measurements in the x-y plane. To implement this witness, seven measurement settings are required. Fig. (6.3) shows the measurement results, yielding

$$Tr\left(\hat{\mathcal{W}}_G \hat{\rho}_{exp}\right) = -0.093 \pm 0.025, \tag{6.7}$$

which is negative by 3.7 standard deviations and thus proves the presence of genuine sixpartite entanglement.

From the expectation value of the witness, we can directly determine the obtained fidelity as

$$F_{G_6} = \langle G_6|\hat{\rho}_{exp}|G_6\rangle = 0.593 \pm 0.025, \tag{6.8}$$

where $\hat{\sigma}_{exp}$ denotes the experimentally produced state. This is a considerable improvement over the fidelity of the six-atom GHZ states of [123] ($F = 0.509 \pm 0.004$).

For the cluster state of Eq. (6.3), a possible witness would be

$$\hat{\mathcal{W}}_C = \hat{I}/2 - |C_6\rangle\langle C_6|. \tag{6.9}$$

Similar to the constructions of ref. [128], we use a slightly different witness $\tilde{\hat{\mathcal{W}}}_C$, the implementation of which requires only six measurements. Using the results of ref. [128], the observable of Eq. (6.9) is a witness detecting genuine multipartite

entanglement around the cluster state. Then, we consider the observable

$$\begin{aligned}\tilde{\hat{\mathcal{W}}}_C &= \frac{3}{2}\hat{I} - \prod_{i=1,3,5}\frac{1}{2}\left(\hat{g}_i + \hat{I}\right) - \prod_{i=2,4,6}\frac{1}{2}\left(\hat{g}_i + \hat{I}\right) \\ &\quad -\frac{1}{2}\left(\hat{I}\otimes\hat{A}_0 + \hat{A}_0\otimes\hat{I}\right) - \left(\hat{A}_1\otimes\hat{B}_1 + \hat{B}_1\otimes\hat{A}_1\right) \\ &= \frac{1}{2}\hat{I} - |C_6\rangle\langle C_6| + |\tilde{C}_6\rangle\langle\tilde{C}_6|,\end{aligned} \tag{6.10}$$

where $\hat{g}_i$ denotes the stabilizing operators of the cluster state (Fig. 6.4). Furthermore, we use

$$\begin{aligned}\hat{A}_0 &= \hat{I} - |HHH\rangle\langle HHH| - |VVV\rangle\langle VVV| \\ \hat{A}_1 &= |VVV\rangle\langle VVV| - |HHH\rangle\langle HHH| \\ \hat{B}_1 &= \frac{2}{\sqrt{3}}\left(\hat{M}^{\otimes 3}_{(1)} + \hat{M}^{\otimes 3}_{(-1)}\right),\end{aligned} \tag{6.11}$$

where $\hat{M}_i$ is defined as for the GHZ state (see Eq. 6.6). Finally, $|\tilde{C}_g\rangle$ denotes a cluster state with different signs, namely

$$\begin{aligned}|\tilde{C}_g\rangle = \frac{1}{2} \quad &(-|HHHHHH\rangle + |HHHVVV\rangle \\ &+|VVVHHH\rangle + |VVVVVV\rangle).\end{aligned} \tag{6.12}$$

It is clear that $\tilde{\hat{\mathcal{W}}}_C - \hat{\mathcal{W}}_C \geq 0$, which implies that $\tilde{\hat{\mathcal{W}}}_C$ is a valid witness [128]. Furthermore, this implies that the fidelity of the cluster state can be estimated as

$$F_{C_6} = \langle C_6|\hat{\rho}_{exp}|C_6\rangle \geq (1/2) - \langle\tilde{\hat{\mathcal{W}}}_C\rangle. \tag{6.13}$$

The witness $\tilde{W}_C$ (Eq. 6.10) detects genuine entanglement from the states of the form

$$\hat{\rho}(p) = p|C_6\rangle\langle C_6| + \frac{(1-p)\hat{I}}{64} \tag{6.14}$$

for $p > 0.5$. The determination of the expectation value of the witness $\tilde{\hat{\mathcal{W}}}_C$ requires six measurement settings, namely $\hat{\sigma}_z^{\otimes 3}\hat{\sigma}_x^{\otimes 3}$, $\hat{\sigma}_x^{\otimes 3}\hat{\sigma}_z^{\otimes 3}$, $\hat{\sigma}_z^{\otimes 3}\hat{M}^{\otimes 3}_{(\pm 1)}$ and $\hat{M}^{\otimes 3}_{(\pm 1)}\hat{\sigma}_z^{\otimes 3}$. The results are shown in Fig. (6.5) and yield

$$Tr\left(\tilde{\hat{\mathcal{W}}}_C\hat{\rho}_{exp}\right) = -0.095 \pm 0.036. \tag{6.15}$$

Thus, the genuine six-partite entanglement of the cluster state is also proved. Furthermore, from this result, we can obtain a lower bound of the fidelity of our cluster state as

$$F_{C_6} \geq 0.595 \pm 0.036. \tag{6.16}$$

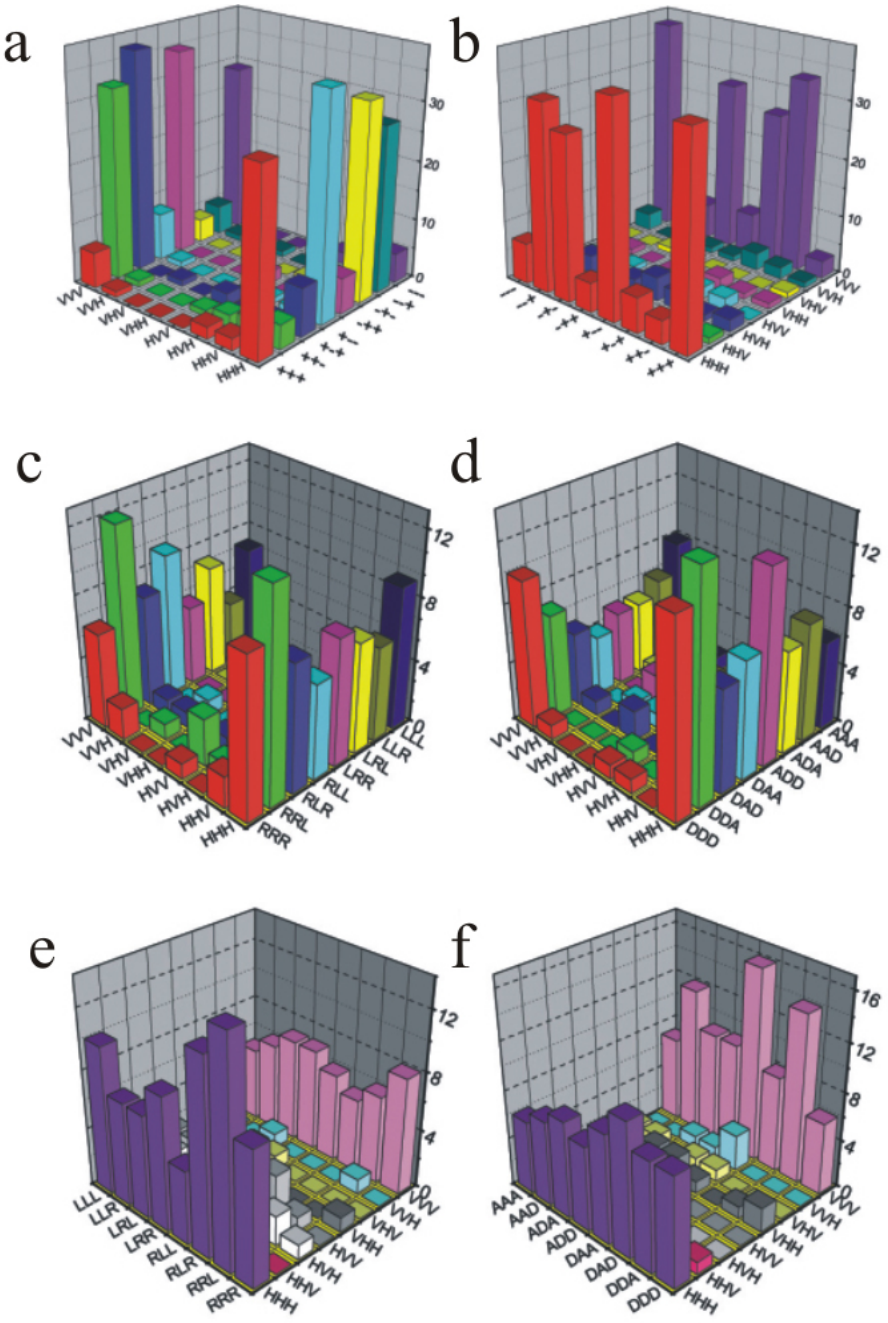

Figure 6.5: *Experimental results for the six-photon cluster state. Six-fold coincidence counts measured in the* **(a)** $\hat{\sigma}_z^{\otimes 3}\hat{\sigma}_x^{\otimes 3}$ *and* **(b)** $\hat{\sigma}_x^{\otimes 3}\hat{\sigma}_z^{\otimes 3}$ *basis in 3 hours, and in the* **(c)** $\hat{\sigma}_z^{\otimes 3}\hat{M}_{(+1)}^{\otimes 3}$, **(d)** $\hat{\sigma}_z^{\otimes 3}\hat{M}_{(-1)}^{\otimes 3}$, **(e)** $\hat{M}_{(+1)}^{\otimes 3}\hat{\sigma}_z^{\otimes 3}$ *and* **(f)** $\hat{M}_{(-1)}^{\otimes 3}\hat{\sigma}_z^{\otimes 3}$ *basis in 1.5 hours. Here we use the notations* $|P\rangle = \left(|H\rangle + e^{i\frac{\pi}{6}}|V\rangle\right)/\sqrt{2}$, $|Q\rangle = \left(|H\rangle - e^{i\frac{\pi}{6}}|V\rangle\right)/\sqrt{2}$, $|M\rangle = \left(|H\rangle + e^{-i\frac{\pi}{6}}|V\rangle\right)/\sqrt{2}$ *and* $|N\rangle = \left(|H\rangle - e^{-i\frac{\pi}{6}}|V\rangle\right)/\sqrt{2}$. *Each measurement signals the observation of an eigenstate of the stabilizer operator* $(\hat{g}_i)$ *with the corresponding eigenvalue of* $v_j = +1$ *or* -1. *From the probabilities of multi-photon detections* p_j, $j = 1, 2, ..., 64$, *we can then compute the expectation values of the stabilizer operators by* $Tr\left(\hat{g}_i\hat{\rho}\right) = \sum_{j=1}^{64} p_j v_j$.

6.4.2 Estimation of Entanglement Measures

Characterization of entanglement has been an interesting and basic task both from the foundational and the practical point of view. Besides for detecting six-particle genuine entanglement, the experimental data obtained in the experiment can be used for a stronger, quantitative measurement of the entanglement in the states. This is very useful information by which one may give an answer to the question of how useful a given state is, say, to perform a certain quantum information task.

In order to quantify the entanglement in the experiment, we estimated two important entanglement measures. The first one is the entanglement of formation [100]. This is an entanglement measure for two parties, defined for pure states as

$$E_F(|\Psi\rangle) = -Tr\left(\hat{\rho}_A \log(\hat{\rho}_A)\right) \tag{6.17}$$

i.e. as the von Neumann entropy of the reduced state. This definition can be extended to mixed states via the so-called convex roof construction [100, 129]. Physically, the entanglement of formation quantifies the entanglement (measured in singlet pairs) that must be invested for the realization of one copy of the state.

For the analysis we considered the bipartitions which arise if the six parties are divided into two groups. Since only incomplete information on the state is available, it is impossible to compute the exact value of E_F. To obtain a lower bound on E_F we use the method and the algorithm presented in Ref. [129] and apply it to the expectation value of the witness, which allows to calculate the best possible bound on entanglement measures from experimentally obtained information about the states.

For the six-photon GHZ state we arrive at a bound of

$$E_F\left(\hat{\rho}_{exp}\right) \geq 0.073 \pm 0.032 \tag{6.18}$$

for all bipartitions, in comparison with the perfect GHZ state that would result in a value of

$$E_F\left(|G_6\rangle\right) = 1. \tag{6.19}$$

For the cluster state, different bipartitions have to be taken into account. The values are given in Table (6.20). Due to the permutation symmetry of the witness, the values for other bipartitions follow from the values in the table. The fact that some values in the table coincide, can be understood from the symmetry of the witness concerning the Legendre transform [129].

Bipartition	value for $\|C_6\rangle$	bound for $\hat{\rho}_{exp}$
1|23456	1	0.074 ± 0.047
12|3456	1	0.074 ± 0.047
14|2356	2	0.729 ± 0.106
123|456	1	0.074 ± 0.047
124|356	2	0.729 ± 0.106

(6.20)

As a second entanglement measure, we estimated the geometric measure of entanglement E_G [130]. This is an entanglement measure for multipartite systems. For pure states, it is defined as

$$E_G\left(|\Psi\rangle\right) = 1 - \sup_{|\Phi\rangle=|a\rangle|b\rangle|c\rangle\ldots} |\langle\Psi|\Phi\rangle|^2 \tag{6.21}$$

i.e. it is one minus the maximal overlap with fully separable states. Physically, it can be used to estimate the distinguishability of states via local operations and classical communication [131]. It also quantifies the distance of an entangled state to the fully separable states. However, it takes not only the genuine multipartite entanglement into account, also for bi-separable states it can be strictly positive. For the GHZ state, we have

$$E_G\left(|G_6\rangle\right) = 1/2 \tag{6.22}$$

in theory, and

$$E_G\left(\hat{\rho}_{exp}\right) \geq 0.0088 \pm 0.0047 \tag{6.23}$$

for the experimentally realized six-photon GHZ state. For the cluster state, we have

$$E_G\left(|C_6\rangle\right) = 3/4 \tag{6.24}$$

in theory and find experimentally

$$E_G\left(\hat{\rho}_{exp}\right) \geq 0.181 \pm 0.0.023. \tag{6.25}$$

The fact that the estimates for the GHZ state and the cluster state differ significantly can be understood by that for the GHZ state the mean value $\langle\hat{\mathcal{W}}_G\rangle = 0$ is compatible with a fully separable state with $E_G\left(\hat{\rho}\right) > 0$. Similarly, the different values in Table I origin from the fact that $\langle\tilde{\hat{\mathcal{W}}}_G\rangle = 0$ is for some bipartitions in agreement with separability, while for other bipartitions it is not.

6.5 Discussion

The imperfections of our graph states are mainly caused by two reasons. First, high-order emissions of entangled photons give rise to the undesired components in the computational basis (see Fig. 6.3). Second, the partial distinguishability of independent photons causes some incoherent mixtures. In spite of the imperfections, genuine entanglements of the six-photon graph states are strictly confirmed. It is possible to improve the fidelity in future experiments, for example, by using photon-number discriminating detectors to filter out the events of double emissions of photon pairs. Moreover, graph states with high purity can be obtained efficiently using an existing entanglement purification scheme [132]. Linear optical elements such as a

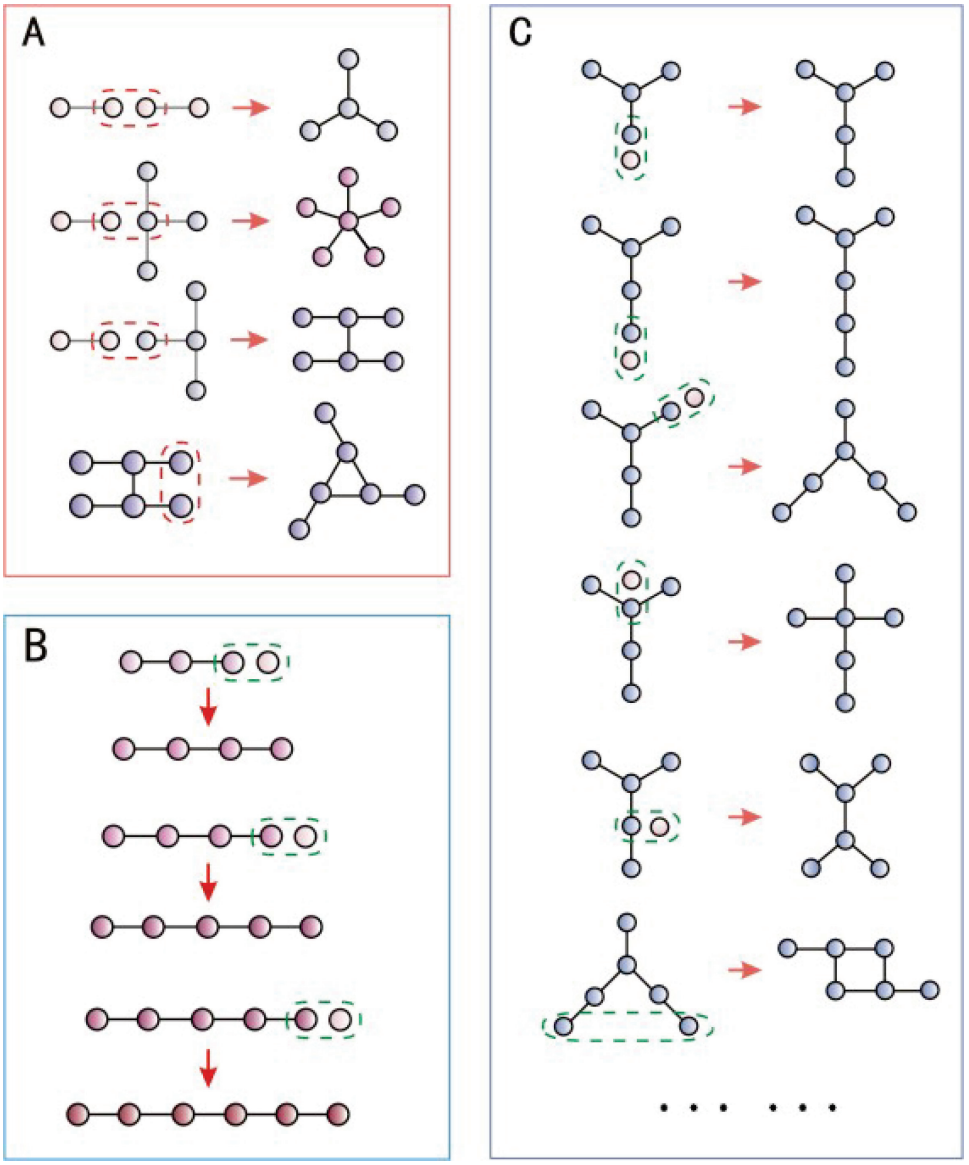

Figure 6.6: *Scheme to construct various six-photon graph states.* ***(a)*** *Generation of a graph state by fusion of two photon entangled states.* ***(b)*** *Generation of larger linear graph states by fusion with a single photon.* ***(c)*** *Generation of Y-shaped and other graph states.*

PBS may offer a high accuracy tool for this task [49]. It leaves a crucial open question of how to reach the noise thresholds for optical cluster-state quantum computation [125].

Some further remarks are warranted here. We have demonstrated the creation of the six-photon GHZ state and cluster state, which are two special instances of graph states. We generate the graph states conditioned on there being one and only one photon in each of the six outputs. This post-selective feature, together with the fusion method, provides a flexible and economical way to create various multi-photon graph states. Slight modifications of the fusion method and our experimental setup will readily allow the experimental generation of a number of other graph states, which are selectively shown in the graph-state representation in Fig. (6.6). This result implies that photons manipulated by linear optics are excellent candidates for graph state engineering, which, together with the intrinsic advantages of photons such as long de-coherence time and precise single-qubit operations and the recent encouraging theoretical progresses on one-way quantum computation [133, 68] (see chapter 2.2.2), appear to offer an extremely promising approach to quantum computation. We envision that such a fascinating capacity will open up prospects for many exciting experiments and applications such as studies of multi-particle entanglement, implementations of quantum algorithms and investigations of fault-tolerant one-way quantum computation.

Furthermore, the post-selective feature does not prohibit subsequent applications such as tests of quantum non-locality [56, 57, 58] and in-principle verifications of linear optical QIP tasks where photons need to be eventually detected. Finally, concerning the scalability issue, we refer to ref. [68], which has shown that if combined with quantum memory, the post-selection method can even be used for scalable generation of tree-graph states using realistic linear optics. Along this line, however, technically extensive efforts still need to be undertaken to make a quantum memory usable for this purpose.

In this chapter, we have discussed the realization of two special graph states, the six-photon GHZ state, the largest photonic Schrödinger cat so far, and the six-photon cluster state – a state-of-the-art one-way quantum computer. We have demonstrated the ability to entangle six photons and to engineer multiqubit graph states, and have created a versatile test-bed for experimental investigations of one-way quantum computation [68], quantum error correction [55], studies of multi-particle entanglement [53] and foundational tests of quantum physics [56, 57, 58, 60]. Combined with quantum memory, our experimental method could lead to the generation of large-scale tree-graph states [68]. The high efficiency and flexibility of the six-photon graph-state generation we demonstrated here suggest that photons manipulated with linear optics are promising candidates for engineering of multi-qubit graph states. Various applications of our six-photon graph-state test-bed can be imagined. For instance, the six-qubit cluster states allow full implementations of the quantum game of prisoners' dilemma [124] and a proof-of-principle demonstration of the basic elements of

loss-tolerant one-way quantum computation [126]. Most remarkably, the six-qubit star-ring graph state corresponds to the codeword and encoding procedure of the five-qubit quantum error-correction code that is able to correct all one-qubit errors [55]. In addition, our six-photon cluster state also enables a novel test of non-locality, namely a GHZ argument of non-locality for mixed states [57]. Lastly, the graph-state test-bed is well suited for studies of the stabilities of different types of multi-particle entanglement (for example, GHZ and cluster) under the influence of de-coherence, which may provide experimental evidence for the surprising conclusion in ref. [60] that genuine entanglement of a macroscopic number of particles is possible and can persist for timescales that are independent of the size of the system.

Chapter 7

One-Way Quantum Computing with Two-Photon Four-Qubit Cluster States

7.1 Introduction

As we have seen in the previous chapter (6), preparing photonic cluster states still suffers from several serious limitations. Due to the probabilistic nature and Poissonian distribution of the parametric down-conversion process (see chapter 2.3.1), the generation rate of four-photon cluster states is quite low [10, 59, 64, 69], and largely restricts the speed of computing. Furthermore, the quality and fidelity of prepared cluster states are relatively low [59, 64, 69] and are difficult to be improved substantially. These disadvantages consequently impose great challenges of advancement even for few-qubit quantum computing.

Fortunately, motivated by the experimental generation of *hyper-entangled* states [134, 135, 136, 137], we have the possibility to produce a new type of cluster state (two-photon four-qubit cluster state) with nearly perfect fidelity and high generation rate. The hyper-entangled states have been used to test "All-Versus-Nothing" (AVN) quantum non-locality (see chapter 2.2) [138, 139, 134, 135], and are shown to lead to an enhancing violation of local realism [140, 141]. The states also enable us to perform a complete deterministic Bell state analysis [142] as demonstrated in [137, 143].

In this chapter, we discuss an experimental realization of one-way quantum computing with such a two-photon four-qubit cluster state. The key idea is to develop and employ a bright source which produces a two-photon state entangled both in polarization and spacial modes. We are thus able to implement the Grover's algorithm and quantum gates with excellent performances. The genuine four-partite entanglement and high fidelity of better than 88% are characterized by an optimal entanglement witness. Inheriting the intrinsic two-photon character, our scheme

promises a brighter source by four orders of magnitude than the usual multi-photon source, which offers a significantly higher efficiency for optical quantum computing. It thus provides a simple and fascinating alternative to complement the latter. With ease of manipulation and control, the nearly perfect quality of this source allows to perform highly faithful and precise quantum computing.

7.2 Experimental Setup

The desired four-particle cluster state is up to local unitary transformations the same as in Eq. (5.2) of chapter (5) and is given by

$$|C_4\rangle = \frac{1}{2}\left(|0000\rangle_{1234} + |0011\rangle_{1234} + |1100\rangle_{1234} - |1111\rangle_{1234}\right). \tag{7.1}$$

To generate the cluster state, we use a slightly different method than in the experiments described in the previous chapters. Instead of type-II SPDC (see chapter 2.3.1), we use a technique developed in previous experiments [134], which is based on type-I SPDC. The experimental setup is shown in Fig. (7.1a). A pump pulse of ultraviolet light (UV) passes through two contiguous BBOs with their optic axes aligned in perpendicular planes. With this configuration there is a small probability for the UV to produce a pair of equally polarized photons in the first BBO via type-I SPDC. Accordingly, there also exists a small probability to produce a pair of equally, but perpendicular to the first pair, polarized photons in the second BBO. The paths of the two pairs overlap almost completely and their coherence length is larger than the dimension of the BBO's. We thus, have to add the probability amplitudes of the two pairs which results in a polarization entangled photon pair in the forward direction in the state [134]

$$\frac{1}{\sqrt{2}}\left(|H\rangle|H\rangle + e^{i\varphi_1}|V\rangle|V\rangle\right) \tag{7.2}$$

in spacial (path) modes $L_{A,B}$. Now if the pump pulse is reflected and passes through the BBO crystal a second time, there again is a possibility to generate a polarization entangled photon pair in the backward direction. By inserting a quarter wave plate (QWP) in mode L_A and R_B, respectively, we can tune the phases $\varphi_{1,2}$ as desired. We thus generate a pair in the state

$$\frac{1}{\sqrt{2}}\left(|H\rangle_A|H\rangle_B + |V\rangle_A|V\rangle_B\right)|L_A\rangle_A|L_B\rangle_B \tag{7.3}$$

or in the state

$$\frac{1}{\sqrt{2}}\left(|H\rangle_A|H\rangle_B - |V\rangle_A|V\rangle_B\right)|R_A\rangle_A|R_B\rangle_B \tag{7.4}$$

Through perfect temporal overlaps of modes R_A and L_A and of modes R_B and L_B, once again the probability amplitudes have to be added and we obtain a state

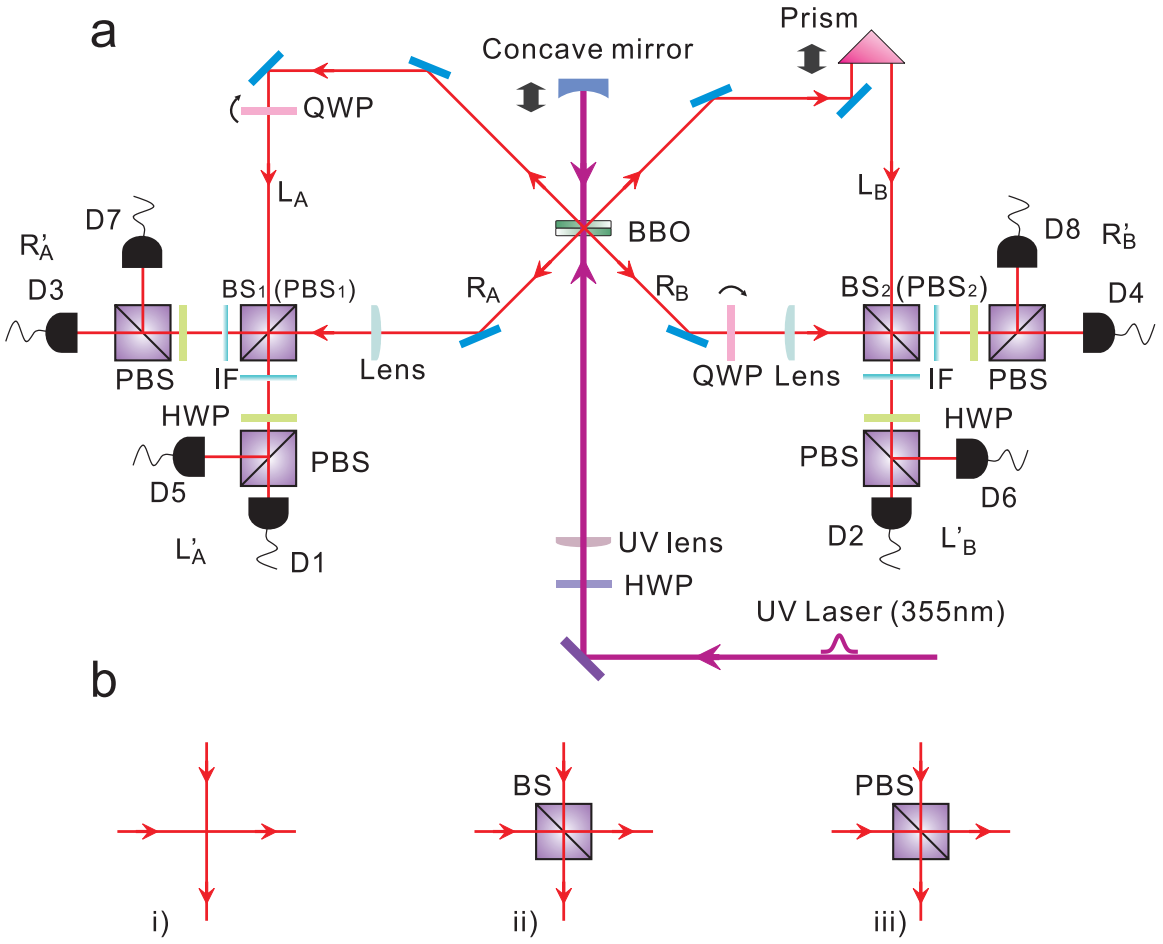

Figure 7.1: *Schematic of experimental setup.* ***(a)*** *By pumping a two-crystal structured BBO in a double pass configuration, one polarization entangled photon pair is generated either in the forward direction or in the backward direction. The ultraviolet laser pulse (5ps) has a central wavelength of 355 nm with a repetition rate of 80 MHz and an average power of 200 mW. Two quarter wave plates (QWPs) are tilted along their optic axis to vary relative phases between polarization components to attain two desired possibilities for entangled pair creation. Concave mirror and prism are mounted on translation stages to optimize interference on two beam splitters($BS_{1,2}$) or polarizing beam splitters ($PBS_{1,2}$) for achieving the target cluster state. Half wave plates (HWPs) together with PBSs and 8 single-photon detectors (D1-D8) are used for polarization analysis of the output state. IF are 3 nm filters with a central wavelength of 710 nm.* ***(b)*** *The position marked with $BS_{1,2}$ or $PBS_{1,2}$, three different apparatuses are used to measure all necessary observables. Setup* ***(i)*** *corresponds to a Z measurement while setup* ***(ii)*** *is used for a X measurement for spacial modes. If an α phase shifter is inserted at one of the input modes in (ii), an arbitrary measurement along basis $B(\alpha)$ can be achieved. Setup* ***(iii)*** *can be used for a Z measurement in the spacial mode and, simultaneously, for a Z measurement in the polarization mode.*

with coherent superposition:

$$\frac{1}{2}\Big(\big(|H\rangle_A|H\rangle_B+|V\rangle_A|V\rangle_B\big)|L\rangle_A|L\rangle_B+ e^{i\theta}\big(|H\rangle_A|H\rangle_B-|V\rangle_A|V\rangle_B\big)|R\rangle_A|R\rangle_B\Big) \tag{7.5}$$

By properly adjusting the distance between the concave mirror and the crystal so that $\theta = 0$, the state of Eq. (7.5) becomes

$$\frac{1}{2}\Big(\big(|H\rangle_A|H\rangle_B+|V\rangle_A|V\rangle_B\big)|L\rangle_A|L\rangle_B+ \big(|H\rangle_A|H\rangle_B-|V\rangle_A|V\rangle_B\big)|R\rangle_A|R\rangle_B\Big). \tag{7.6}$$

In order to tune the phase θ, in the experiment the concave mirror and a prism in spacial mode L_B are scanned by a piezo translation stage and a motor translation stage, respectively. Interference fringes (Fig. 7.2) can be observed by measuring the two-fold coincidence counts between the output modes monitored by detectors D_1 and D_2 behind half wave plates HWPs at an angle of 22.5° and corresponding PBSs. By setting the piezo translation system to a position where we observe maximum two-fold coincidences between detectors D_1 and D_2, we tune the phase to $\theta = 0$.

Following this procedure, the generated state will exactly be the desired cluster state of Eq. (7.1) if we identify photon A to be qubits 2,3 and photon B to be qubits 1,4 and encode logical qubits as

$$\begin{aligned} |H(V)\rangle_B &\leftrightarrow |0(1)\rangle_1 \\ |H(V)\rangle_A &\leftrightarrow |0(1)\rangle_2 \\ |L(R)\rangle_A &\leftrightarrow |0(1)\rangle_3 \\ |L(R)\rangle_B &\leftrightarrow |0(1)\rangle_4. \end{aligned} \tag{7.7}$$

The state $|C_4\rangle$ (Eq. 7.1) can be represented by a box cluster graph shown in Fig. (2.7c) and Fig. (7.3a), up to a local unitary transformation.

We observe a cluster state generation rate of about 1.2×10^4 per second for 200 mW UV pump, which is four orders of magnitude brighter than the usual four-photon cluster state production [64, 69, 59] where only a rate of about 1 per second is achieved.

7.3 Experimental Results

7.3.1 Quality of the Four-Qubit Cluster State

To evaluate the quality of the state, we apply an optimal entanglement witness [128] (see chapter 2.2.3). The witness is of the form

$$\hat{\mathcal{W}} = \tfrac{1}{2}\Big(4\cdot\hat{I}^{\otimes 4}-(\hat{\sigma}_x\hat{\sigma}_x\hat{I}\hat{\sigma}_z+\hat{\sigma}_x\hat{\sigma}_x\hat{\sigma}_z\hat{I}+\hat{I}\hat{I}\hat{\sigma}_z\hat{\sigma}_z +\hat{I}\hat{\sigma}_z\hat{\sigma}_x\hat{\sigma}_x+\hat{\sigma}_z\hat{I}\hat{\sigma}_x\hat{\sigma}_x+\hat{\sigma}_z\hat{\sigma}_z\hat{I}\hat{I})\Big), \tag{7.8}$$

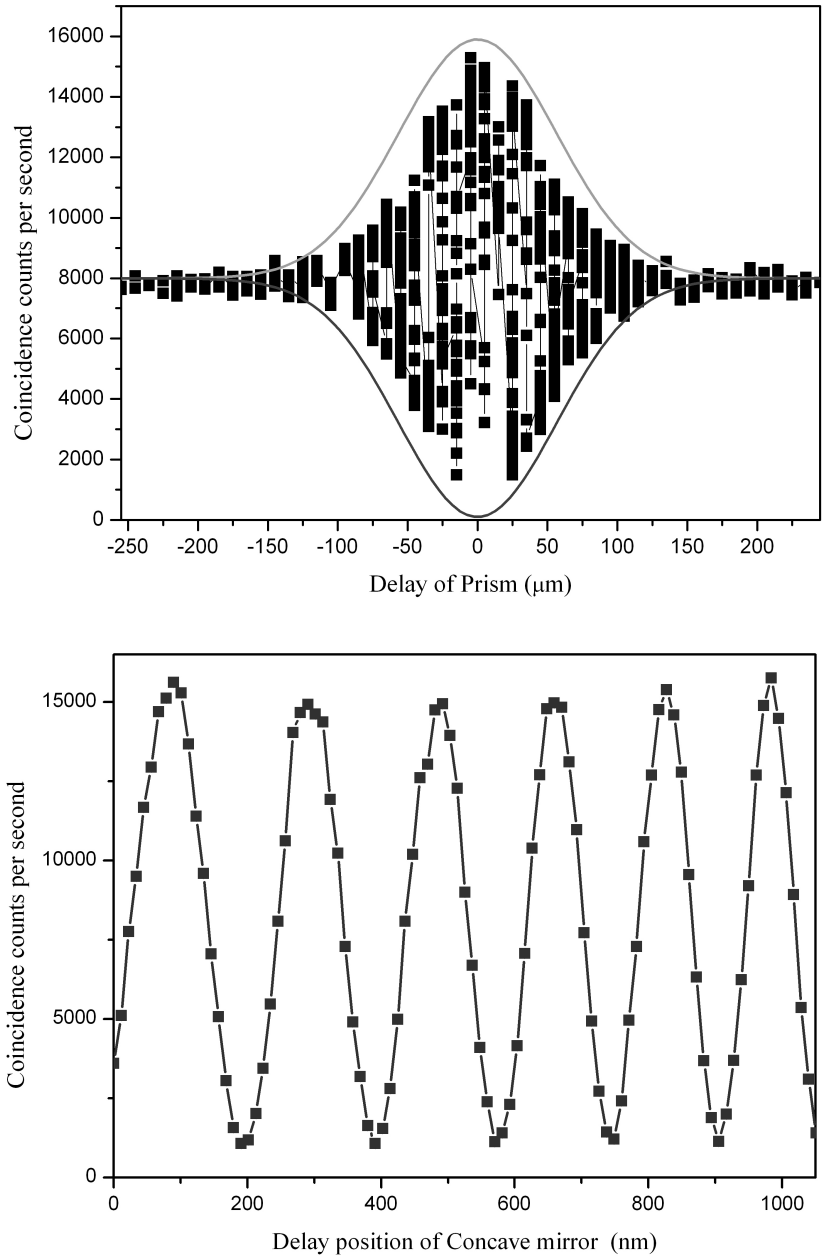

Figure 7.2: *Interference fringes used to adjust the phase of the cluster state. They are observed when the concave mirror and the prism are moved to achieve perfect temporal overlap and to adjust the phase to* $\theta = 0$. ***(a)*** *Two-fold coincidence counts observed between detectors* D_1 *and* D_2 *behind HWPs at* $22.5°$ *and PBSs by scanning the position of the prism. The envelope over the curve of the observed two-fold coincidences indicates the visibility of the two-photon coherence. Inside the coherent region, the best visibility is obtained at the position where perfect temporal overlap is achieved.* ***(b)*** *Fine scan around the center of the envelope of (a) with a piezo translation stage underneath the concave mirror. The optimum position of* $\theta = 0$ *is achieved by setting the piezo system to a position of maximum two-fold coincidences between* D_1 *and* D_2.

Observable	Value	Observable	Value
$\hat{\sigma}_x\hat{\sigma}_x\hat{I}\hat{\sigma}_z$	0.9070 ± 0.0036	$\hat{I}\hat{\sigma}_z\hat{\sigma}_x\hat{\sigma}_x$	0.9071 ± 0.0037
$\hat{\sigma}_x\hat{\sigma}_x\hat{\sigma}_z\hat{I}$	0.9076 ± 0.0035	$\hat{\sigma}_z\hat{I}\hat{\sigma}_x\hat{\sigma}_x$	0.8911 ± 0.0040
$\hat{I}\hat{I}\hat{\sigma}_z\hat{\sigma}_z$	0.9812 ± 0.0016	$\hat{\sigma}_z\hat{\sigma}_z\hat{I}\hat{I}$	0.9372 ± 0.0030

Table 7.1: *Experimental values for the observables of the entanglement witness $\hat{\mathcal{W}}$ to detect the cluster state $|C_4\rangle$. The experimental integration time for each measurement is 1 sec. The errors correspond to Poissonian counting statistics.*

where $\hat{I}$ and $\hat{\sigma}_x$, $\hat{\sigma}_y$, $\hat{\sigma}_z$ are the usual two-dimensional identity matrix and the Pauli matrices, respectively.

A negative value for the witness implies four-partite entanglement for a state close to $|C_4\rangle$ (see chapter 2.2.3) and will be $\hat{\mathcal{W}} = -1$ for a perfect cluster state. The two experimental settings $\hat{\sigma}_x\hat{\sigma}_x\hat{\sigma}_z\hat{\sigma}_z$ and $\hat{\sigma}_z\hat{\sigma}_z\hat{\sigma}_x\hat{\sigma}_x$ are needed. $\hat{\sigma}_x\hat{\sigma}_x\hat{\sigma}_z\hat{\sigma}_z$ can be attained by measuring in the diagonal basis for the polarization in each output arm after apparatus **(i)** in Fig. (7.1b). while $\hat{\sigma}_z\hat{\sigma}_z\hat{\sigma}_x\hat{\sigma}_x$ can be realized by measuring in the computational basis after apparatus **(ii)**. This is because a BS acts exactly as a Hadamard transformation for the path modes, i.e. it changes the measurement basis from the computational ($\hat{\sigma}_z$) to the diagonal basis ($\hat{\sigma}_x$), namely,

$$\begin{aligned} |L\rangle_{A,B} &\rightarrow \frac{1}{\sqrt{2}}(|R'\rangle_{A,B} + |L'\rangle_{A,B}) \\ |R\rangle_{A,B} &\rightarrow \frac{1}{\sqrt{2}}(|R'\rangle_{A,B} - |L'\rangle_{A,B}). \end{aligned} \tag{7.9}$$

All observables for evaluating the witness and their results are listed in Table 7.1. Substituting their experimental values into Eq. (7.8) yields $\langle\hat{\mathcal{W}}\rangle_{exp} = -0.766 \pm 0.004$, which clearly proves genuine four-partite entanglement by about 200 standard deviations. As shown in [128], one can obtain a lower bound for the fidelity (see chapter 2.2.3) of the experimentally prepared state:

$$F \geq \frac{1}{2} - \frac{1}{2}\langle\hat{\mathcal{W}}\rangle_{exp} = 0.883 \pm 0.002. \tag{7.10}$$

This proves to be a better cluster state source than the ones in [64, 69, 59] where the measured fidelities are about 0.63 [64, 69] and 0.74 [59], respectively. We attribute impurity of our state to imperfect overlapping on the BSs, deviations of the BSs from 50%, as well as imperfections in the polarization and path modes analysis devices.

7.3.2 Grover's Search Algorithm

For an unsorted database, Grover's search algorithm gives a quadratic speed-up compared to any classical search algorithm. For a database with N entries only $\sim \sqrt{N}$ consultations are needed in comparison to $\sim N$ [20]. Striking linear optics

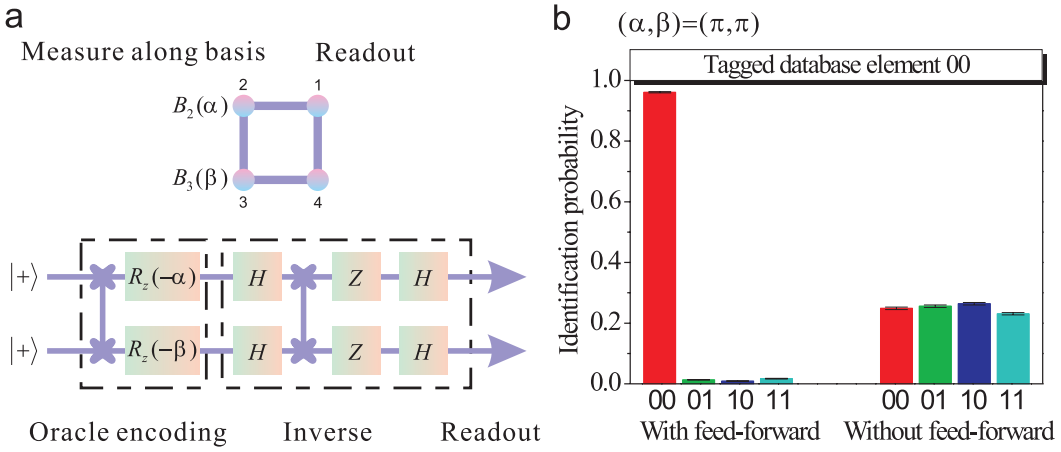

Figure 7.3: *Demonstration of Grover's search algorithm.* ***(a)*** *One-way quantum circuit of Grover's search algorithm using the box cluster state. The 'oracle' encodes the element '00' by measuring along the basis $B_2(\pi)$ and $B_3(\pi)$, while the inverse and readout sections will find this entry with certainty by a single query.* ***(b)*** *A successful identification probability of* $(96.1\pm0.2)\%$ *is achieved deterministically with feed-forward, while it is* $(24.9 \pm 0.4)\%$ *without feed-forward. This is in excellent agreement with theoretical expectations.*

implementations have been achieved in [144, 145], although it is questionable whether the algorithm is truly 'quantum' due to a demonstration [145], based on interference of classical waves. One-way realizations have been carried out [64, 69] recently. In the case of four entries $|00\rangle, |01\rangle, |10\rangle, |11\rangle$, a single quantum search will already find the marked element. An execution goes as follows (see also chapter 2.2.2): The input state of an oracle is in an equal superposition of all possible entries. In our case this is the state $|{+}{+}\rangle$. The oracle tags the desired entry by changing its sign (e.g. $|00\rangle \rightarrow -|00\rangle$). After an inversion-about-the-mean operation, the labeled element will be found with certainty by the readout. It is shown in [64] that this can exactly be finished with the box cluster state in Fig. (7.3a) (see also Fig. (2.7c)) by read out in the basis $B(\pi)$ (see chapter 2.2.2). In the experiment, we choose to tag the element $|00\rangle$ on the cluster qubits $2, 3$ and make the readout on the cluster qubits $1, 4$ along the basis $B(\pi)$. Taking into account that the state of Eq. (7.1) differs from the box cluster by a Hadamard transformation on every qubit and a swap between qubits 2 and 3, this amounts to measure along the computational basis (and multiply by a factor of -1) after apparatus (iii) in Fig. (7.1b). The output of the algorithm denotes the tagged entry and thus consists of two bits: $\{s_3 \oplus s_4\}$ and $\{s_1 \oplus s_2\}$. Here, s_i is the measurement result on cluster qubit i and $\oplus$ denotes 'modulo two addition'. Note, that measurement result s_2 and s_3 are feed-forward outcomes (see chapter 2.2.2). The experimental results are sketched in Fig. (7.3b).

We want to remark that on the one hand the PBSs of the two apparatuses (iii) are used to generate the desired box cluster state by two-photon interference. On

the other hand, they are also used to ensure perfect temporal overlap of two spacial modes to implement apparatus (i).

7.3.3 Quantum Gates

Non-trivial two-qubit quantum gates such as the C-Phase gate are at the heart of universal quantum computation. They can be realized by one-way computing conveniently via corresponding cluster states (see chapter 2.2.2). Depending on the initial cluster state and measurement basis, states with different degrees of entanglement can be generated. The horseshoe (Fig. 7.4a, Fig. 2.7b) or box cluster (Fig. 7.4c, Fig. 2.7c) can be used to realize such important gates. For the case of the horseshoe cluster, depending on the outcomes when measuring along basis $B_2(\alpha)$ and $B_3(\beta)$, the output state on qubits 1,4 will be

$$|\Omega_{out}\rangle = (\hat{\sigma}_x^{s_2} \otimes \hat{\sigma}_x^{s_3})(\hat{H} \otimes \hat{H})\big(\hat{R}_z(-\alpha) \otimes \hat{R}_z(-\beta)\big)\hat{U}^{\text{C-Phase}} |\Omega_{in}\rangle \tag{7.11}$$

where $|\Omega_{in}\rangle = |{+}{+}\rangle$. The state $|\Omega_{out}\rangle$ is always a maximally entangled state. We choose $\alpha = \beta = 0$ and consider only the case with outcomes '00' in qubits 2,3. This implies a final Bell state of

$$|\Omega_{out}\rangle = \frac{1}{\sqrt{2}}(|+\rangle\,|0\rangle + |-\rangle\,|1\rangle). \tag{7.12}$$

Note that the horseshoe cluster state is equivalent to the state of Eq. (7.1) up to a $\hat{H}\hat{I}\hat{I}\hat{H}$ transformation. To characterize the quality of the quantum gate output, we put a birefringent crystal in path R_B to perform the polarization transformation $|+\rangle \leftrightarrow |-\rangle$. Thus, behind BS_2, all Bell states on qubits 1,4 will undergo the following transformations:

$$\begin{array}{l} \frac{1}{\sqrt{2}}(|+\rangle_1\,|0\rangle_4 \pm |-\rangle_1\,|1\rangle_4) \longrightarrow |+\rangle_1\,|\pm\rangle_4 \\ \frac{1}{\sqrt{2}}(|-\rangle_1\,|0\rangle_4 \pm |+\rangle_1\,|1\rangle_4) \longrightarrow |-\rangle_1\,|\pm\rangle_4 \end{array} \tag{7.13}$$

These states can be completely and deterministically discriminated by measuring along the diagonal basis. The fidelities of the output states are shown in Fig. (7.4b). Analogous, for the box cluster state, measurements on qubits 2,3 along basis $\{B_2(\alpha), B_3(\beta)\}$ will give an output state on qubits 1,4 of

$$|\Omega_{out}\rangle = (\hat{\sigma}_z \otimes \hat{\sigma}_x)^{s_3}(\hat{\sigma}_x \otimes \hat{\sigma}_z)^{s_2}\hat{U}^{\text{C-Phase}}(\hat{H} \otimes \hat{H})\big(\hat{R}_z(-\alpha) \otimes \hat{R}_z(-\beta)\big)\hat{U}^{\text{C-Phase}} |\Omega_{in}\rangle \tag{7.14}$$

which is a product state when $\alpha = \pi$ and $\beta = 0$. Since we can completely distinguish the four different products states, output fidelities can be obtained directly, as shown in Fig. (7.4d). By employing the techniques developed in [69] with active feed-forward, one can expect to achieve deterministic quantum computation with excellent output qualities.

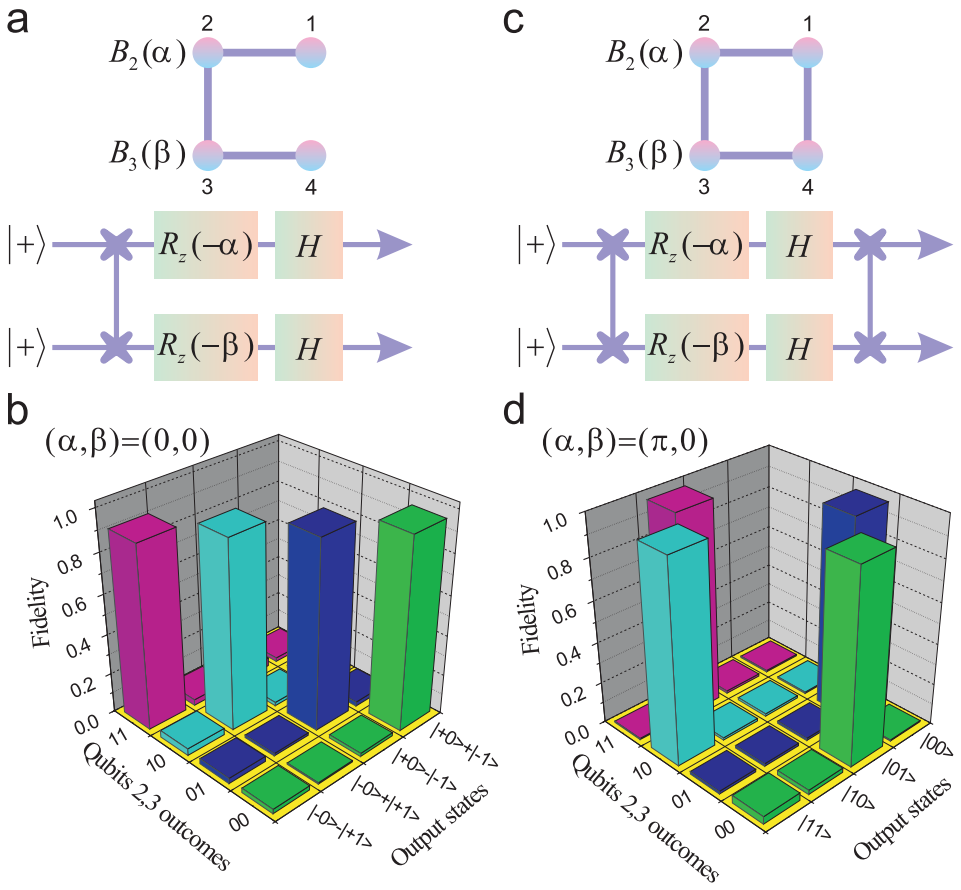

Figure 7.4: *Scheme and experimental results for the realization of two-qubit quantum gates.* ***(a)*** *Realization of a C-Phase gate with a horseshoe cluster.* ***(b)*** *Experimentally measured fidelities of the output states to the ideal Bell states. The fidelities are* 0.954 ± 0.003, 0.940 ± 0.004, 0.936 ± 0.005 *and* 0.910 ± 0.005 *for outcomes 00, 01, 10 and 11 on qubits 2,3, respectively.* ***(c)*** *Implementation of a quantum gate that does not generate entanglement with the box cluster.* ***(d)*** *Measured fidelities of the output states to the ideal product states. The fidelities are* 0.935 ± 0.005, 0.962 ± 0.004, 0.969 ± 0.003 *and* 0.975 ± 0.003 *for outcomes 00, 01, 10 and 11 on qubits 2,3, respectively.*

7.4 Discussion

We want to remark that other two-qubit states can be generated by suitable measurements on qubits 2 and 3. However, an arbitrary single-qubit rotation needs three single-qubit measurements on a cluster for one-way implementation [64, 69], which is a rather large consumption of resources. Fortunately, this rotation can easily be attained by linear optical components both for polarization and spacial modes. Therefore a hybrid framework would be more practical for one-way realizations of single and two-qubit gates. Like the source presented in [69], our source is not yet scalable. However, the scheme developed here leads to quantum computing with a quality and efficiency at present largely unmatched by previous methods.

In this chapter, we have discussed a scheme for the preparation of a two-photon four-qubit cluster state, thereby we have designed and demonstrated the first proof-of-principle realization of one-way quantum computing employing such a source. An excellent quality of the state with a fidelity better than 88% is achieved. The high count rates enable quantum computing more efficient than previous methods by four orders of magnitude. We have implemented Grover's search algorithm with a successful probability of about 96% and two-qubit quantum gates with high fidelities of about 95% on average. Our scheme helps to make a significant advancement of QIP, and the source constitutes a promising candidate for efficient and high quality one-way optical quantum computation. By using more photons and more degrees of freedom, one can expand our scheme to generate many-qubit cluster states for performing quantum computing and other complex tasks. Our results can also find rapid applications in quantum error correction codes, multi-partite quantum communication protocols [55, 91], as well as novel types of AVN tests for non-locality [138, 139].

Chapter 8

Conclusions, Outlook and Remarks

In this thesis, we have reported our research on the field of quantum information processing. We have used pairs of polarization-entangled photons as produced by pulsed parametric down-conversion to experimentally explore interference phenomena of multi-particle quantum systems. Along this research, we have designed and developed a new generation of a high power EPR source, which we have exploited to assemble a six-photon interferometer – the first of its kind.

Our research has been mainly concentrated on the following topics: (i) We have experimentally demonstrated quantum teleportation of a two-qubit composite system. We have been able to teleport a polarization entangled photon pair, which on the one hand denotes an important step towards the teleportation of complex systems but on the other hand and even more importantly constitutes the basis for various QIP schemes and protocols. – (ii) We have further demonstrated entanglement swapping over multiple stages, which is a crucial requirement for the realization of quantum repeaters. By this we have generated entanglement between particles that have never interacted in the past with the help of ancillary particles that also do not share any common history. – (iii) The coupling of qubits to the environment imposes a major challenge to realistic implementations of QIP. Quantum error correction codes and fault-tolerant quantum gates are therefore critical components within the framework of QIP. We have reported the first successful realization of the scheme by Gottesman and Chuang for fault-tolerant quantum gates. The in-principle demonstration shows the feasibility of the scheme and opens doors for possible future large scale implementations of quantum networks. – (iv) Multipartite entangled states are on the one hand of fundamental interest, since they can be used for conceptually new ways to test locality and realism of quantum mechanics and on the other hand they form the resource for various quantum computation schemes. We have generated for the first time six-photon graph states, such as a Schrödinger cat and a cluster state. – (v) The model of one-way quantum computation is a recent approach that with the resource of highly entangled cluster states, active

feed-forward and classical measurements enables the implementation of quantum computers. With a two-photon four-qubit cluster state we have implemented a simple version of this model to perform Grover's algorithm and a quantum gate. With an improvement of the cluster state generation rate by four orders of magnitude we have provided a significant step towards the realization of quantum computation on a larger scale.

Although significant theoretical and experimental progress in the field of linear optic QIP has been demonstrated over the last few years, we are still at the beginning on the way towards large-scale implementations of QIP in the lab or even in everyday life.

An obvious drawback of the current realization of linear optic QIP is the process of generating entangled photons. Even though the process of SPDC yields high quality entanglement of photons and via a pulsed laser setup can be used to generate multi-photon entanglement, its probabilistic nature makes scalable and thus large-scale implementations impossible. It has been very useful to test fundamental properties of multipartite entanglement and to develop techniques and methods for the manipulation of multi-photon entanglement. However, with our six-photon interferometer we are approaching the maximum number of entangled photons that can be generated via SPDC. There exist various promising alternatives to generate photonic entanglement. Quantum dots can be used to generate single photons on demand [146]. However, poor quality and the lack of ability to develop a large number of identical sources still makes the use of quantum dots unpractical. Another promising approach is the application of atomic ensembles as quantum memories and single photon sources [104]. The emission of a *Stokes* photon conditioned on the detection of an *Anti-Stokes* photon in an atomic system with a λ-level-configuration has proven to be an alternative process to generate single photons and could be used to construct a scalable quantum network.

A further problem of the current technology is the poor overall coupling efficiency, i.e only $\sim 15\%$ of the generated photons are actually detected. This deficiency is mainly caused by insufficient mode matching and additional loses at the filters. Thus, even with a deterministic single photon source, large scale quantum operations are severely limited by this drawback. A miniaturization of the setup could on the one hand constitute a potential solution to this problem and on the other hand dramatically enhanced its performance and reduce the resource requirements, as it has been for conventional computers.

Concluding, the developed techniques and obtained knowledge of linear optics within this dissertation need to be combined with other physical systems to merge its different strengths and advantages.

As a final remark, we would like to note that a number of text paragraphs were taken from joint papers of our group because the formulations found there are difficult to improve.

Acknowledgment

Many people have contributed to the work presented in this thesis and supported me during my Ph.D. studies. I would like to take this opportunity to thank them all.

I would like to thank my advisor Prof. Jian-Wei Pan for giving me the opportunity to conduct research in this very exciting field and for his guidance and support. I am very thankful for his introduction to experimental physics, many hours of helpful discussions and generous availability.

I also would like to thank my second advisor Prof. Jörg Schmiedmayer for many fruitful discussions in which I have profited from his deep understanding and natural feeling of the experiment.

Special thanks are due to Dr. Yu-Ao Chen, Dr. Qiang Zhang and Dr. Alois Mair from whom I have learned most of my skills in the lab and to Dr. Kai Chen for support on the theoretical side. I especially enjoyed the discussions with Claudia Wagenknecht and Thorsten Strassel about physics and the general meaning of life. I further would like to thank all members of the QUO group for their general support: Dr. Shuai Chen, Dr. Zhen-Sheng Yuan, Dr. Che-Ming Li, Dr. Chih-Sung Chuu, Dr. Youjin Deng, Yong Zhao, Bo Zhao and Chao-Yang Lu.

This work would not have been possible without the great support of the electronic workshop, especially by Mr. v. Walter, the mechanical workshop and our secretaries.

I am grateful to Florian Lenz, Bernd Hezel, Christoph Petri and all others at the *Physikalisches Institut* for fun times at the *Kicker* Table and at institute events.

Während der Zeit als Doktorand hat mir mein großes Hobby Basketball als Ausgleich zu der Arbeit im Physikalischen Institut gedient. Ich möchte mich bei meiner Mannschaft, der Herren 2 des HTV, für unzählige schöne Stunden bedanken, bei denen ich manchen Frust abbauen konnte. Besonders möchte ich mich auch bei *"meinen Mädels"* der U18 Mannschaft bedanken; Ihr habt mir viel Freude bereitet.

Ich habe das Glück, im Laufe meines Lebens sehr gute Freunde kennen gelernt zu haben, von denen ich vielfältige Unterstützung erfahren habe. Ich danke Euch allen

und möchte einige hier erwähnen: Torsten, Olli, Steve, Mareike, Frank, Yvonne, Mo, Tina, Markus, Robert, Micha, Dave, Ruben, Jan, Lukas, Frederike.

Ein besonderer Dank gilt Sabrina, für die vielen Male, die sie mir Mut zugesprochen hat. Ich danke Dir sehr!

Meinem Bruder Florian bin ich dankbar für seine Unterstützung seit meiner Kindheit. Unsere Gespräche haben mein Verständnis und Interesse an der Physik entscheidend beeinflusst und mich in meiner persönlichen Entwicklung geprägt. Ich danke Dir dafür!

Zum Abschluss möchte ich meinen Eltern danken, für die unzähligen Momente, in denen sie mich auf vielfältigste Art und Weise unterstützt, mir Mut zugesprochen, mich begeistert oder begleitet haben. Ich danke Euch!

Bibliography

[1] L. Marton, J.A. Simpson, and J.A. Suddeth. Electron beam interferometer. *Phys. Rev.*, 90:490, 1954.

[2] H. Rauch, W. Treimar, and U. Bonse. Test of a single crystal neutron interferometer. *Phys. Lett. A*, 57:369, 1974.

[3] O. Carnal and J. Mlynek. Young s double-slit experiment with atoms: A simple atom interferometer. *Phys. Rev. Lett.*, 66:2689–2692, 1991.

[4] D.W. Keith, C.R. Ekstrom, Q.A. Turchette, and D.E. Pritchard. An interferometer for atoms. *Phys. Rev. Lett.*, 66:2693–2696, 1991.

[5] A. Einstein, B. Podolsky, and N. Rosen. Can quantum mechanical description of physical reality be considered complete? *Phys. Rev.*, 47:777, 1935.

[6] J. S. Bell. On the Einstein Poldolsky Rosen paradox. *Physics (Long Island City, N.Y.)*, 1:195, 1964.

[7] A. Aspect, P. Grangier, and G. Roger. Experimental tests of realistic local theories via Bell's theorem. *Phys. Rev. Lett.*, 47:460–463, 1981.

[8] A. Aspect, P. Grangier, and G. Roger. Experimental realization of Einstein-Podolsky-Rosen-Bohm gedankenexperiment: A new violation of Bell's inequalities. *Phys. Rev. Lett.*, 49:91–94, 1982.

[9] A. Aspect, J. Dalibard, and G. Roger. Experimental test of Bell's inequalities using time- varying analyzers. *Phys. Rev. Lett.*, 49:1804–1807, 1982.

[10] P. Walther, M. Aspelmeyer, K. J. Resch, and Anton Zeilinger. Experimental violation of a cluster state Bell inequality. *Phys. Rev. Lett.*, 95:020403, 2005.

[11] C. Simon and W. T. M. Irvine. Robust long-distance entanglement and a loophole-free Bell test with ions and photons. *Phys. Rev. Lett.*, 91:110405, 2003.

[12] E. Schrödinger. Die gegenwärtige Situation in der Quantenmechanik. 23:807–812; 823–828; 844–849, 1935.

[13] C. H. Bennett. "Quantum and classical information: Transmission and computation". *Physics Today*, 48(10):24–30, 1995.

[14] D. Bouwmeester, A. Ekert, and A. Zeilinger. *The Physics of quantum information*. Springer-Verlag Berlin: Heidelberg, 2000.

[15] C. H. Bennett and G. Brassard. Quantum cryptography: Public key distribution and coin-tossing. *in Proc. IEEE Int. Conf. on Computers, systems, and signal processing*, Bangalore, India:(IEEE, New York, 1984), 175.

[16] A. K. Ekert. Quantum cryptography based on Bell's theorem. *Phys. Rev. Lett.*, 67:661–663, 1991.

[17] C. H. Bennett and S. J. Wiesner. Communication via one- and two-particle operators on Einstein-Podolsky-Rosen states. *Phys. Rev. Lett.*, 69:2881–2884, 1992.

[18] M. Aspelmeyer, H. R. Böhm, T. Gyatso, T. Jennewein, R. Kaltenbaek, M. Lindenthal, G. Molina-Terriza, A. Poppe, K. Resch, M. Taraba, R. Ursin, P. Walther, and A. Zeilinger. Long-distance free-space distribution of quantum entanglement. *Science*, 301:621–623, 2003.

[19] R. Ursin, F. Tiefenbacher, T. Schmitt-Manderbach, H. Weier, T. Scheidl, M. Lindenthal, B. Blauensteiner, T. Jennewein, J. Perdigues, P. Trojek, B. Ömer, M. Fürst, M. Meyenburg, J. Rarity, Z. Sodnik, C. Barbieri, H. Weinfurter, and A. Zeilinger. Entanglement-based quantum communication over 144 km. *Nature Physics*, 3:481, 2007.

[20] L. K. Grover. Quantum mechanics helps in searching for a needle in a haystack. *Phys. Rev. Lett.*, 79:325, 1997.

[21] P. W. Shor. Polynomial-time algorithms for prime factorization and discrete logarithms on a quantum computer. In *Proceedings of the 35th Annual Symposium on Foundations of Computer Science*, 1994.

[22] D. Deutsch and R. Jozsa. Rapid solutions of problems by quantum computation. *Proceedings of the Royal Society of London A*, 439:553, 1992.

[23] H. J. Briegel, W. Dur, J. I. Cirac, and P. Zoller. Quantum repeaters: the role of imperfect local operations in quantum communication. *Phys. Rev. Lett.*, 81:5932–5935, 1998.

[24] W. Dür, H.-J. Briegel, J. I. Cirac, and P. Zoller. Quantum repeaters based on entanglement purification. *Phys. Rev. A*, 59:169–181, 1999.

[25] H. Häffner, W. Hänsel, C. F. Roos, J. Benhelm, D. Chek al kar1, M. Chwalla, T. Körber, U. D. Rapol, M. Riebe, P. O. Schmidt, C. Becher, O. Gühne, W. Dür, and R. Blatt. Scalable multiparticle entanglement of trapped ions. *Nature*, 438:643–646, 2005.

[26] L. M. K. Vandersypen, M. Steffen, G. Breyta, C. S. Yannoni, M. H. Sherwood, and I. L. Chuang. Experimental realization of shor's quantum factoring algorithm using nuclear magnetic resonance. *Nature*, 414:883–887, 2001.

[27] D. Loss and D. P. DiVincenzo. Quantum computation with quantum dots. *Phys. Rev. A*, 57:120, 1998.

[28] Y. Nakamura, Y. A. Pashkin, and J. S. Tsai. Coherent control of macroscopic quantum states in a single-cooper-pair box. *Nature*, 398:786, 1999.

[29] E. Knill, R. Laflamme, and G. J. Milburn. A scheme for efficient quantum computation with linear optics. *Nature*, 409:46–52, 2001.

[30] P. G. Kwiat, K. Mattle, H. Weinfurter, A. Zeilinger, A. V. Sergienko, and Y. Shih. New high-intensity source of polarization-entangled photon pairs. *Phys. Rev. Lett.*, 75:4337–4341, 1995.

[31] C. S. Wu and I. Shaknov. The angular correlation of annihilation radiation. *Phys. Rev.*, 77:136, 1950.

[32] C. A. Kocher and E.D. Commins. Polarization correlation of photons emitted in an atomic cascade. *Phys. Rev. Lett.*, 18:575–577, 1967.

[33] J. F. Clauser. Experimental limitations to the validity of semiclassical radiation theories. *Phys. Rev. A*, 6:49–54, 1972.

[34] J. F. Clauser. Experimental distinction between the classical and quantum field - theoretical predictions for the photoelectric effect. *Phys. Rev. D*, 9:853–860, 1974.

[35] C. H. Bennett, G. Brassard, C. Crepeau, R. Jozsa, A. Peres, and W. K. Wootters. Teleporting an unknown quantum state via dual classic and Einstein-Podolsky-Rosen channels. *Phys. Rev. Lett.*, 70:1895–1899, 1993.

[36] D. Bouwmeester, J.-W. Pan, K. Mattle, M. Eibl, H. Weinfurter, and A. Zeilinger. Experimental quantum teleportation. *Nature*, 390:575–579, 1997.

[37] K. Mattle, H. Weinfurter, P. G. Kwiat, and A. Zeilinger. Dense coding in experimental quantum communication. *Phys. Rev. Lett.*, 76:4656–4659, 1996.

[38] A. Barenco, D. Deutsch, A. Ekert, and R. Jozsa. Conditional quantum dynamics and logic getes. *Phys. Rev. Lett.*, 74:4083–4086, 1995.

[39] A. Barenco, C.H. Bennett, D.P. DiVincenzo, N. Margolus, P. Shor, T. Sleator, J. Smolin, and H. Weinfurter. Elementary gates for quantum computation. *Phys. Rev. A*, 52:3457–3467, 1995.

[40] D. Gottesman and I. L. Chuang. Demonstrating the viability of universal quantum computation using teleportation and single-qubit operations. *Nature*, 402:390–393, 1999.

[41] L. K. Grover. Quantum telecomputation. arXiv:quant-ph/9704012.

[42] M. Żukowski, A. Zeilinger, M. A. Horne, and A. K. Ekert. "event-ready-detectors" Bell experiment via entanglement swapping. *Phys. Rev. Lett.*, 71:4287–4290, 1993.

[43] S. Bose, V. Vedral, and P.L. Knight. Multiparticle generalization of entanglement swapping. *Phys. Rev. A*, 57:822–829, 1998.

[44] W. K. Wootters and W. H. Zurek. A single quantum cannot be cloned. *Nature*, 299:802–803, 1982.

[45] D.M. Greenberger, M.A. Horne, and A. Zeilinger. *Bell's Theorem, Quantum Theory, and Conceptions of the Universe*, page 69. Kluwer, Dordrecht, 1989.

[46] J.-W. Pan, D. Bouwmeester, M. Daniell, H. Weinfurter, and A. Zeilinger. Experimental test of quantum nonlocality in three-photon Greenberger-Horne-Zeilinger entanglement. *Nature*, 403:515–519, 2000.

[47] C. H. Bennett, G. Brassard, S. Popescu, B. Schumacher, J. A. Smolin, and W. K. Wootters. Purification of noisy entanglement and faithful teleportation via noisy channels. *Phys. Rev. Lett*, 76:722–725, 1996.

[48] J.-W. Pan, C. Simon, C. Brukner, and A. Zeilinger. Entanglement purification for quantum communication. *Nature*, 410:1067–1070, 2001.

[49] J.-W. Pan, S. Gasparoni, U. Rupert, G. Weihs, and A. Zeilinger. Experimental entanglement purification of arbitrary unknown states. *Nature*, 423:417–422, 2003.

[50] W. Dür, G. Vidal, and J. I. Cirac. Three qubits can be entangled in two inequivalent ways. *Phys. Rev. A*, 62:062314, 2000.

[51] A. Cabello. Bell's theorem with and without inequalities for the three-qubit greenberger-horne-zeilinger and w states. *Phys. Rev. A*, 65:032108, 2002.

[52] N. Gisin. Nonlocality criteria for quantum teleportation. *Phys. Lett. A*, 210:157–159, 1996.

[53] M. Hein, J. Eisert, and H. J. Briegel. Multiparty entanglement in graph states. *Phys. Rev. A*, 69:062311, 2004.

[54] H. J. Briegel and R. Raussendorf. Persistent entanglement in arrays of interacting particles. *Phys. Rev. Lett.*, 86:910–913, 2001.

[55] D. Schlingemann and R. F. Werner. Quantum error-correcting codes associated with graphs. *Phys. Rev. A*, 65:012308, 2002.

[56] D. M. Greenberger, M. A. Horne, A. Shimony, and A. Zeilinger. Bell's theorem without inequalities. *Am. J. Phys.*, 58:1131–1143, 1990.

[57] V. Scarani, A. Acín, E. Schenck, and M. Aspelmeyer. Nonlocality of cluster states of qubits. *Phys. Rev. A*, 71:042325, 2005.

[58] O. Gühne, G. Tóth, P. Hyllus, and H.J. Briegel. Bell inequalities for graph states. *Phys. Rev. Lett.*, 95:120405, 2005.

[59] N. Kiesel, C. Schmid, U. Weber, G. Tóth, O. Gühne, R. Ursin, and H. Weinfurter. Experimental analysis of a four-qubit photon cluster state. *Phys. Rev. Lett.*, 95:210502, 2005.

[60] W. Dür and H.J. Briegel. Stability of macroscopic entanglement under decoherence. *Phys. Rev. Lett.*, 92:180403, 2004.

[61] R. Raussendorf and H. J. Briegel. A one-way quantum computer. *Phys. Rev. Lett.*, 86:5188–5191, 2001.

[62] M. A. Nielsen. Optical quantum computation using cluster states. *Phys. Rev. Lett.*, 93:040503, 2004.

[63] M. Hein, W. Dür, and H. J. Briegel. Entanglement properties of multipartite entangled states under the influence of decoherence. *Phys. Rev. A*, 71:032350, 2005.

[64] P. Walther, K. J. Resch, T. Rudolph, E. Schenck, H. Weinfurter, V. Vedral, M. Aspelmeyer, and A. Zeilinger. Experimental one-way quantum computing. *Nature*, 434:169–176, 2005.

[65] A.-N Zhang, C.-Y. Lu, X.-Q. Zhou, Y.-A. Chen, Z. Zhao, T. Yang, and J.-W. Pan. Experimental construction of optical multiqubit cluster states from bell states. *Phys. Rev. A*, 73:022330, 2006.

[66] C.-Y. Lu, X.-Q. Zhou, O. Gühne, W.-B. Gao, J. Zhang, Z.-S. Yuan, A. Goebel, Tao Yang, and Jian-Wei Pan. Experimental entanglement of six photons in graph states. *Nature Physics*, 3:91–95, 2007.

[67] D. E. Browne and T. Rudolph. Resource-efficient linear optical quantum computation. *Phys. Rev. Lett.*, 95:010501, 2005.

[68] T. P. Bodiya and L.-M. Duan. Scalable generation of graph-state entanglement through realistic linear optics. *Phys. Rev. Lett.*, 97:143601, 2006.

[69] R. Prevedel, P. Walther, F. Tiefenbacher, P. Böhi, R. Kaltenbaek, T. Jennewein, and A. Zeilinger. High-speed linear optics quantum computing using active feed-forward. *Nature*, 445:65–69, 2007.

[70] M. S. Tame, R. Prevedel, M. Paternostro, P. Böhi, M. S. Kim, and A. Zeilinger. Experimental realization of Deutsch's algorithm in a one-way quantum computer. *Phys. Rev. Lett.*, 98:140501, 2007.

[71] S. Hill and W. K. Wootters. Entanglement of a pair of quantum bits. *Phys. Rev. Lett.*, 78:5022–5025, 1997.

[72] W. K. Wootters. Entanglement of formation of an arbitrary state of two qubits. *Phys. Rev. Lett.*, 80:2245–2248, 1998.

[73] M. Bourennane, M. Eibl, C. Kurtsiefer, S. Gaertner, H. Weinfurter, O. Gühne P. Hyllus, D. BruSS, M. Lewenstein, and A. Sanpera. Experimental detection of multipartite entanglement using witness operators. *Phys. Rev. Lett.*, 92:087902, 2004.

[74] Y.-A. Chen, S. Chen, Z.-S. Yuan, B. Zhao, C.-S. Chuu, J. Schmiedmayer, and J.-W. Pan. Memory-built-in quantum teleportation with photonic and atomic qubits. *arXiv:quant-ph/07051256*, 2007.

[75] L. De Caro and A. Garuccio. Reliability of bell inequality measurements using polarization correlations in parametricdown-conversion photons sources. *Phys. Rev. A*, 50:R2803–R2805, 1994.

[76] M. H. Rubin, D. N. Klyshko, Y. H. Shih, and A. V. Sergienko. Theory of two-photon entanglement in type-II optical parametric down-conversion. *Phys. Rev. A 50, 5122 - 5133 (1994)*, 50:5122–5133, 1994.

[77] A. Zeilinger. General properties of lossless beam splitters in interferometry. *Am. J. Phys.*, 49:882, 1981.

[78] D. Boschi, S. Branca, F. De Martini, L. Hardy, and S. Popescu. Experimental realization of teleporting an unknown pure quantum state via dual classical and Einstein-Podolsky-Rosen channels. *Phys. Rev. Lett.*, 80:1121–1125, 1998.

[79] J.-W. Pan, D. Bouwmeester, H. Weinfurter, and A. Zeilinger. Experimental entanglement swapping: entangling photons that never interacted. *Phys. Rev. Lett.*, 80:3891–3894, 1998.

[80] M. D. Barrett, J. Chiaverini, T. Schaetz, J. Britton, W. M. Itano, J. D. Jost, E. Knill, C. Langer, D. Leibfried, R. Ozeri, and D. J. Wineland. Deterministic quantum teleportation of atomic qubits. *Nature*, 429:737–739, 2004.

[81] M. Riebe, H. Häffner, C. F. Roos, W. Hänsel, J. Benhelm, G. P. T. Lancaster, T. W. Körber, C. Becher, F. Schmidt-Kaler, D. F. V. James, and R. Blatt. Deterministic quantum teleportation with atoms. *Nature*, 429:734–737, 2004.

[82] I. Marcikic, H. de Riedmatten, W. Tittel, H. Zbinden, and N. Gisin. Long-distance teleportation of qubits at telecommunication wavelengths. *Nature*, 421:509–513, 2003.

[83] R. Ursin, T. Jennewein, M. Aspelmeyer, R. Kaltenbaek, M. Lindenthal, P. Walther, and A. Zeilinger. Communications quantum teleportation across the danube. *Nature*, 430:849, 2004.

[84] Z. Zhao, Y.-A. Chen, A.-N. Zhang, T. Yang, H. Briegel, and J.-W. Pan. Experimental demonstration of five-photon entanglement and open-destination teleportation. *Nature*, 430:54–57, 2004.

[85] B. C. Jacobs, T. B. Ptitman, and J. D. Franson. Quantum relays and noise suppression using linear optics. *Phys. Rev. A*, 66:052307, 2002.

[86] A. R. Calderbank and P. W. Shor. Good quantum error-correcting codes exist. *Phys. Rev. A*, 54:1098–1105, 1996.

[87] J. Lee and M. S. Kim. Entanglement teleportation via Werner states. *Phys. Rev. Lett.*, 84:4236–4239, 2000.

[88] Y. Yeo and W. K. Chua. Teleportation and dense coding with genuine multipartite entanglement. *Phys. Rev. Lett.*, 96:060502, 2006.

[89] G. Rigolin. Quantum teleportation of an arbitrary two-qubit state and its relation to multipartite entanglement. *Phys. Rev. A*, 71:032303, 2005.

[90] M. Hillery, V. Bužek, and A. Berthiaume. Quantum secret sharing. *Phys. Rev. A*, 59:1829–1834, 1999.

[91] R. Cleve, D. Gottesman, and H.-K. Lo. How to share a quantum secret. *Phys. Rev. Lett.*, 83:648–651, 1999.

[92] M. Żukowski, A. Zelinger, and H.Weinfurter. Entangling photons radiated by independent pulsed source. *Ann. N.Y. Acad. Sci.*, 755:91, 1995.

[93] Y.H. Shih and C.O. Alley. New type of einstein-podolsky-rosen-bohm experiment using pairs of light quanta produced by optical parametric down conversion. *Phys. Rev. Lett.*, 61:2921, 1988.

[94] C. K. Hong, Z. Y. Ou, and L. Mandel. Measurement of subpicosecond time intervals between two photons by interference. *Phys. Rev. Lett.*, 59:2044–2046, 1987.

[95] J.-W. Pan, M. Daniell, S. Gasparoni, G. Weihs, and A. Zeilinger. Experimental demonstration of four-photon entanglement and high-fidelity teleportation. *Phys. Rev. Lett.*, 86:4435, 2001.

[96] J.-W. Pan and A. Zeilinger. Greenberger-Horne-Zeilinger-state analyzer. *Phys. Rev. A*, 57:2208–2211, 1998.

[97] A. Hayashi, T. Hashimoto, and M. Horibe. Reexamination of optimal quantum state estimation of pure states. *Phys. Rev. A*, 72:032325, 2005.

[98] D. Collins, N. Gisin, and H.D. Riedmatten. Quantum relays for long distance quantum cryptography. *J. Mod. Opt.*, 52:735, 2005.

[99] J.I. Cirac, L.M. Duan, and P. Zoller. Experimental quantum computation and information. In *Proceedings of the International School of Physics ŞEnrico FermiŤ, Course CXLVIII, edited by F. Di Martini and C. Monroe (IOS Press, Amsterdam)*, 2002.

[100] C. H. Bennett, D. P. DiVincenzo, J. A. Smolin, and W. K. Wootters. Mixed-state entanglement and quantum error correction. *Phys. Rev. A*, 54:3824–3851, 1996.

[101] P.G. Kwiat, S. Barraza-Lopez, A. Stefanov, and N. Gisin. Experimental entanglement distillation and 'hidden' non-locality. *Nature*, 409:1014, 2001.

[102] T. Chanelière, D. N. Matsukevich, S. D. Jenkins, S.-Y. Lan, T. A. B. Kennedy, and A. Kuzmich. Storage and retrieval of single photons transmitted between remote quantum memories. *Nature*, 438:833–836, 2005.

[103] D. Felinto, C. W. Chou, J. Laurat, E. W. Schomburg, H. de Riedmatten, and H. J. Kimble. Conditional control of the quantum states of remote atomic memories for quantum networking. *Nature Physics*, 2:844, 2006.

[104] Y.-A. Chen, S. Chen, Z.-S. Yuan, B. Zhao, C.-S. Chuu, J. Schmiedmayer, and J.-W. Pan. Memory-built-in quantum teleportation with photonic and atomic qubits. *Nature Phys.*, 4:103, 2008.

[105] T. Jennewein, G. Weihs, J.-W. Pan, and A. Zeilinger. Experimental nonlocality proof of quantum teleportation and entanglement swapping. *Phys. Rev. Lett.*, 88:017903, 2002.

[106] H. de Riedmatten, I. Marcikic, J. A. W. van Houwelingen, W. Tittel, H. Zbinden, and N. Gisin. Long-distance entanglement swapping with photons from separated sources. *Phys. Rev. A*, 71:050302, 2005.

[107] R. E. S. Polkinghorne and T. C. Ralph. Continuous variable entanglement swapping. *Phys. Rev. Lett.*, 83:2095–2099, 1999.

[108] X. Jia, X. Su, Q. Pan, J. Gao, C. Xie, and K. Peng. Experimental demonstration of unconditional entanglement swapping for continuous variables. *Phys. Rev. Lett.*, 93:250503, 2004.

[109] N. Takei, H. Yonezawa, T. Aoki, and A. Furusawa. High-fidelity teleportation beyond the no-cloning limit and entanglement swapping for continuous variables. *Phys. Rev. Lett.*, 94:220502, 2005.

[110] O. Gühne, P. Hyllus, D. Bruß, A. Ekert, M. Lewenstein, C. Macchiavello, and A. Sanpera. Detection of entanglement with few local measurements. *Phys. Rev. A*, 66:062305, 2002.

[111] M. Barbieri, F. De Martini, G. Di Nepi, P. Mataloni, G. M. D'Ariano, and C. Macchiavello. Detection of entanglement with polarized photons: Experimental realization of an entanglement witness. *Phys. Rev. Lett.*, 91:227901, 2003.

[112] V. Scarania, H. de Riedmatten, I. Marcikic, H. Zbinden, and N. Gisin. Four-photon correction in two-photon bell experiments. *Eur. Phys. J. D*, 32:129, 2005.

[113] M. Barbieri. Effects of frequency correlation in linear optical entangling gates operated with independent photons. *Phys. Rev. A*, 76:043825, 2007.

[114] J. Preskill. Reliable quantum computers. *Proc. R. Soc. Lond. A*, 454:385–410, 1998.

[115] A. M. Steane. Efficient fault tolerant quantum computing. *Nature*, 399:124–126, 1999.

[116] D. Gottesman. Theory of fault-tolerant quantum computation. *Phys. Rev. A*, 57:127–137, 1998.

[117] P. W. Shor. Scheme for reducing decoherence in quantum computer memory. *Phys. Rev. A*, 52:R2493–R2496, 1995.

[118] A. M. Steane. Error correcting codes in quantum theory. *Phys. Rev. Lett.*, 77:793–797, 1996.

[119] D. Gottesman. Stabilizer codes and quantum error correction. *arXiv:quant-ph/9705052*, 1997.

[120] R. Laflamme, C. Miquel, J. P. Paz, and W. H. Zurek. Perfect quantum error correcting code. *Phys. Rev. Lett.*, 77:198–201, 1996.

[121] R. Raussendorf, D. E. Browne, and H. J. Briegel. Measurement-based quantum computation on cluster states. *Phys. Rev. A*, 68:022312, 2003.

[122] Q. Zhang, A. Goebel, C. Wagenknecht, Y.-A. Chen, B. Zhao, T. Yang, A. Mair, J. Schmiedmayer, and J.-W. Pan. Experimental quantum teleportation of a two-qubit composite system. *Nature Physics*, 2:678–682, 2006.

[123] D. Leibfried, E. Knill, S. Seidelin, J. Britton, R. B. Blakestad, J. Chiaverini, D. B. Hume, W. M. Itano, J. D. Jost, C. Langer, R. Ozeri, R. Reichle, and D. J. Wineland. Creation of a six-atom 'Schrödinger cat' state. *Nature*, 438:639–642, 2005.

[124] M. Paternostro, M. S. Tame, and M. S. Kim. Hybrid cluster state proposal for a quantum game. *New J. Phys.*, 7:226, 2005.

[125] C. M. Dawson, H. L. Haselgrove, and M. A. Nielsen. Noise thresholds for optical quantum computers. *Phys. Rev. Lett.*, 96:020501, 2006.

[126] M. Varnava, D. E. Browne, and T. Rudolph. Loss tolerance in one-way quantum computation via counterfactual error correction. *Phys. Rev. Lett.*, 97:120501, 2006.

[127] A. Zeilinger, M. A. Horne, H. Weinfurter, and M. Zukowksi. Three-particle entanglements from two entangled pairs. *Phys. Rev. Lett.*, 78:3031–3034, 1997.

[128] G. Tóth and O. Gühne. Entanglement detection in the stabilizer formalism. *Phys. Rev. A*, 72:022340, 2005.

[129] O. Gühne, M. Reimpell, and R. F. Werner. Estimating entanglement measures in experiments. *Phys. Rev. Lett.*, 98:110502, 2007.

[130] T. C. Wei and P. M. Goldbart. Geometric measure of entanglement and applications to bipartite and multipartite quantum states. *Phys. Rev. A*, 68:042307, 2003.

[131] M. Hayashi, D. Markham, M. Murao, M. Owari, and S. Virmani. Bounds on multipartite entangled orthogonal state discrimination using local operations and classical communication. *Phys. Rev. Lett.*, 96:040501, 2006.

[132] W. Dür, H. Aschauer, and H.-J. Briegel. Multiparticle entanglement purification for graph states. *Phys. Rev. Lett.*, 91:107903, 2003.

[133] P. Kok, W. J. Munro, K. Nemoto, T. C. Ralph, J. P. Dowling, and G. J. Milburn. Linear optical quantum computing with photonic qubits. *Rev. Mod. Phys.*, 79:135–174, 2007.

[134] T. Yang, Q. Zhang, J. Zhang, J. Yin, Z. Zhao, M. Żukowski, Z.-B. Chen, and J.-W. Pan. All-versus-nothing violation of local realism by two-photon, four-dimensional entanglement. *Phys. Rev. Lett.*, 95:240406, 2005.

[135] C. Cinelli, M. Barbieri, R. Perris, P. Mataloni, and F. De Martini. All-versus-nothing nonlocality test of quantum mechanics by two-photon hyperentanglement. *Phys. Rev. Let..*, 95:240405, 2005.

[136] J. T. Barreiro, N. K. Langford, N. A. Peters, and Paul G. Kwiat. Generation of hyperentangled photon pairs. *Phys. Rev. Lett.*, 95:260501, 2005.

[137] C. Schuck, Gerhard Huber, C. Kurtsiefer, and Harald Weinfurter. Complete deterministic linear optics Bell state analysis. *Phys. Rev. Lett.*, 96:190501, 2006.

[138] A. Cabello. "all versus Nothing" inseparability for two observers. *Phys. Rev. Lett.*, 87:010403, 2001.

[139] Z.-B. Chen, J.-W. Pan, Y.-D. Zhang, C. Brukner, and A. Zeilinger. All-Versus-Nothing violation of local realism for two entangled photons. *Phys. Rev. Lett.*, 90:160408, 2003.

[140] A. Cabello. Bipartite Bell inequalities for hyperentangled states. *Phys. Rev. Lett.*, 97:140406, 2006.

[141] Marco Barbieri, F. De Martini, P. Mataloni, G. Vallone, and A. Cabello. Enhancing the violation of the Einstein-Podolsky-Rosen local realism by quantum hyperentanglement. *Phys. Rev. Lett.*, 97:140407, 2006.

[142] P. G. Kwiat and H. Weinfurter. Embedded Bell-state analysis. *Phys. Rev. A*, 58:R2623–R2626, 1998.

[143] M. Barbieri, G. Vallone, P. Mataloni, and F. De Martini. Complete and deterministic discrimination of polarization Bell states assisted by momentum entanglement. *Phys. Rev. A*, 75:042317, 2007.

[144] P.G. Kwiat, J.R. Mitchell, P.D.D. Schwindt, and A. G. White. Grover's search algorithm: An optical approach. *J. Mod. Opt.*, 47:257, 2000.

[145] N. Bhattacharya, H.B. van Linden van den Heuvell, and R.J.C. Spreeuw. Implementation of quantum search algorithm using classical fourier optics. *Phys. Rev. Lett.*, 88:137901, 2002.

[146] R. M. Stevenson, R. J. Young, P. Atkinson, K. Cooper, D. A. Ritchie, and A. J. Shields. A semiconductor source of triggered entangled photon pairs. *Nature*, 439:179–182, 2006.